BONE-ON-BONE FORCES AT THE ANKLE AND KNEE IN FIGURE SKATERS DURING LOOP JUMPS : CLINICAL IMPLICATIONS

by

Michelle Elisabeth Kho

A thesis
presented to the University of Waterloo
in fulfilment of the
thesis requirement for the degree of
Master of Science
in
Kinesiology

Waterloo, Ontario, Canada, 1996

The University of Waterloo requires the signatures of all persons using or photocopying this thesis. Please sign below, and give address and date.

ABSTRACT

Success in competitive figure skating is dependent upon the number of triple revolution jumps a skater can successfully complete in competition. Figure skating injury studies indicated that the knee and the ankle were the most common injury sites. To gain insight into potential injury mechanisms, a model of the ankle and knee joints was created to predict the bone-on-bone forces during jump landings and takeoffs.

Three male National level figure skating competitors participated in this study, which was divided into laboratory and on-ice components. On ice, the skaters were videotaped performing single and double loop jumps. Muscle activity of vastus lateralis, tibialis anterior, biceps femoris, and lateral gastrocnemius was recorded with a portable EMG data unit. An estimate of the location and magnitude of the ground reaction force vector was obtained by laboratory simulations of jump takeoffs and landings. Similar to the on-ice collection, all trials were videotaped and muscle activity recorded. Muscle activation, video, and force plate data were used as inputs to an inverse dynamic model of the lower limb.

A 2-dimensional, dynamic, sagittal plane model of the lower limb was programmed to calculate the bone-on-bone forces at the ankle and knee from the laboratory and on-ice data. An updated version of McGill and Norman's (1986) multiplicative muscle model was incorporated into the lower limb model. Representative force plate trials of jump takeoffs and jump landings were used as the kinetic complement to on-ice video and electromyographic information.

Peak vertical ground reaction forces in the laboratory simulations ranged from 2.12 to 2.21 times body weight in jump takeoffs and 3.65 to 4.88 times body weight in jump landings. Muscle activity patterns revealed a high degree of cocontraction on impact

in jump landings. Joint reaction forces at the ankle and knee were larger in jump landings than in jump takeoffs in both laboratory and on-ice trials. Joint moment analysis indicated that jump takeoffs elicited a plantarflexor moment at the ankle and extensor moment at the knee. Jump landings resulted in an ankle plantarflexor moment and knee extensor moment.

Peak bone-on-bone forces ranging from 6.6 to 11.7 and 4.5 to 47.1 times body weight at the ankle and knee, respectively, were calculated during jump takeoff conditions. Jump landing conditions resulted in peak bone-on-bone forces ranging from 5.8 to 17.3 and 21.5 to 69.3 times body weight at the ankle and knee, respectively.

Bone-on-bone forces during jump landings were characterized by bimodal peaks at the ankle and a high-intensity, short duration peak, at the knee. These peaks occurred within the first 125 ms of impact. Bone-on-bone forces at the ankle remained fairly constant throughout jump takeoffs, while a high-intensity, short duration peak was noted at the knee prior to takeoff. These short, explosive periods of force may be a window onto understanding why skaters experience knee and ankle injuries.

ACKNOWLEDGEMENTS

First and foremost, I am very grateful to my supervisor, Dr. Patrick Bishop, for his guidance, insight, and unfailing optimism throughout this project. I treasure the friendship we have developed and hope that I may one day attain some of the accomplishments he has achieved in his career and extracurricular activities.

To my examination committee members, Dr. Stuart McGill and Dr. Richard Wells, thank you for your time and inputs to this study. Your wealth of knowledge helped make this project a reality.

To my enthusiastic and incredibly patient skaters, thank you for your time and perspectives from the athlete's point of view.

To my brother, Michael, the guinea pig in pilot studies right from the beginning. Thank you so much--the patience and tolerance you demonstrated in all situations were well above and beyond the call of sibling duty. May the force be with you.

To the coaches and therapist who helped me understand jump technique, thank you.

Thank you to John Pezzack--without your help, the computer model would still be somewhere on paper.....okay, so the programming wasn't that bad!

To Wendell Prime, thank you for your instrumentation insights and expertise throughout this project. Shelter anyone?

To my emotional crises network, Lesley Allan, Jacqueline Hooper, Carolyn Kovacs, Melissa Harder, and Ann Marie Klein--thanks for the smiles and hugs. To my social convenor, Danny Ljubisic and the members of the after-hours club, thanks for making sure I had fun.

To Nancy Bestic, a true friend through good and bad. Thanks for being you. I'm grateful for the support from Martine Mientjes, Tammy Lindover, and Elaine Little - people who see things the same way too. Thanks to all the KINGRADS-- you guys are awesome!

To the Staff and Faculty in the Department of Kinesiology, thank you for your guidance and friendship--the last seven years here have made some of my best memories.

Finally, I never could have done this project without the support and unfailing faith from my parents, Ay and Hans Kho. You have set an example of selflessness and unconditional love for which I am eternally grateful, even though I may not always say it. I love you both very much.

TABLE OF CONTENTS

Chapter 1 - Introduction

Chapter 2 - Review of Related Literature

Chapter 3- Methods

Chapter 4 - Model Development

Chapter 5 - Results and Discussion

Chapter 6 - Summary, Conclusions, and Recommendations

LIST OF TABLES

LIST OF FIGURES

Chapter I - Introduction

International competitive figure skating is a sport which requires that participants strike a complementary balance between musical artistry and athletic ability. In singles events, elite competitors must successfully complete multi-revolution jumps precisely choreographed into musical highlights and phrases. International achievement is directly related to the technical superiority exhibited by the number of different triple revolution jumps (triple jumps) a skater can complete in a standard 4 - 4½ minute free skating programme. Serious competitors are pushing the limits of their abilities by repetitive practice, often at the expense of their own bodies' capacity, to reach perfect execution and consistency of triple jumps. This drive is also evident in younger skaters aspiring to reach international levels of competition as they learn double and triple jumps.

Competitive figure skating has changed considerably in the last 10 years. Before 1991, a skating competition consisted of compulsory figures (the tracing of specified patterns on the ice with the skate blade) and of free skating. The Canadian Figure Skating Association (1995) defined compulsory figures as, "the skating of prescribed movements on one or more circles." In free skating, the skater chooses the number and type of elements (ie jumps, spins, and connecting movements) included in a programme of specified length skated to music of his or her choice (Canadian Figure Skating Association, 1995). Compulsory figures were removed from international figure skating competitions in 1991, and this has shifted skating's training emphasis to free skating.

In 1982, Smith and Micheli reported that high level skaters spent at least 30 minutes a day practising triple jumps. Based on a schedule of six sessions a week, 48 weeks per year, this amounted to 144 hours of practice per year on triple jumps alone.

Survey data before 1991 showed that compulsory figures occupied between five and 21 hours of weekly practice time (Smith et al., 1982, Brock and Striowski, 1986, Brown and McKeag, 1987). Comper (1996) reported that skaters at the 1993 Canadian Figure Skating Championships (no compulsory figure component) had not reduced their on-ice skating time. From this, one may extrapolate that present-day skaters are now spending more time subjecting their bodies to the forces and moments imposed on their system as they practice to perfect triple jumps.

An extensive review of existing injury data on figure skaters revealed poor epidemiological injury reporting techniques. Reports ranged from review articles (Niinimaa, 1982), to patient chart reviews (Garrick, 1985), to interviews (Pecina, Bojanic, and Dubravcic, 1990), to questionnaires (Smith and Micheli, 1982; Brock and Striowski, 1986; Brown and McKeag; 1987), and prospective studies (Smith and Ludington, 1989; Kjaer and Larsson, 1990). Of these studies, only Brock et al. (1986), Brown et al. (1987), Smith et al. (1989), Pecina et al. (1990), and Kjaer et al. (1990) solely examined national and international competitors. Despite these varied approaches to studying injuries, trends emerged. Lower extremity injuries were more common than upper extremity injuries, and of the lower extremity injuries, the knee and ankle were the most common injury sites. Similar trends have been reported in other jumping and landing activities such as running and basketball (Dufek and Bates, 1991).

Few biomechanical studies have been conducted on figure skating jumps (Aleshinsky, 1986; King, Arnold, and Smith; 1994, Albert and Miller, 1996). The results of these studies have been mainly qualitative in nature, emphasizing takeoff velocities, jump lengths, and skid lengths. Some previous studies (Aleshinsky, 1986; King et al. 1994; Albert et al., 1996) have emphasized a kinematic approach to jump analysis. However, to gain insight into injury mechanisms, knowledge about how the body responds to external forces must be known. Nigg (1985) defined the term "load

on the human locomotor system" as, "the sum of the forces and moments acting on the body of interest." He further stated that excessive loads may be the reason for micro- or macro- damages of anatomical structures (Nigg, 1988). Thus, as suggested by others, a kinetic approach to determine the forces acting externally on the human system and how they affect movement is required (Winter, 1990).

Despite many technological advances, biomechanists still cannot directly measure muscle force in the human system without surgical intervention (Norman, 1989). Force platforms, which measure ground reaction vectors, and electromyography, an indicator of a muscle's electrical activity, are used by researchers as indirect tools of force measurement. Coupled with a video record of motion, these methods can relate ground reaction forces and muscle activity to specific body positions in time during motion. By merging the information from these sources, a model may be formulated to estimate forces acting on the human body.

Biomechanical models are commonly used to predict loads acting on the human body. Link segment modelling (LSM) uses anthropometric and kinematic data to calculate reaction forces and moments at different joints (Winter, 1990). Two different types of reaction forces may be calculated - joint reaction (JRX) and bone-on-bone (BOB). Joint reaction forces represent the moment of force about a hinge joint and assume that the force across the joint surface is the same as the reaction force at the joint. However, muscles contribute compressive and shear forces to joint surfaces, and the inclusion of these muscle forces to a LSM represents the calculation of BOB force.

Researchers who have examined BOB forces have shown the importance of studying the takeoff phase in addition to landings. Scott and Winter (1990) predicted BOB forces of 9.0 - 11.7 times body weight (BW) at the ankle and 10.3 - 14.1 times BW at the knee during running. These forces occurred during midstance and at the start of

push off. Galea's (1983) model predicted that ballet dancers experienced peak ankle BOB forces of 12 times BW during relevés en pointe (a rapid dynamic movement where the dancer begins flatfoot and ends on the toes). Similar to Scott and Winter, these values occurred just as the heel was leaving the ground.

Many researchers have examined ground reaction forces (GRF) in landing activities. McNitt-Gray (1991) reported peak GRFs of 11.0, 6.3, and 3.9 times BW in landings from 1.28, 0.72, and 0.32 m in elite gymnasts. Dufek and Bates (1991) reported average peak GRFs of three times BW in landings from 0.6 m. Peak GRFs of 15 - 17 times BW were recorded in one foot landings of gymnasts from double back somersaults (Panzer, 1987). Adding the effects of muscle activation to these forces would result in much larger BOB forces at the joint surfaces in a combined link segment and anatomical model. For example, the reported GRFs in Scott and Winter's (1990) study only ranged from 1.6 - 3.0 times BW.

To date, little if any data exists on the magnitude of the BOB forces experienced by skaters during jumping activities. Since most skating injuries occur at the knee and ankle, insight into the loads experienced at these sites would improve the knowledge of how and why certain athletes may be predisposed to injury (Scott and Winter, 1990).

1.1 Purpose

The purpose of this study was to use a link segment biomechanical model to determine bone-on-bone forces at the ankle and knee in takeoffs and landings of a figure skating jump that begins and ends on the same leg (loop jump).

1.2 Subproblems

1. The magnitude of ground reaction force in on-ice take-offs and landings could not be measured directly. The first sub-problem was to measure these forces during simulated jumps in the laboratory.
2. A second sub-problem was a comparison of the bone-on-bone forces determined from laboratory simulations and on-ice performances.
3. Skaters were asked to perform both single and double loop jumps. The third subproblem was to determine differences in the magnitudes of the bone-on-bone forces in takeoffs and landings for these two jumps.

1.3 Hypotheses

It was hypothesized that:

1. The peak bone-on-bone forces predicted at the knee and ankle for jump takeoffs were different than those predicted for jump landings.
2. Double jumps would produce substantially higher peak BOB forces than single jumps for both takeoffs and landings.

1.4 Assumptions

1. Ground reaction forces recorded by a force platform during simulated takeoffs and landings in the laboratory were representative of the forces experienced by skaters during jumping on-ice.
2. The magnitude of ground reaction force was independent of the number of revolutions completed in the air (ie single or double) in both takeoffs and landings. Previous research has indicated that jump height was constant across single, double, and triple jumps (Aleshinsky, 1986; King et al., 1994).
3. Jump takeoffs and landings occurred in the sagittal plane.
4. Electromyographic-based muscle force predictions were representative of

actual muscle force contributions at the joint of interest.

1.5 Limitations

1. This study was limited to a 2-dimensional sagittal plane analysis of the ankle and knee joints.
2. Jump takeoffs and landings were examined separately.
3. Landing ground reaction forces measured in the laboratory were based on vertical landings from a raised platform. There was no simulation of the angular velocity or rotation experienced in an on-ice jump.
4. Takeoff ground reaction forces measured in the laboratory were based on stationary one foot jump takeoffs.
5. Ground reaction forces were measured on a force platform with the skaters wearing their skates and plastic blade guards.
6. Maximum muscle activity was estimated by a static, maximum voluntary contraction.
7. This study was limited to 3 national-level participants.

1.6 Definitions

(Single) Loop Jump- A jump where the skater leaves the ice from a backward outside edge, completes one revolution in the air and lands on a backward outside edge. The take-off foot and the landing foot are the same.

Double/Triple Loop Jump- Same as single loop, except the skater completes 2 or 3 revolutions.

Figure Skate- The figure skate consists of the skating boot and a stainless steel blade.

Blade- The skating blade, made of stainless steel, represents the interface between the skating boot and the ice.

I.7 Justification

The most common injuries in figure skaters have been documented at the knee and ankle. Injury rates in similar jump sports, and a concentration of reported lower extremity injuries suggest that potential injury situations exist in a variety of landing environments (Dufek and Bates, 1991). Nigg et al. (1981) have suggested that if a potential for injury exists in a movement activity, then the external forces associated with performance should be measured and their effects evaluated.

One goal of the sport biomechanist is to help aspiring athletes by comparing their movement patterns to those that are successfully employed by highly skilled performers (Sprigings, 1987). This study will add to the growing database of biomechanical studies of elite skaters.

Previous studies examining figure skating jumps were hindered by two areas of data collection. First, in many studies, only one trial was used from each subject (Aleshinsky, 1986; King et al., 1994; Albert et al., 1996). As well, the means and standard deviations that were reported were based on collapsed data from a small group of skaters (Aleshinsky, 1986; King et al., 1994; Albert et al., 1996). By combining individual data trials, these methods assumed that all subjects performed the task using a similar strategy. Dufek and Bates (1991) recommended the use of within-subject designs to evaluate individual movement strategies. Previous studies by this group (1990) showed that individual performer information was lost by combining single trials of different subjects.

Secondly, jump inclusion criteria were based on the best camera view (Aleshinsky, 1986; King et al., 1994; Albert et al., 1996). King et al. (1994) were fortunate that

their data set included several trials that were of good jump quality and camera view. This group solicited skating experts to choose an appropriate trial for analysis from each skater, based on jump quality. A weakness in the study of Albert et al. (1996) was that successful and unsuccessful jump characteristics were reported as a combined average. This inconsistency in jump quality did not accurately reflect true, successful jump characteristics.

The goal of this study was to predict the magnitude of bone-on-bone forces at the ankle and knee based on multiple trials of takeoffs and landings of single and double loop jumps. The database of multiple trials from this study will provide further insights about how the body tissues responded to forces and help identify individual jumping strategies. This will help coaches and rehabilitation professionals develop individual training and rehabilitative strategies so that aspiring athletes can improve their jump technique. In addition, further understanding about how these forces may contribute to a potential injury in jumping will be enhanced.

Chapter 2 - Review of Related Literature

Figure skating is a beautiful, yet very complex sport to analyze biomechanically. This section reviews the existing literature on figure skating, mechanisms of lower body injury, biomechanical modelling, and studies on jump takeoffs and landings.

2.1 Figure Skating and Science

The available literature on skaters and skating in general is sparse and not reported in a uniform manner. This section provides the reader a brief introduction to the sport of figure skating, discusses some of the physical characteristics of figure skaters, reports on injury data, and concludes with a synopsis of biomechanical studies of figure skating.

2.1.1 Skating Background

Jumps are a spectacular part of a singles figure skating (skating) programme. A skater's technical prowess in jumping is determined by three factors:

I) The number of different ways a skater can propel him/herself into the air (ie starting backwards or forwards),

ii) The number of times a skater can rotate in the air (about the vertical axis; the more revolutions, the better), and

iii) The total number of the above conditions successfully landed backward on one leg.

Skating jumps are identified by the final approach of the skater prior to takeoff. For a given skater, all successful jumps finish the same way - travelling backward, balancing on a stainless steel blade 4 mm wide.

Triple and quadruple jumps have become an integral portion of the technical component of figure skating. Knoll and Hildebrand (1992, as cited by King, Arnold,

and Smith, 1994) observed that at the 1992 Olympic games, 13 skaters successfully completed triple axels (3½ revolutions in the air) and four skaters successfully completed a quadruple toe loop (4 revolutions). Twelve years earlier, no skater attempted either of these jumps at the Olympic games. At least two different triple jumps are required in the "Short Programme," the first of two programmes skated in competition. Failure to successfully complete these elements results in mandatory penalization by the judges of the event (International Skating Union, 1994; Canadian Figure Skating Association, 1995).

The composition of skating competitions has changed substantially over the last 10 years. Prior to 1991, compulsory figures (the repetitive tracing of circles based on the figure-eight) occupied from five to more than 21 hours per week of skaters' practice time (Smith and Micheli, 1982; Brock and Striowski, 1986; Brown and McKeag, 1987). The removal of compulsory figures from international competition in 1991 increased the amount of ice time available to skaters to practice "free skating" moves (jumps, spins, and footwork).

In 1982, Smith et al. reported that high-level skaters spent at least 30 minutes a day practicing triple jumps. Based on six sessions per week and a training schedule of 48 weeks per year, this amounted to 144 hours per year on triple jumps. Comper (1996) reported that skaters at the 1993 Canadian Figure Skating Championships had not reduced their on-ice skating time, presumably increasing their bodies' exposure to the forces and moments of multi-revolution jumps.

2.1.2 Physical Characteristics of Skaters

Table 1 outlines the reported anthropometric characteristics of skaters from various studies. These values are contrasted against those reported in the Canadian Standardized Test of Fitness (CSTF) Operations Manual 50th percentile Canadian (Fitness Canada, 1986). Due to the disparity in report techniques, it was difficult to

Table 1: Physical Characteristics of Figure Skaters

			Age (years)		Height (m)		Weight (kg)		BMI (kg/m^2)	
	Males	Females	Males	Females	Males	Females	Males	Females	Males	Females
Niinimaa, Woch, and Shephard (1979)	5	4	22.6±8.3	18.0±1.4	1.67±0.04	1.60±0.07	57.7±3.3	55.6±4.8	20.7	21.7
Ninimaa (1982)	9	9	21.3±6	16.5±2.2	1.67±0.06	1.58±0.06	59.6±6.1	48.6±5.4	21.4	19.5
Brock and Striowski (1986)	27	33	20.8	17.6	1.73	1.59	65.6	50.6	22.0	20.0
Roi, Merlo, Occhi, Gemma, Fochini (1989)	8	8	21.1±5	16.8±2.7	1.75±0.04	1.60±0.04	62.3±5.5	52.2±5.4	20.3	20.4
Smith and Ludington (1989)	24	24	21.9±3.7	18±3.6	1.71±0.09	1.56±0.06	66±8	46±5	22.6	18.9
Podolsky, Kaufman, Cahalan, Ateshinsky, and Chao (1990)	10	8	17.5±1.6	14.7±1.6	1.69±0.09	1.58±0.05	64.7±10.1	53.4±4.6	22.7	21.4
Delistraty, Reissman, and Snipes (1992)	0	13	/	12.9±2.1	/	1.55±0.11	/	47.2±6.4	/	20.0
Slemenda and Johnston (1993)	0	22	/	17.7±3.2	/	1.59±0.07	/	50.45±7.3	/	20.0
50th Percentile Canadian Age 15-19	/	/	15-19	15-19	1.74	1.64	66	56	22	21
50th Percentile Canadian Age 20-29	/	/	20-29	20-29	1.76	1.63	73	56	23	21

draw firm conclusions about the anthropometric characteristics of figure skaters. Between studies, different groups of skaters have been used, ranging from recreational skaters (Delistraty, Reissman, and Snipes, 1992; Slemenda and Johnston, 1993) to national and international competitors (Niinimaa, Woch, and Shephard, 1979; Brock et al., 1986; Brown et al., 1987; Roi, Merlo, Occhi, Gemma, and Fochini 1989; Smith and Ludington, 1989; Podolsky, Kaufman, Cahalan, Aleshinsky, and Chao, 1990). Overall, the reported study groups were slightly shorter and had a smaller mass than the CSTF norms. However, the calculated body mass index did not appear to differ from the 50th percentile Canadian.

2.1.3 Injuries in Figure Skaters

An extensive view of existing injury data on figure skaters revealed little uniformity in injury reporting techniques. Reports ranged from review articles (Niinimaa, 1982), to patient chart reviews (Garrick, 1985), to interviews (Pecina, et al., 1990), to questionnaires (Smith et al., 1982; Brock et al., 1986; Brown et al., 1987), and prospective studies (Smith et al., 1989; Kjaer and Larsson, 1990). Of these studies, only Brock et al. (1986), Brown et al. (1987), Smith et al. (1989), Pecina et al. (1990), and Kjaer et al., (1992) solely examined national and international competitors. Despite these methodological differences, definite trends developed in that lower extremity injuries were more dominant than upper extremity injuries. Of the lower extremity injuries, the knee and ankle were the most common injury sites.

The constant trauma of a take off and landing causes stress to the ankles, knees, and hips of skaters (Nash, 1988). Significantly higher bone mineral density in the legs and pelvis of skaters than non-skaters has been reported ($n=22$, $p>= 0.04$, and $p>= 0.0001$ respectively) (Slemenda et al., 1993). Of 18 injuries sustained by eight elite Danish skaters during one skating season, 15 were lower limb related (Kjaer et al., 1992). Pecina et al. (1990) found that nine of 42 skaters at two international competitions had suffered stress fractures in the lower limb during their skating

careers. Brown et al. (1987) documented a history of lower extremity injuries in figure skaters. Hickey (1980, as cited by Brown et al., 1987) examined the effects of compensatory pronation on the competitive ice skater and reported that of 45 female skaters, 40% of the subjects complained of "intermittent foot pain severe enough to require medical consultation or periods off the ice." Unpublished data by M.E. Herring (1983, cited by Brown et al., 1987) showed that of 94 subjects, ankle and knee injuries accounted for 24.5% and 23.4% of the injuries respectively. Garrick (1985) reported that of 242 figure skating injuries seen at a San Francisco sports medicine clinic, 28.9% were attributable to the knee, 24.4% to the ankle, and 11.6% to the foot. Smith et al. (1982) reported 52 injuries in 19 skaters over their skating careers, 25% related to the foot and ankle, and 15% to the knee.

From these studies, the most common knee and ankle injuries experienced by skaters were patellar-femoral pain syndrome (including chondramalacia patellae) (Smith et al., 1982; Brock et al., 1986; Smith et al., 1989), patellar tendinitis (Smith et al., 1989) peroneal tendinitis (Smith et al., 1989), and Achilles tendinitis (Smith et al., 1989). Brock et al. (1986) and Garrick (1985) did not report specific conditions, however, lower limb "overuse" injuries accounted for a large proportion of injuries. Finally, stress fractures have also been documented as common injuries sustained by figure skaters (Smith et al., 1982; Pecina et al, 1990). While stress fractures do not specifically involve the knee and ankle joints, they are indicative of the load transmitted through physically connected structures (Speer and Braun, 1985).

2.1.4 Biomechanics and Figure Skating

Few biomechanical studies have been published on figure skating jumps. Jumps are very complex to study biomechanically because they involve rotation about the body's vertical axis in addition to linear displacement in the horizontal and vertical planes. Advancements in technology have made qualitative jump evaluation much more manageable.

Aleshinsky (1986a) proposed the use of Direct Linear Transformation (DLT) in the biomechanical assessment of figure skating. The three-dimensional nature of skating jumps was captured by forming an image based on multiple camera views of the same movement. Two (or more) cameras placed at known angles to each other were synchronized to record the skating element from all axes (x, y, z). Each camera view was digitized and used to form a 3-dimensional image of the movement. To date, all of the published biomechanical skating articles have used this method to determine jump kinematic parameters.

Aleshinsky (1986b) applied a 15-link segment model (1978) to examine jump takeoff velocity, mechanical energy, rotation, and moment of inertia in jumps completed by four skaters. From the single trials of different jumps, Aleshinsky pioneered research that formed the foundation and present directions of skating biomechanics. He found that in jump takeoffs, the values of absolute velocity at the instant of takeoff tended to decrease as the difficulty level of the jump increased. In the double Axel (a jump of 2.5 revolutions), a total of 1,096 joules of energy was lost during the 0.5s approach and landing, accounting for over half the initial translation energy. In examination of pelvis motion, he detected that skaters did not actually rotate the number of revolutions implied by the title of the jump they were performing. For example a double Axel of 2½ revolutions was only rotated 2.09 revolutions by one skater and 2.15 revolutions by another skater. He also determined that the flight time of the jumps ranging from 0.5 to three revolutions (by name) did not change significantly from lower revolution jumps to triple revolution jumps. Limitations to his study included the small sample size (n=4) and the large range of subject skill level.

Podolsky et al. (1990) determined that jump height was directly related to muscle strength about the knee, hip and shoulder. Using Aleshinsky's (1978) link segment model to determine jump height, this group determined there was a high correlation between jump height in Axel (a 1½ revolution jump) and double Axel jumps and knee

extension (single Axel $r = 0.89$ $p < 0.0001$; double Axel $r = 0.88$, $p < 0.0001$) and shoulder abduction (single Axel $r = 0.859$ $p < 0.0001$; double Axel $r = 0.87$, $p < 0.0001$). A limitation of this study was that male and female data were combined to arrive at this conclusion.

King, Arnold, and Smith (1994) kinematically examined single, double, and triple axels in five elite male figure skaters. Three video cameras were used to collect three single, three double, and two triple axels from each of the five skaters. A 12-link segment model was produced with the PEAK5 motion measurement system. One trial from each condition (single, double, and triple) was digitized per skater. Descriptive statistics from this study determined there was little difference in jump height between single (0.68 ± 0.12 m), double (0.65 ± 0.08 m), and triple (0.66 ± 0.09 m) jumps, implying that skaters increased their angular velocity in jumps requiring more rotation. On average, jump lengths for triple axels were 15% smaller than for double axels and 28% smaller than for single axels. Average horizontal takeoff velocity was highest for single axels ($5.3\ m \cdot s^{-1}$) and smallest for triple axels ($3.6 m \cdot s^{-1}$), while average double Axel take off velocity was intermediate ($4.7\ m \cdot s^{-1}$). Conversely, skid width, skid length, takeoff angles, and rotational velocity increased as jump difficulty increased. Vertical velocity and tilt in air (with respect to vertical) remained constant across jumping conditions.

Miller and Albert (1994, 1995, 1996) investigated the kinematics of single and double axels using a DLT approach. One single and one double Axel from each of eight males and eight females were analyzed. No significant difference was found between single and double axels in the vertical velocity at the start of the jump or in the magnitude of angular momentum (about the vertical axis). Contrary to King et al. (1994), flight time was longer for double axels than for single axels. In double axels, the skater initiated the jump with a smaller moment of inertia than in single axels, and reduced it further to complete the additional rotation.

This study was limited by the choice of subjects evaluated and the final analysis. The authors reported that, "In total, the single and double Axel performances of 44 different skaters were videotaped." Three trials of each jump were recorded. Of these 44 skaters, (264 trials in total), only eight males and eight females were included in the final analysis. Of these possible 96 trials available, only 16 trials, one single and one double Axel were analyzed. A major limitation of the final analysis of these 16 trials was that in the female participants, of eight double axels, only three were successfully landed.

The conclusions drawn from combining the information from successful and unsuccessful trials in this study may be misleading. Research has not yet been conducted to show whether or not differences exist between successful and unsuccessful jump attempts. However, this study did collect very valuable information that could be interpreted more meaningfully and effectively with the consultation of an international level coach.

Few authors have biomechanically evaluated figure skating jump landings. Foti (1990) compared jump landings in a traditional skate and a newly-designed articulated skating boot. A force plate covered with an artificial ice surface and a video analysis system were used to measure impact force and lower extremity angular position data during a simulated one foot backward landing from a 0.3 m high platform. The mean normalized peak force scaled to body weight (BW) was 4.12 ± 0.67 BW in the conventional boot and 3.18 ± 0.60 BW in the articulated skating boot. These simulated landing heights, however, were not necessarily representative of the jump height attained by figure skaters in previous studies. King et al., (1994) reported average jump heights of 0.68, 0.65, and 0.66 m for single, double, and triple axels respectively.

2.2 Jump Takeoffs and Landings

A jump sport is classified as an activity containing an airborne phase which results in a subsequent need for landing (Dufek and Bates, 1991b). A large range of activities are encompassed in this broad definition, ranging from running (which may be considered to be a series of repetitive jump-land sequences), to aerobic dance, to gymnastics and volleyball and, the focus of this thesis, singles figure skating. This section reviews some findings from models used in jump sports.

2.2.1 Jump Takeoffs

Galea (1983) examined bone-on-bone forces at the first metatarsalphalangeal and talocrural joints in ballet dancers during relevés en pointe. A link segment and anatomical model were used in a 2-dimensional, sagittal plane analysis. Peak bone-on-bone forces at the ankle ranged from 5255N to 7030N on full pointe. These values corresponded to 12 times body weight and occurred just as the heels left the ground and on full pointe. Peak bone-on-bone forces at the first metatarsalphalangeal joint were approximately 2.5 times body weight when the heels left the ground at the onset of the motion.

Scott and Winter (1990) created a lower limb model to estimate the magnitude of bone-on-bone loads at the ankle and knee during running. A model of the lower extremity yielded force predictions ranging from 10.3-14.1 times body weight (BW) at the ankle and 7.0-11.1 times BW at the patello-femoral joint. These forces occurred during midstance and at the start of push off.

2.2.2 Jump Landings

McNitt-Gray (1991) examined landing kinematics in elite male gymnasts (n = 6, height = 172.3 ± 2.4 cm, weight 670.8 ± 30.2 N). Vertical landing velocities representing dismounts from different apparati (ie balance beam, parallel bars) were simulated in

different heights (0.32 m, 0.72 m, 1.28 m). Of 4 trials, one trial was included in the analysis, based on the subject's choice of "best" landing. Ground reaction forces ranged from 3.9 - 11.0 times body weight. Kinematic analysis determined that proximal segments were always brought to rest before distal segments. As platform height increased, the peak vertical ground reaction force and joint angular velocity increased, while time to peak vertical force and minimum knee and hip angles decreased. Curiously, minimum ankle angle remained constant across all height conditions (80°). A study of female gymnasts (McNitt-Gray, Yokoi, and Millward, 1993a) yielded similar results (n = 9, height = 161.5 ± 7.9 cm, weight 560.3 ± 57.3 N, platform heights: 0.69 m, 1.25 m, 1.82m).

McNitt-Gray's (1991) study was re-analyzed kinetically to gain insight into joint moments experienced by gymnasts (1993b). An inverse dynamics model using the ground reaction force vector as input yielded peak extensor moments of 525.84 Nm at the ankle and 520.37 Nm at the knee for a drop jump from 1.78 m (data corrected to average subject body weight). Increased vertical velocities resulted in an increase in the magnitude of joint extensor moments and subsequent demand on the lower extremity to control motion.

Dufek and Bates (1990) studied the effect of height, distance and landing technique in landing forces. Subjects were filmed jumping backwards onto a force platform from towers of 3 different heights (40, 60 and 100 cm), located 3 distances away from the force plate (40, 70, and 100 cm), and instructed to employ 3 landing techniques (stiff knee, relative knee angle (RKA) greater than 110°; slightly bent knee, RKA between 75° and 119°; and flexed knee, RKA less than 75°). Each subject (n = 3) performed 3 trials in each of the 27 different conditions. Peak maximum vertical ground reaction forces ranged from 3.74 - 5.43 times body weight.

Panzer, Wood, Bates, and Mason (1987) created a 2-dimensional sagittal plane link

Panzer, Wood, Bates, and Mason (1987) created a 2-dimensional sagittal plane link segment model of the lower limb to evaluate one foot landings in single and double back somersaults. Six elite Australian gymnasts participated in this study. Peak vertical ground reaction forces in double back somersaults ranged from 8.8 - 14.4 times body weight, representing an increase of 6.7 times body weight compared to single back somersaults. Average knee compression and shear forces were reported at 2106 N and 2875 N (in the posterior direction) respectively. Within subject comparison of double back somersault trials in the best male subject revealed the greatest loads at the knee and hip occurred during a fully flexed landing.

2.3 Injury Mechanisms

Section 2.1.3 listed common injuries experienced by figure skaters. This section relates biomechanical events to clinical injury mechanisms at the knee and ankle.

Tendinitis refers to inflammation of the tendon (Hagberg, Silverstein, Smith, Hendrick, Carayon, and Pérusse, 1995). The inflammation may be the result of inflammatory disease (ie rheumatoid arthritis) or may be due to mechanical irritation and friction, which may lead to local inflammation in the tendons and in the tendon sheath (Kurppa, Waris, and Rokkanen, 1979, cited by Hagberg et al., 1995). Repetitive stretching and contraction of the tendon, and impact force on the tendon during jumping were exposure factors associated with Achilles tendinitis in ballet dancers (Fernandez-Palazzi, Rivas, and Mujica, 1990). These similar motions in figure skating, as well as the form-fitting, custom-made skate boot, which may compress the Achilles tendon, may explain why skaters experience Achilles tendinitis.

The growth plate is cartilage interposed in growing bone and allows the axial and diametric growth of bone (Speer and Braun, 1985). Its complex topography between metaphyseal and epiphyseal bone was designed to resist shear forces across the growth plate. The growth plate is ideally suited to axial loading, as deviations from

axial loading impose stress in its weaker planes. Osgood-Schlatter disease is a term that refers to a group of conditions that involve the tibial tubercle epiphysis. At this site, the separation of the cartilaginous apophysis (non-weight bearing epiphysis) from the proximal epiphysis results in swelling over the tibial tubercle. Patellar tendinitis at the tibial insertion occurs due to inflammation of the bursa between the tibia and patellar tendon. An avulsion fracture of the tibial tubercle may occur due to rapid contraction of the quadriceps.

Winter and Bishop (1992) discussed biomechanical factors associated with chronic injury to the lower extremity in runners. Patellofemoral pain syndrome is aggravated in running by the quadriceps muscle forcing the patella against the groove, creating a compressive component, and by the lateral shearing of the patella on the femur due to the quadriceps activation during the knee range of motion. Stress fractures of the tibia, common in individuals with pronated feet, is associated with an increase in tibial torsion during the support phase of running.

Forces on the human body act through many different structures that are physically connected (bone, cartilage, ligaments, tendons) (Speer et al., 1985). These components must share the magnitude of forces experienced at the joint to alleviate loading of one structure. During load sharing, one structure may be overstressed, resulting in micro- or macrodamage. Butler, Grood, Noyes, Zernicke, and Brackett (1984) calculated the failure level of the central and medial third of the patellar tendon-bone unit from young human donors (n=18; mean age = 26 years). They determined that the central patellar tendon could withstand 1154 kN of tensile force prior to failure, while the medial patellar tendon failed at 1136 kN of tensile force.

2.4 Modelling

2.4.1 Link Segment Models and the Inverse Dynamic Approach

Inverse dynamics modelling has been used to estimate or predict the internal moments generated at various joints during a movement.

An inverse solution requires the formation of a link segment model that incorporates several assumptions (Winter, 1990):

i) The human body is modelled as a chain of rigid segments, representing human body segments (de Looze, Kingma, Bussmann, and Toussaint, 1992).

ii) Individual segment mass proportions and radii of gyration are based on established anthropometric tables (ie Dempster, 1958).

iii) Each segment in the model has a fixed mass located as a point mass at its centre of mass and its location remains constant during the movement.

iv) Joints are considered hinge (or ball and socket) joints.

v) The mass moment of inertia of each segment about its mass centre is constant during the movement.

vi) The lengths of each segment remains constant during the movement .

2.4.1.1 Validation of Inverse Dynamics Calculations

Estimations of joint stress and compressive forces are based on reactive forces computed using link segment models of the human body. Bresler and Frankel's landmark paper (1950) predicted joint forces and moments in three dimensions using a force platform and cinematographic analysis. This paper provided comprehensive detail about the forces and moments incurred during walking, but the model was not validated.

Several groups have attempted to validate the link segment approach to predicting joint reaction forces and moments with different models. One disadvantage of link segment modelling is that error is cumulative through the linked segments. Pezzack

and Norman (1981) validated the link segment model with a computer model and determined that errors in prediction increased as the number of segments incorporated into the model increased.

deLooze, Kingma, Bussmann, and Toussaint, (1992) compared calculated and known external vertical reaction forces, resulting in a correlation of 0.88 for their model of a dynamic lifting task. Fukashiro, Komi, Jarvinen, and Miyashita (1993) compared in-vivo Achilles tendon force transducer measurements with ground reaction force measurements. This study determined that force plate output was similar to transducer output, yet reinforced the notion that force plate output is a global measurement, not representative of individual structures (ie muscle activity).

Despite the assumptions and limitations of link segment modelling, the inverse dynamic solution is a viable method of determining joint reaction forces and moments. Its strengths and weaknesses lie in the assumptions made by the researcher modelling the situation.

2.4.2 Anatomical Models

Joint reaction forces obtained from a link segment model do not accurately represent the forces experienced at joint the surfaces, because they do not reflect the forces contributed by the surrounding muscles and ligaments that act during movement. When muscle activation is included, the resulting forces are those experienced at the joint articulation and are designated as bone-on-bone force.

2.4.2.1 Muscle Models

The execution of any activity represents the successful coordination of muscle agonists and antagonists. Different degrees of muscle activation are unique to any specific task and individual. Each task has a different desired outcome and requires a distinctive pattern of muscle activation. Within a task, individuals may elicit

different strategies of muscle recruitment. The purpose of this section is to address the factors that must be considered in creating a muscle model and discuss the development of some models of human muscle.

One obstacle in biomechanics is the inability to directly measure force in the human body (Norman, 1989). Surrogates have been used to measure external force production (ie force exerted on a linear variable differential transducer may be extrapolated to biceps force production), but in-vivo measurement is invasive and expensive. Besides the risks involved with surgery, the implantation of measurement devices such as force transducers may result in damage to the structure of interest, thus resulting in an inaccurate record of activity. Despite these drawbacks, a few groups have attempted to measure force production in-vivo (Butler, Sheh, Stouffer, Samaranayake, and Levy, 1990, Crawshaw, Hastings, and Dove, 1991, Xu, Butler, Stouffer, Grood, and Glos, 1992, Fukashiro, Komi, Järvinen, and Miyashita, 1993). Their results suggested that patterns of force production for a specific site (ie Achilles tendon) were consistent with electromyographic (EMG) activity or mathematical models.

Muscle activity is a very complex entity to model. Many factors influence the final force output of a muscle, including the neural drive, instantaneous muscle length, instantaneous muscle velocity, physiological cross-sectional area, and the contribution of series and passive elasticity.

The neural drive represents the degree of activation of the muscle in question. Impairment to the neural drive suggests disruption of pathways to higher control centres.

Instantaneous muscle length influences force output by the relative muscle length with respect to optimal length. Actively, muscle tension begins at a sarcomere length

of 1.87 - 2.0μm; any smaller distance is not possible due to the barrier imposed to the actin filaments by z-disks. Muscle tension increases linearly with increased sarcomere distance until a plateau is reached. Maximum muscle tension occurs at a sarcomere length of 2.0 - 2.2μm. Tension then decreases from 2.2 - 3.65μm; at 3.6μm, no tension is produced because the actin and myosin filaments cannot interdigitate (Gordon, Huxley, and Julian, 1966, Lieber and Bodine-Fowler, 1993).

The velocity of shortening is inversely related to muscle tension output. As shortening velocity is increased concentrically, force production is reduced. At zero velocity, force production is at a maximum concentrically. Maximum shortening velocity results in no force output. Eccentrically, an increase in muscle lengthening results in a constant force output (approximately 150% of maximum isometric force) greater than that of a concentric contraction (Hill, 1938, Lieber and Bodine-Fowler, 1993). The relationship between velocity of shortening and force output is given by A.V. Hill's (1938) equation:

$$(P+a)v=b(P_o-P)$$

Where: **a** and **b** are derived experimentally (usually approximately 0.25)
P is muscle force
$\mathbf{P_o}$ is the maximum muscle force
v is the muscle velocity

Physiological cross sectional area is the sum of the total muscle fibre cross sectional area, accounting for the pinnation of muscle fibres. Because of this, different muscles have different force-production capabilities depending on their fibre orientation and fibre length (Alexander and Vernon, 1975). Pennate muscles have larger force production capabilities due to the parallel arrangement of fibres. Fusiform muscles have larger velocity potential due to the series arrangement of sarcomeres. Depending on the function of the muscle, the architecture and resulting moment arm length will result in different moment production capabilities (Lieber and Bodine-Fowler, 1993).

The passive elastic component of muscle is not a major factor unless the muscle is stretched beyond its rest length. Once the muscle is stretched beyond rest length, the passive elements of the muscle (titin, connecting myosin filaments end to end) add to the active component of the muscle. Hence, more force is produced in eccentric contractions (Lieber and Bodine-Fowler, 1993).

In 1983, Galea examined the magnitude of bone-on-bone forces in ballet dancers at the first metatarsophalangeal joint and talocrural joint during relevés en pointe. A dynamic EMG-driven model incorporating isometric force, neural drive, velocity of shortening, and muscle length was developed to predict muscle forces acting at the joints of interest. This work was an extension of Norman's (1977) model that indicated that maximum isometric force was modulated by an EMG factor based on muscle activation.

Muscle force was calculated by the following equation:

$$F_m = F_i * \frac{EMG}{EMG_i} * \frac{F_{(Vel)}}{F_{i(Vel)}} * \frac{F_{(L)}}{F_{(Lo)}}$$

Where: F_m is the instantaneous muscle force
F_i is the instantaneous force output of a calibration contraction
EMG is the instantaneous EMG reading
EMG_i is the EMG normalization level recorded from Fi
$F_{(Vel)}/Fi_{(Vel)}$ is the ratio of muscle force as a proportion of its force output of the muscle isometrically (ie velocity =0)
$F_{(L)}/F_{(Lo)}$ is the ratio of muscle length as a proportion of its capabilities of resting length

Individual muscle torques were partitioned as the product of the proportion of the relative muscle cross sectional area to the total cross sectional area of the muscle group examined and the torque produced by an external moment. This value was

divided by the muscle moment arm length.

McGill and Norman (1986) further refined this model by taking it one step further to a 3-dimensional model of the low back that partitioned the reactive moment from L4/L5 into restorative components provided by the intervertebral disk, ligaments, and active musculature. This model advanced Galea's (1983) model by the augmentation of a gain factor to the final individual muscle force and, prior to this gain, the addition of force due to passive elasticity. Limitations of this model included eliciting maximal voluntary contractions from each of the 12 EMG-monitored muscles.

$$F_m = P_o * \frac{EMG}{EMG_i} * \frac{F_{(Vel)}}{F_{i(Vel)}} * \frac{F_{(L)}}{F_{(Lo)}} + Pec$$

Where: F_m is the instantaneous muscle force
Po is the maximum force producing ability of the muscle
EMG is the instantaneous EMG reading
EMG_i is the EMG normalization level recorded from Fi
$F_{(Vel)}/Fi_{(Vel)}$ is the ratio of muscle force as a proportion of its force output of the muscle isometrically (ie velocity =0)
$F_{(L)}/F_{(Lo)}$ is the ratio of muscle length as a proportion of its capabilities of resting length
Pec is the force contribution due to passive components beyond muscle rest length

This chapter has outlined the status of figure skating research and common skating injury sites. A rationale for predicting bone-on-bone forces in figure skating jumps has been developed. The use of link segment modelling combined with an accurate anatomical model will hopefully lead to a better understanding of muscle activation patterns and jump characteristics.

Chapter 3- Methods

3.0 Participants

Three male national level figure skaters participated in this study. All participants had competed at the Canadian Figure Skating Championships in either singles or pairs within the last three years and were actively training for the upcoming competitive skating season. All skaters preferentially rotated in the counter-clockwise direction in the air (right landing leg). Each subject's initials were used as the first two units of all trial identifiers. Subject characteristics are summarized in Table 2.

Prior to participation, each subject signed a document acknowledging Informed Consent, approved by the University of Waterloo Office of Human Research and Animal Care (OHR # 7349).

Table 2: Subject Characteristics

Subject	Age (years)	Mass (with Skates on)	Height (with Skates on)	Current Competitive Level	# Years Competitive Skating
MK	22	60.9 kg	181.6 cm	Senior Singles	10
SM	25	72.5 kg	185.4 cm	Senior Pairs	10
ES	18	60.0 kg	179.1 cm	Junior Singles	8
$\bar{x}$	21.67	64.47	182.03		9.33
σ	2.87	5.69	2.59		0.94

3.1 Data Collection

Data collection was divided into two components: on-ice and off ice.

3.1.1 General Protocol

On-ice, skaters were videotaped performing multiple trials of single and double loop jumps. Takeoffs and landings were videotaped from different camera views. Skaters were instrumented with a portable unit that allowed EMG collection on-ice. Electromyographic information was synchronized with video information with a light trigger.

Off-ice, jump takeoffs and landings were simulated in the laboratory. Wearing skates, the participants simulated a loop jump takeoff on a force platform (Figure 1). Jump landings were simulated by having the skater jump backwards from a raised platform, custom built for each skater (Figure 2). Skaters wore their skates and landed on one foot on the force plate. Each trial was videotaped, and EMG was obtained via the same portable unit as that used on-ice.

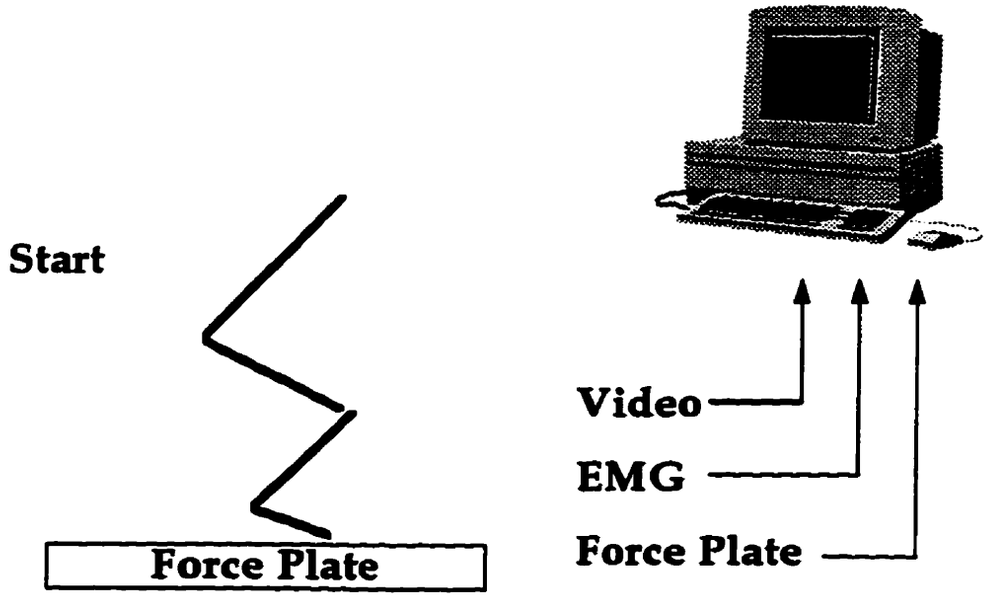

Figure 1: Laboratory Takeoff Schematic

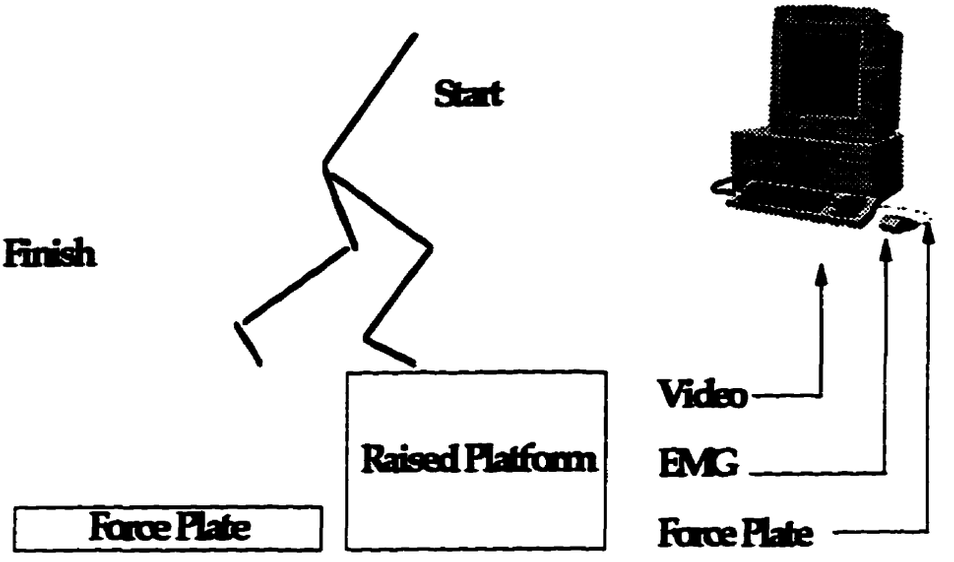

Figure 2: Laboratory Landing Schematic

3.1.2 Instrumentation

3.1.2.1 Video

3.1.2.1.1 Takeoffs

Takeoff trials were video taped at 60 Hz using two cameras placed at 90° to each other. In both on- and off-ice conditions, the video screen was equally split vertically to provide simultaneous sagittal and frontal views of the skater prior to the start of a trial. Pilot work indicated that skaters rotated approximately 90° on the ice prior to jump takeoff.

In on-ice takeoffs, the camera recording the sagittal plane of the skater was used to pan the skater as he moved through the designated jumping area. The second camera remained stationary throughout the data collection and was used to capture the final sagittal view of jump takeoff (Figure 3, Camera 2).

Simulated takeoffs in the laboratory were recorded with both cameras stationary throughout the collection.

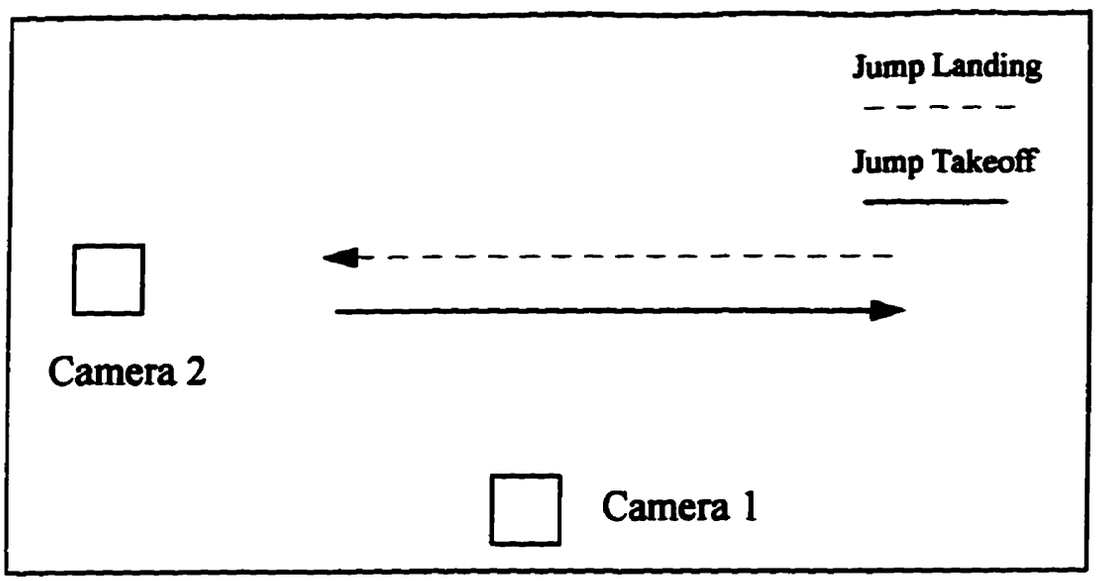

Figure 3: Camera Position Schematic

3.1.2.1.2 Landings

All landings were recorded with one camera (Camera 1, Figure 3) in the sagittal plane only. On-ice, the camera panned the skater as he moved through the designated jumping space. Off-ice, the camera remained stationary throughout the collection.

3.1.2.2 Electromyography

To ultimately calculate bone-on-bone forces, muscle activation patterns were recorded to determine the contribution of various muscles to the support moment at the joint of interest. A portable data acquisition system to collect muscle activity on-line was used so that skaters could perform their tasks in an unrestricted manner.

The Muscle Tester ME 3000 Professional (MEGA)(Kuopio, Finland), a clinically-oriented portable data acquisition system, was used. This system permitted the

simultaneous collection of up to four independent channels of raw or averaged EMG at different sampling frequencies and durations. Accompanying software allowed downloading of the EMG information for further processing in ASCII format or within the software itself. A major advantage of this system was its compact size (166 mm x 77 mm x 30 mm) and light weight (600 g). The unit was securely strapped at the waist of all participants for data collection. It was felt that by having the unit secured on the body close to the axis of rotation, its effects on increasing the moment of inertia of the subject were negligible.

Signal gains were modulated by manufacturer-supplied cables. For the purpose of this study, 360 gain cables were very suitable.

The memory capacity of the system (1024 KB static RAM) allowed 4 channels of raw EMG to be collected simultaneously at 1000 Hz for 2 minutes. Once the system memory reached capacity, information was downloaded to a 486 DX notebook personal computer (Impulse) via optic cable supplied with the system.

Data collection was controlled directly on the portable unit by means of an event marker which was triggered by the skater prior to jumping. A 2-minute window of data collection allowed the skaters to complete 7-10 complete jump trials on-ice and 10 trials off-ice. A switch hardwired to a synchronization light also pulsed on depression of the event marker and was used to indicate the start and finish of a trial on the video tape.

3.1.2.3 Force Plate

An AMTI model OR-6 force platform was used to measure takeoff and landing ground reaction forces in the laboratory. Force information was collected at 1000 Hz in digital format using the National Instruments A/D board and software. Ground reaction forces and moments about the vertical, antero-postero, and medial-lateral

axes were measured .

Manufacturer-supplied shunt calibrations were used to calibrate the force plate. The force plate was allowed to warm up for at least 2 hours before data collection. An LED triggered by the researcher was used to initiate trial collection and to indicate the onset of force signal collection on the video.

3.1.3 On-Ice Data Collection

Skaters were instructed to wear form-fitting clothing for the collection protocol. Each participant was fitted with surface Ag-AgCl electrodes longitudinally on the muscle belly of the vastus lateralis, tibialis anterior, biceps femoris, and lateral gastrocnemius of the right leg. Standardized electrode sites were used for recording and ground electrode placement (Zipp, 1982; Mega Electronics Ltd., 1983) (Figure 4). Recording electrodes were separated by a 3 cm centre-to-centre distance. Electrode sites were prepared by cleaning the area thoroughly with rubbing alcohol and paper tissues.

The electrodes were hardwired to the MEGA unit and movement artefact was reduced by securing the cables to the skater with medical tape after allowing for full range of motion by the subject. The participants wore form-fitting trousers over the cables to further reduce their movement.

The MEGA unit was securely attached to the waist of the participant by means of a nylon belt attached to a manufacturer-supplied protective case. The synchronization lights were located at the waist (in the sagittal plane) and at the shoulder (in the frontal plane) of the participant to ensure that at least one synch light per trial would be in view of a video camera.

Reflective joint markers were placed on the right side of the body of the skater. On the skate, markers were located at the head of the metatarsal, malleolus, and heel of

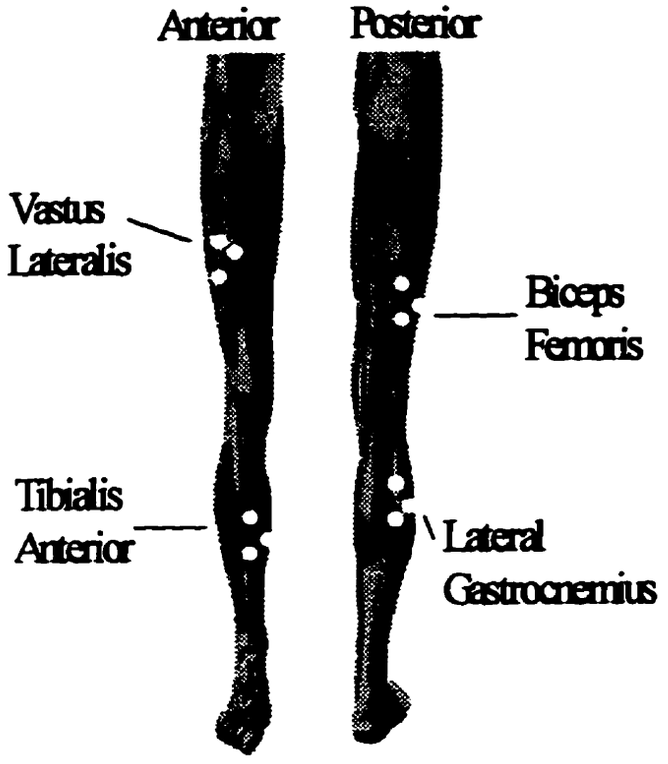

Figure 4: Electrode Placement Schematic

the boot on both the medial and lateral sides. Additional markers were placed on the medial and lateral aspects of the knee, on the lateral side of the hip at the greater trochanter, and on the lateral side of the shoulder at the head of the humerus.

Video cameras were situated at right angles to each other on the ice (one to view the skater in the sagittal plane, the other to view the skater in the frontal plane, Figure 3). The distance from the camera lens to the collection areas was recorded for each camera for later geometric correction. The collection space was marked on the ice and skaters were instructed to jump and land within this area as much as possible. The camera view from the frontal plane was focused and fixed, while the sagittal view was focused and panned through the movement as the skater jumped.

Skaters were videotaped on-ice performing single and double loops. Since all

skaters had competed at the National level, it was felt that these jumps posed little difficulty for the skaters to complete. No learning effects were expected to confound the data collection.

Skaters were instructed to complete as many trials of single and double loops as possible within the 2-minute collection window allowed by the MEGA system. For each trial, skaters were instructed to mark the onset and completion of each trial. It was felt that this protocol elicited a physical exertion level similar to that of a 2.5 minute skating programme.

Landings were videotaped in the sagittal plane by having the skater approach the jump from the right of the camera (Figure 3, Camera 1).

Takeoffs were videotaped on splitscreen in the sagittal and frontal planes by having the skater approach the jump from the left of the sagittal plane camera (Figure 3, Camera 2). This allowed full view of the skating foot as it turned from the sagittal plane to the frontal plane, and back to the sagittal plane prior to takeoff.

In total, skaters completed a total of 20 - 30 trials each of single and double loops (10-15 filmed takeoff, 10-15 filmed landing).

3.1.4 Off-Ice Data Collection

All laboratory testing was conducted at facilities available through the Biomechanics Laboratories at the University of Waterloo.

Subjects were fitted with EMG electrodes and joint markers as described previously. In the laboratory sessions, subjects wore shorts and form-fitting shirts. For calibration trials, skaters wore running shoes. Skaters wore their skates, with blade guards for

simulated take-off and landing trials.

3.1.4.1 Maximum EMG Calibration

Prior to the laboratory testing protocol, subjects participated in a series of calibration tasks. These tasks were designed to elicit a maximum muscle activity from each monitored muscle.

Gastrocnemius and tibialis anterior calibration trials were conducted as per Galea (1983). An apparatus was fabricated to immobilize the structures below the knee Participants were seated and the right thigh was immobilized as much as possible. The participant's right foot was securely fastened in place by a velcro strap over the metatarsal heads of the foot.

Gastrocnemius trials were conducted with the participant at an angle of 15° knee flexion. The participant was instructed to try to raise his heel as high as possible from the foot platform. The participant's knee angle was changed to 90° knee flexion for tibialis anterior trials. The participant's instructions for this calibration were to try to lift the ball of the foot as high as possible.

Vastus lateralis and biceps femoris trials were collected by having the participant extend or flex maximally at the knee against a cuff secured via a series of chain links to the wall. Vastus lateralis trials were conducted with the participant seated comfortably with a knee flexion angle of 70°. A cuff was placed around the participant's right ankle and the participant was instructed to extend his knee as much as possible. In biceps femoris trials, the participant was seated with his right knee at a 90° angle of knee flexion. The cuff was placed at the ankle and the participant was instructed to flex his knee as much as possible.

In all conditions, participants were instructed to maintain maximal contractions for 3

seconds. Each calibration trial was repeated 3 times. Muscle activity was recorded as described previously using the MEGA system. Participants marked the start and finish of each calibration trial. EMG information was downloaded after each set of calibration trials, yielding four separate files of 3 trials each for further processing.

3.1.4.2 Simulated Takeoffs

The skater was instructed to step onto the force platform and perform a loop jump takeoff as if on-ice. Approximately 20 trials were completed by each skater.

Video information was recorded throughout the collection session. Force plate data collection was triggered by a synch pulse initiated by the researcher. This triggered an LED viewed by the frontal video camera. EMG collection was controlled by the skater who marked the beginning and end of each trial. Individual trials were identified on video by a systematic alphanumeric code.

3.1.4.3 Simulated Landings

Participants jumped backwards from a wooden platform onto the force plate. Custom platforms were fabricated for each skater, based on the average on-ice jump height. Skaters landed on their right leg and held the final landing position for 3 seconds. Approximately 20 trials were completed by each skater, with video, force plate, and EMG information collected as described above.

3.2 Data Reduction

3.2.1 Video

Videotapes were carefully labelled and time encoded using the Peak Performance video digitizing system.

From the on-ice video, frame numbers were manually recorded corresponding to the following events: EMG synchronization pulse, takeoff (last frame the skate blade was in contact with the ice), and landing (first frame the skate blade was in contact with the ice).

From the off-ice video, simulated takeoff frame numbers were manually recorded according to the following events: force plate LED synchronization pulse, EMG synchronization pulse, and the last frame the skate blade was in contact with the force plate. In landing conditions, the force plate LED synchronization pulse, EMG synchronization pulse, and impact (first frame the skate blade contacted the force plate) events were recorded.

These event frames were used as the time base/event coordination for all EMG activity.

Takeoff and landing trials were separately digitized for on- and off-ice conditions. Takeoffs were operationally defined as 200 ms prior to the last frame in which the skater's blade was in contact with the ground/ice. Landings were defined as the first frame the skater's blade was in contact with the ground to 350 ms post-impact. A 4-link segment model was established in the PEAK system. To accommodate the finite difference differentiation used in the link segment model, one video frame was digitized before and after the start and finish of a trial.

All video trials were carefully reviewed by the researcher to determine inclusion or exclusion in the analysis. Factors which disqualified trials were incomplete rotation, poor control on the landing (extreme trunk forward flexion), and quality of video image. If a trial was excluded due to poor jump quality, both the takeoff and the landing files were removed from the analysis.

Joint centres were filtered in the Peak software with a Butterworth filter at optimal cutoff frequencies determined for each marker. Peak Performance files were converted into ASCII files for further processing by in-house software (PEAKTABL, written by John Pezzack, 1996).

3.2.2 Electromyography

MEGA files were converted to ASCII files using accompanying MEGA programme software. Subsequent processing was completed using the WATSCOPE series of data analysis programmes.

EMG data was full wave rectified and digitally filtered using a single pass Butterworth low pass filter. Residual analysis confirmed that Olney and Winter's (1982) optimal lower limb cutoff frequencies were appropriate for this study. The following cutoff frequencies were used: vastus lateralis - 2.0 Hz, tibialis anterior - 1.7 Hz, biceps femoris - 1.5 Hz, lateral gastrocnemius - 1.5 Hz.

Each on-ice data collection session yielded approximately 20-30 trials of single and double loop takeoffs and landings. The beginning and end of each EMG trial was related back to the video events to match EMG activity to motion/body position. EMG trial clipping information was accomplished by creating a linked spreadsheet in EXCEL that related the time base between video events (and the known frame rate) to time in the EMG trial.

Filtered trials were clipped according to previously described takeoff and landing definitions. All trials were graphed in EXCEL. After applying video trial exclusion criteria, an ensemble average of EMG activity for each participant was calculated. These were created from the remaining files of single loop takeoffs and landings, double loop takeoffs and landings, simulated takeoffs, and simulated landings.

3.2.3 Force Plate

Force plate data was scaled according to slope and bias values determined for each channel. Individual trial files were edited to correspond to video and EMG files. Edited trial files were converted to ASCII format for further processing.

Chapter 4 - Model Development

> *"The accuracy of biomechanical modelling depends upon the extent to which the mechanical approximation of the body faithfully represents the true anatomical structure."*
>
> Pearsall and Reid, 1994

A myoelectrically driven, 2-dimensional, sagittal plane model of the lower limb calculated bone-on-bone (BOB) forces at the ankle and knee joints for the takeoff and landing phases of the loop jump. The model was subdivided into three parts: a link segment model, an anatomic model, and a muscle model. Software written by the author in Mathcad Plus 6.0 Professional Edition was used to process conditioned video, forceplate, and electromyographic data. A discussion of each model's assumptions follows the description of the model. The entire model is presented in Appendix A.

4.1 Link Segment Model

Peak Performance video coordinate data and force plate information were the inputs to the link segment model (Figure 5). For calculating the takeoff and landing forces, force plate information, derived from simulated loop jump takeoffs and landings in a laboratory, was linearly interpolated to correspond in time to video frame data.

From filtered body marker coordinates, a stick figure diagram of the motion under consideration was produced. Two-point finite difference differentiation (Winter, 1990) was used to calculate individual marker linear velocities and linear accelerations using the following equations:

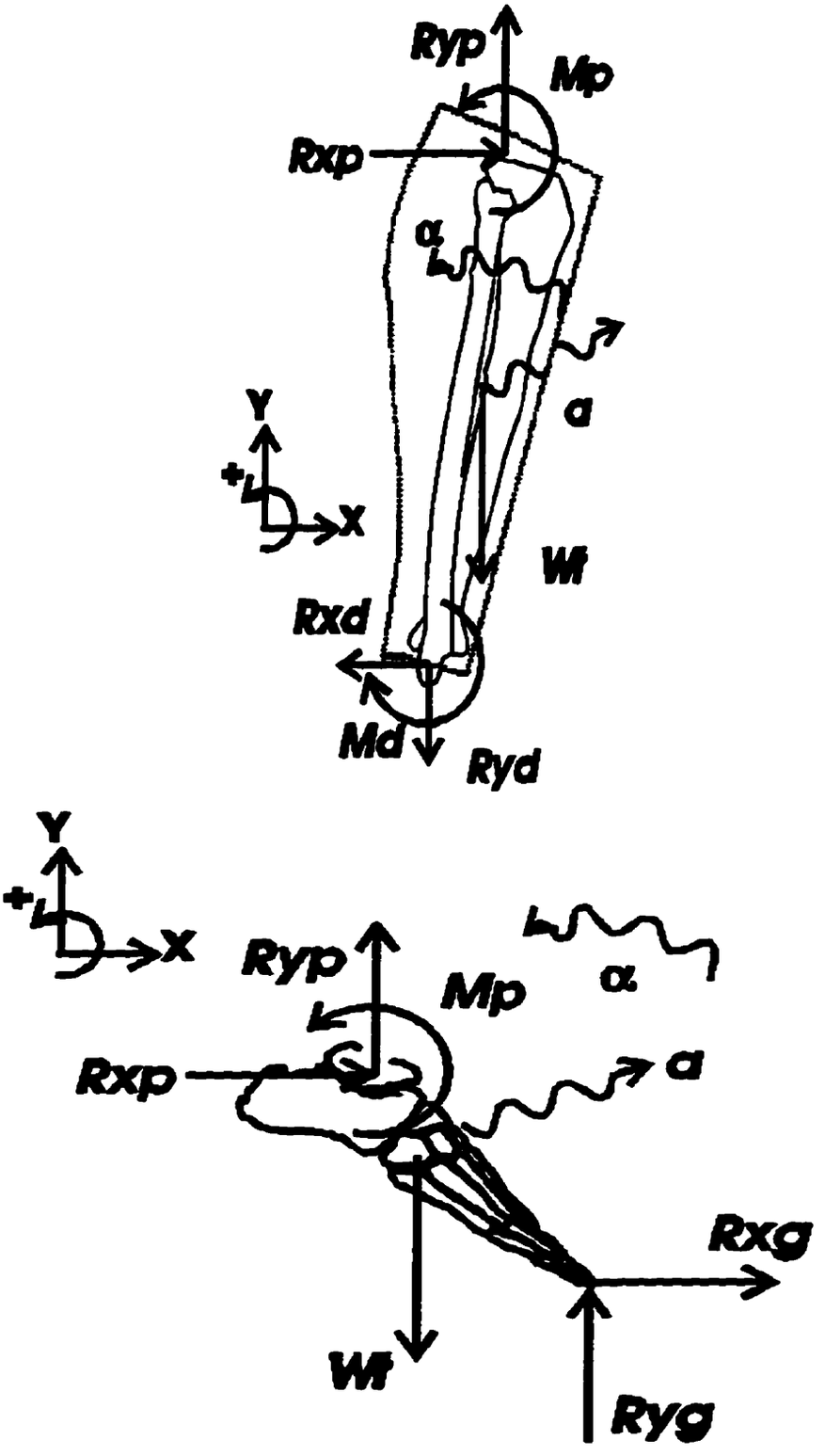

Figure 5: Free body diagrams of the ankle and knee

$$vx_{ij}=\frac{(x_{ij+1}-x_{ij-1})}{2\Delta t}$$ **(1)** Linear Velocity

$$ax_{ij}=\frac{(x_{ij+1}-2x_{ij}+x_{ij+1})}{\Delta t^2}$$ **(2)** Linear Acceleration

Where: v refers to velocity
a refers to acceleration
x refers to marker coordinate position
i refers to the specific marker (hip, knee, etc.)
j refers to the frame of interest
t refers to the time between frames

Absolute angular kinematics for each segment were calculated. The segment angle with respect to the horizontal was first determined. Finite difference differentiation of the change in segment angle was used to calculate segmental angular velocity and angular acceleration. The following equations were used to calculate angular kinematics (Winter, 1990):

$$\omega_{ij}=\frac{(\theta_{ij+1}-\theta_{ij-1})}{2\Delta t}$$ **(3)** Angular Velocity

$$\alpha_{ij}=\frac{(\theta_{ij+1}-2\theta_{ij}+\theta_{ij+1})}{\Delta t^2}$$ **(4)** Angular Acceleration

Where: θ refers to absolute segment angle
ω refers to angular velocity
α refers to angular acceleration
i refers to the specific marker (hip, knee, etc.)
j refers to the frame of interest
t refers to the time between frames

Absolute segment displacements, velocities, and accelerations were used to determine the relative angular kinematics for each joint. The knee angle was defined as the internal angle between the thigh and shank, while the ankle angle was the internal angle subtended between the shank and foot (Figure 6). The ankle angle was corrected for bias introduced by the location of the malleolus and metatarsal markers by subtracting 30°. This allowed flatfoot standing to be represented by 90°.

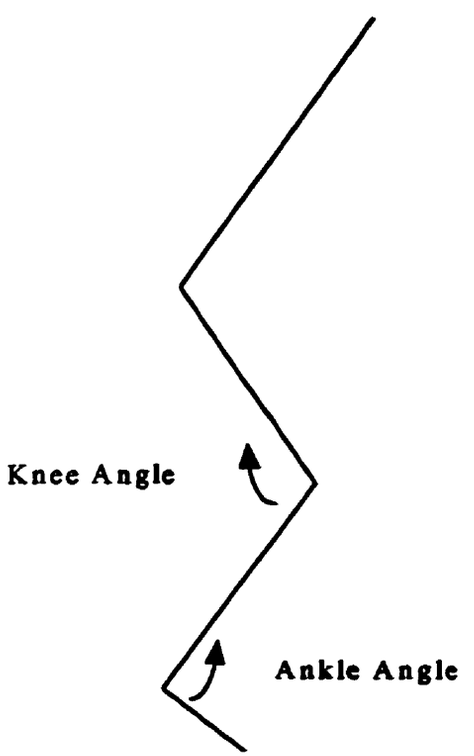

Figure 6: Joint Angle Conventions

Anthropometric characteristics were based on work by Plagenhof, Evans, and Abdelnour (1983). This group calculated the body segment parameters of 35 healthy, college-age male athletes based on Dempster's (1958) planes of dissection and equations. Segment mass, length, centre of gravity, and radius of gyration were calculated.

In the present study, the mass of the skate was added directly to the mass of the foot segment. It was assumed to act at the centre of mass of the foot (Albert and Miller, 1996). Table 3 outlines the body segment parameters used in this study.

Table 3: Anthropometric Characteristics (Plagenhof et al., 1983)

Parameter	Thigh	Shank	Foot
Mass	0.105 * BW	0.475 * BW	(0.0143 * BW) + mass of skate
Proximal proportion of segment length to segment centre of mass	0.433 * segment length	0.434 * segment length	0.5 * segment length
Radius of gyration proportion of segment length (centre of mass)	0.107	0.095	0.190

Individual segment masses were calculated by multiplying the segment mass proportion by the total body mass of the participant.

Segment lengths were calculated using the Pythagorean theorem:

$$l_i = \sqrt{(x_{i+1\,j} - x_{i\,j})^2 + (y_{i+1\,j} - y_{i\,j})^2} \qquad \textbf{(5)}\ \text{Segment Length Calculation}$$

Where: l refers to segment length
x refers to the x- coordinate position
y refers to the y- coordinate position
i refers to the specific marker (hip, knee, etc.)
j refers to the frame of interest

The moment of inertia was calculated about the proximal end of the segment and corrected to the centre of mass by the following equation:

$$I_i = m_i*(kp_i*l_i)^2 - m_i*(l_i*(kp_i - rp_i))^2 \qquad \textbf{(6)}\text{Moment of Inertia Calculation}$$

Where: I refers to segment moment of inertia
m refers to segment mass
kp refers to the radius of gyration with respect to the proximal end of the segment
l refers to segment length
rp refers to the length from the radius gyration to segment centre of mass
i refers to the specific marker (hip, knee, etc.)
j refers to the frame of interest

Body segment centre of mass kinematics (linear velocity, linear acceleration) were determined by finite difference differentiation as described earlier (Equations 1 and 2).

Joint reaction forces and moments were calculated at the ankle and knee using the following equations:

$$Rx_{ij} = m_i*ax_{cm_{ij}} - Gx_j \qquad \textbf{(7)}\text{ Ankle x-reaction force}$$

$$Ry_{ij} = m_i*ay_{cm_{ij}} + m_i*g - Gy_j \qquad \textbf{(8)}\text{ Ankle y-reaction force}$$

$$M_a = I_i*\alpha_i - Gx_j*(cpy_j - y_{ij}) - Gy_j*(cpx_j - x_{ij}) - Rx_{ij}*(y_{ij} - y_{cm_{ij}}) - Ry_{ij}*(x_{ij} - x_{cm_{ij}})$$

(9) Ankle Moment

Where: Ma refers to the ankle moment
Gx refers to the antero-postero ground reaction force vector
Gy refers to the vertical ground reaction force vector
cpx and cpy refer to the (x,y) coordinates of the centre of pressure
x and y refer to segment (x,y) marker coordinates
cm refers to the segment centre of mass

$$Rx_{ij} = m_i * axcm_{ij} - Rx_{i+1,j} \qquad \textbf{(10)}\ \text{Knee x-reaction force}$$

$$Ry_{ij} = m_i * aycm_{ij} + m_i * g - Ry_{i+1,j} \qquad \textbf{(11)}\ \text{Knee y-reaction force}$$

$$M_k = I_i * \alpha_i - Rx_{(i+1,j)} * (y_{(i+1,j)} - y_{cm_{ij}}) + Ry_{(i+1,j)} * (x_{(i+1,j)} - x_{cm_{ij}}) + Rx_{ij} * (y_{ij} - y_{cm_{ij}}) - Ry_{ij} * (x_{ij} - x_{cm_{ij}}) + M_a$$

(12) Knee Moment

Where: Ma refers to the ankle moment
Mk refers to the knee moment
Rx i+1 refers to the ankle joint reaction force in the x-direction
Ry i+1 refers to the ankle joint reaction force in the y-direction
x and y refer to segment (x,y) marker coordinates
cm refers to the segment centre of mass

Joint reaction forces and moments were first calculated for the ankle. These values were used as the input forces at the distal end of the shank. Knee moments were calculated from ankle joint reaction forces, knee joint reaction forces and the ankle moment. Joint reaction forces were reported in Newtons and also as a multiple of body weight.

4.1.1 Link Segment Model Assumptions

The link segment model incorporated the following assumptions:

1. Body segments were modelled as rigid links connected by hinge joints.
2. The ankle and knee joints experienced no antero-postero translation during movement.
3. The ankle moment was wholly supported by musculature. The stiffness of the skating boot was considered in the ankle moment calculation.
4. Segment mass proportions and moments of inertia were estimated by tables (Plagenhof et al., 1983) and scaled, based on actual subject heights and

(Plagenhof et al., 1983) and scaled, based on actual subject heights and weights.

5. The mass of the skate was added directly to the mass of the foot and assumed to act at the centre of mass of the foot (Albert and Miller, 1996).
6. Segment centre of gravity positions were based on filtered, digitized segment end points.
7. Ground reaction force profiles generated in the laboratory by simulated jump takeoffs and jump landings were the same as those generated on-ice.
8. The centre of pressure excursion from laboratory takeoff and landing simulations was the same as that experienced by the skaters on-ice.

4.2 Anatomic Model

The anatomic model added muscle lengths, moment arm lengths, and muscle lines of pull to the link segment model. Cadaver measurements scaled to subject proportions were used. A schematic representation of the anatomic model is in Appendix B.

Measurements from a 67-year old male cadaver were taken. It was assumed that the location of muscle origin-insertion points could be represented as a proportion of leg length. All values were expressed as a function of leg length. Leg length was defined as the length of the limb from the greater trochanter to the lateral malleolus.

Recorded values were representative of the paths of the muscle groups responsible for knee flexion/extension and ankle dorsi/plantar flexion. Muscle origin/insertion locations were recorded from the cadaver relative to the location where joint markers were located on the subject. Muscle origin/insertion coordinates were added to the model with respect to their location to the joint centres. The following algebraic rotations ensured that the x,y coordinates "moved" as the stick figure moved:

$$x^1 = x\cos\theta - y\sin\theta \qquad (13) \qquad\qquad y^1 = x\sin\theta + y\cos\theta \qquad (14)$$

Galea (1983) determined that the rest lengths of the lower limb muscles occurred at a knee angle of 131° and ankle angle of 140°. These values were used in this study as rest lengths for the lower limb muscle groups (*tibialis anterior* and *gastrocnemius*).

Muscle lengths and moment arm lengths (the perpendicular distance from the joint centre of rotation to the muscle group line of action) were recorded for the quadriceps group, gastrocnemius, and hamstrings group by moving the cadaver knee in 5° increments through a range of motion from full knee extension to 90° knee flexion while the ankle was fixed at an angle of 140°.

Muscle lengths and moment arm lengths of gastrocnemius/soleus and tibialis anterior were measured by moving the ankle joint was in 5° increments through a range of motion from 15° dorsiflexion to 50° plantarflexion, while the knee angle was fixed at 130°. The angle conventions in this study assigned 90° as the neutral ankle posture. Dorsiflexion angles were subtracted from 90°, while plantarflexion angles were added to 90°.

Muscle lengths were interpolated and scaled to participant dimensions based on the range of motion of the action. Changes in gastrocnemius muscle length were determined by taking the difference in muscle length change from rest length due to knee angle and rest length due to ankle angle and adding this to the muscle rest length value.

Muscle velocities as a function of rest length were determined by finite difference differentiation as described previously (Equations 1 and 2).

4.2.1 Anatomic Model Assumptions

1. Muscle origin-insertion locations measured on a cadaver and scaled to the participants were representative of the participants' muscle origin-insertion

locations.

2. Muscle origin-insertion locations were modelled as point values relative to the link segment model joint centres.
3. Muscle groups were modelled as single muscle equivalents. These were represented by linear point connections defined by muscle origin-insertion points (from (2)) and anatomical landmarks that allowed representation of actual muscle excursion.
4. The effects of the peroneal muscles and hip abductors/adductors were not considered.

4.3 Muscle Model

The most recent version of McGill and Norman's (1986) muscle model was used in this study. Reported parameters reflect the original work and subsequent changes to the original model incorporated by this group. Overall, this model was a multiplicative model of muscle force that predicted force output based on muscle activation, length, velocity, and muscle cross sectional area. Passive effects were added to force output if muscle length was greater than rest length.

The equation to calculate muscle force was:

$$F_m = P_o * \frac{EMG}{EMG_i} * \frac{F_{(Vel)}}{F_{i(Vel)}} * \frac{F_{(L)}}{F_{(Lo)}} + Pec \qquad \textbf{(15)}\ \text{Muscle Force}$$

In this equation: F_m is the instantaneous muscle force
P_o is the maximum force producing ability of the muscle
EMG is the instantaneous EMG reading
EMG_i is the EMG normalization level recorded from Fi
$F_{(Vel)}/Fi_{(Vel)}$ is the ratio of muscle force as a proportion of its force output of the muscle isometrically (ie velocity =0)
$F_{(L)}/F_{(Lo)}$ is the ratio of muscle length as a proportion of its capabilities of resting length
Pec is the force contribution due to passive components beyond muscle rest length

Filtered muscle activation patterns were linearly interpolated to correspond to video frame events because video data was collected at a different frequency (60 Hz) than EMG activity (1000 Hz). Muscle length and velocity values from the anatomic model were used to determine their respective coefficients. Muscle activation was used in conjunction with muscle cross sectional areas obtained from the literature to calculate the overall force production capability.

4.3.1 Maximum Force Production Capability of Muscle

The maximum force a muscle could produce isometrically was estimated by multiplying the physiological cross sectional area of the muscle group by the force producing potential of the muscle group. Literature values of muscle force producing capacity ranged from 30 - 100 N/cm^2 (Winter, 1990). Since the participants in this study were trained athletes, the value assigned to the muscle model was 50 N/cm^2.

The physiological cross sectional areas of the lower limb muscles were obtained from magnetic resonance imaging studies of Narici, Landoni, and Minetti (1992) (quadriceps), and Fukunaga, Roy, Schellock, Hodgson, Day, Lee, Kwong-Fu, and Edgerton (1992) (dorsiflexors and plantarflexors). Narici (1992) did not provide information on the physiological cross sectional area of the knee flexors, so the hamstrings were assigned a value equal to 40% of the quadriceps physiological cross sectional area (Wickiewicz, 1983). Although different subject groups were used in estimating these cross sectional areas, it was felt that combining values from these studies was not unrealistic, because the ratio of hamstrings and quadriceps to ankle plantarflexors and dorsiflexors in Wickiewicz's (1983) study of cadavers ranged widely. Table 4 summarizes the muscle physiological cross sectional areas used in this model.

Table 4: Muscle Physiological Cross Sectional Area Values

Muscle Group	Value (cm^2)	Reference
Quadriceps	280	Narici et al., 1992
Hamstrings (40% of quadriceps)	115	Wickiewicz, 1983
Dorsiflexors	18	Fukunaga et al., 1992
Plantarflexors	326	Fukunaga et al., 1992

Muscles included in the quadriceps group were vastus lateralis, vastus medialis, vastus intermedius, and rectus femoris. The hamstring group consisted of biceps femoris (long and short heads), semimembranosus, and semitendinosus. Tibialis anterior comprised the ankle dorsiflexors, and the ankle plantar flexors were represented by gastrocnemius and soleus.

Muscle force was modelled as slightly nonlinear (Cholewicki and McGill, 1995):

$$F = pcsa * \left(\frac{EMG\ activation}{100}\right)^{\frac{1}{1.3}} \quad (17)$$

4.3.2 Muscle Velocity Coefficient

The muscle velocity coefficient was based on the muscle contraction velocity and activation level of the processed EMG. Velocity coefficients were calculated as follows (Sutarno and McGill, 1995):

i) If EMG activation was greater than 80%:
   a) Muscle velocity < 1.25 Lo/s

$$Velocity\ coefficient = (1.6 * Muscle\ velocity) + 1 \quad (18)$$

b) Muscle velocity ≥1.25 Lo/s

$$Velocity\ coefficient = 1.2 \quad (19)$$

ii) If Muscle velocity was less than 0:

$$Velocity\ coefficient = \beta = \frac{Po * B - |Muscle\ velocity| * A}{(|Muscle\ velocity| + B) * Po} \quad (20)$$

iii) If EMG activation was less than 60%:

$$Velocity\ coefficient = \beta + \frac{1 - \beta}{2} \quad (21)$$

Note that β in equation 21 is the same β from equation 20.

iv) If Muscle velocity was 0:

$$Velocity\ coefficient = 1 \quad (22)$$

A and B were Hill's constants, derived from the literature (Hill, 1938). "A" represented the coefficient of the maximum force producing capability of the muscle:

$$A = 0.25 * Po \quad (23)$$

"B" represented the coefficient of the maximum velocity of the muscle. It assumed a maximum contraction velocity of 3.6 Lo/s:

$$B = 0.25 * 3.6 \quad (24)$$

4.3.3 Length Coefficient

The length coefficient was based on the muscle length compared to rest length (Lo) (McGill and Norman, 1986):

I) If muscle length was less than 1.1 $Lo \cdot s^{-1}$:

$$Length\ coefficient = \sin[\pi * (Muscle\ length - 0.5)] \quad (25)$$

ii) If muscle length was equal to 1.0 $Lo \cdot s^{-1}$:

$$Length\ coefficient = 1 \quad (26)$$

iii) If muscle length was greater than 1.1 $Lo \cdot s^{-1}$ (Gordon, 1967):

$$Length\ coefficient = (-1.092 * Muscle\ length) + 2.15 \quad (27)$$

iv) If muscle length was less than 0.5 $Lo \cdot s^{-1}$ or greater than 1.97 $Lo \cdot s^{-1}$, the length coefficient was set to zero.

4.3.4 Passive Effects

If muscle length was greater than rest length, the force due to passive elasticity was added to muscle force output (Deng and Goldsmith, 1987):

$$Passive = \frac{pcsa(Muscle\ length - 1) \bullet 4.28 * 0.981}{(1 - \frac{Muscle\ length - 1}{0.7})} \quad (28)$$

4.3.5 Muscle Model Assumptions

1. Muscle lengths and, consequently, muscle velocities were based on muscle origin-insertion coordinates and their relative changes from the anatomic model (Section 4.2).
2. Muscle cross-sectional area values were based on magnetic resonance imaging values from literature (Table 4) and are representative of the

subjects in this study.

3. The maximum muscle force output was assumed to be 50 N/cm^2.
4. Muscle force output was assumed to be maximal in all situations, moderated by the relative muscle activation level scaled to a maximal voluntary contraction.
5. A maximal, anisotonic, isometric muscle contraction was used to estimate maximal muscle activity.
6. It was assumed that vastus lateralis was representative of knee extensor activity, tibialis anterior representative of ankle dorsiflexor activity, biceps femoris representative of knee flexor activity, and lateral gastrocnemius representative of ankle plantarflexor activity.

4.4 Calculation of Bone-on-Bone Forces

Bone-on-bone forces were calculated separately at the ankle and at the knee. Muscle angles of pull were calculated for each frame of video data.

The muscle moments were forced to equal the previously calculated reactive moment at each joint (McGill and Norman, 1986). This resulted in 2 gain factors: one was calculated at the knee for the quadriceps/hamstrings muscle group, and one at the ankle for the plantarflexors and dorsiflexors. This was necessary because the previously calculated moments were net joint moments of force that represented the net rotary effect of all internal and external forces acting on the joint.

Bone-on-bone forces were calculated by the following equations:

1) The ankle:

$$BOBax_j = m_s * ax_{cm_{sj}} - Gx_j + (F_d \cos\delta) * gain1_j - (F_p \cos\varsigma) * gain1_j \quad (29)$$

$$BOBay_j = m_s * ay_{cm_{sj}} + m_s * g - Gy_j - (F_d \sin\delta) * gain1 - (F_p \sin\varsigma) * gain1 \quad (30)$$

Where: BOB is the bone-on-bone force
G represents the ground reaction force
j represents the frame
gain1 is the gain applied
Fd is the muscle force due to the ankle dorsi flexors
Fp is the muscle force due to the ankle plantar flexors
δ is the angle of pull of the dorsiflexors
ς is the angle of pull of the plantarflexors

2) The knee:

$$BOBkx_j = m_k * ax_{cm_{kj}} + Rx_{aj} + (F_q \cos\phi) * gain2 - (F_h \cos\gamma) * gain2 \quad (31)$$

$$BOBky_j = m_k * ay_{cm_{kj}} + Ry_{aj} + m_k * g - (F_q \sin\phi) * gain2 - (F_h \sin\gamma) * gain2 \quad (32)$$

Where: BOB is the bone-on-bone force
m is the segment mass
a represents the ankle
k represents the knee
f represents the frame
gain2 is the gain applied
R represents the joint reaction force
Fq is the muscle force due to the quadriceps
Fh is the muscle force due to the hamstrings
ϕ is the angle of pull of the quadriceps
γ is the angle of pull of the hamstrings

Bone-on-bone forces were calculated separately for the ankle and knee. Ground reaction forces (ankle) and joint reaction forces (knee) were the external applied forces. Bone-on-bone forces were expressed in Newtons and as a function of body weight.

4.4.1 Bone-on-Bone Force Calculation Assumptions

1. Gastrocnemius was modelled as a one joint muscle. Its effects were only considered at the ankle.
2. Muscle angles of pull were based on muscle origin-insertion coordinates and anatomical landmarks from Section 4.2.

3. Muscle moment arm lengths were based cadaver measurements scaled to subject dimensions and interpolated to the relevant joint angle (Section 4.2).
4. Bone-on-bone forces were calculated separately at the knee and at the ankle. The calculated joint moment from the link segment model (Section 4.1) was forced to equal the muscle moment of the relevant joint. The difference between the calculated joint moment and the muscle moment was termed a "gain". A separate gain was calculated for the ankle and knee.
5. The effects of ligaments and articular cartilage were not considered.

Chapter 5 - Results and Discussion

5.1 Protocol Synopsis

The purpose of this project was to calculate the bone-on-bone forces at the ankle and knee during figure skating jump takeoffs and landings. This study was divided into two components: laboratory and on-ice. Takeoffs and landings were examined separately.

In the laboratory, participants were videotaped performing jump takeoffs and jump landings on a force platform, used to record the forces and moments about the x, y, and z axes. Skaters were fitted with reflective joint markers at the shoulder, greater trochanter, knee, lateral malleolus, and metatarsal head on the right side of their bodies. Muscle activity patterns of vastus lateralis, tibialis anterior, biceps femoris, and lateral gastrocnemius were monitored with a portable recording unit. Maximum muscle activity calibration trials were also conducted in the laboratory.

In the ice rink, skaters performed four sets of jumping trials. Two jumping conditions were examined: single loop jumps and double loop jumps. Skaters performed one set of takeoff and one set of landing trials (one camera angle for landings and one for takeoffs) in each jump condition. As in the laboratory, skaters were fitted with reflective joint markers and muscle activity patterns were recorded.

The trial exclusion criteria used in this study were poor jump quality (deemed by the author, a National level figure skating judge) and missing input information (ie no force plate data, no EMG data, poor video picture). If any of the input information was unavailable, the entire trial was excluded. If exclusion criteria resulted in fewer than 2 trials, then the data was not included in a group analysis.

Video data was manually digitized and conditioned using the Peak Performance system. Raw electromyographic activity was full-wave rectified and low-pass filtered to yield a linear envelope representation of muscle activation. Force plate data was scaled with manufacturer supplied (AMTI Technologies) shunt calibration values.

MathCad Plus 6.0 Professional Edition was used to programme a 2-dimensional, dynamic, link-segment model that incorporated muscle activation patterns to calculate bone-on-bone forces at the ankle and knee in takeoff and landing conditions. The laboratory analysis used video, electromyographic, and force plate data from each trial as model inputs. For each participant, the force plate data from a representative landing and takeoff trial was used as the force input to this model to estimate the on-ice bone-on-bone forces in jump landings and takeoffs.

This chapter summarizes the calculated bone-on-bone forces at the ankle and knee from the laboratory simulations and on-ice trials. Factors that affected the final bone-on-bone forces from the model are discussed. Due to the small sample size and variable number of trials in each condition, descriptive statistics are reported. As suggested by Dufek and Bates (1990), subjects are examined separately to reduce the masking of individual trends.

5.2 Jump Characteristics

5.2.1 Jump Flight Time

Table 5 outlines the jump flight times of the successful single and double loop jumps in this study.

In this study, the double jumps had consistently longer flight times than the single jumps. Miller et al. (1995) reported similar trends in a study of single and double Axel jumps. This finding contrasted King et al. (1994) and Aleshinsky (1986), who reported no difference in flight time between single, double, and triple jumps. In all of

those studies, however, the reported means were the result of combining one trial of one jump from different skaters.

Table 5: Jump Flight Times (time in seconds; $\bar{x}$ (sd); [number of trials])

Skater	Single Loop	Double Loop
MK	**0.43** (0.10) [24]	**0.50** (0.02) [23]
SM	**0.45** (0.03) [30]	**0.47** (0.02) [27]
ES	**0.42** (0.02) [34]	**0.45** (0.03) [24]

5.1.2 Jump Heights

Table 6 outlines the on-ice jump heights. The reported values were based on all of the successful jumps landed by each skater in this study. The maximum jump height from on-ice jumps was used as the simulated jump height from which the skaters jumped in the laboratory force plate trials.

Table 6: On-ice Jump Heights (height in metres; $\bar{x}$ (sd))

Skater	Single Loop	Double Loop
MK	**0.21** (0.03)	**0.31** (0.02)
SM	**0.24** (0.03)	**0.26** (0.02)
ES	**0.21** (0.04)	**0.25** (0.03)

Jump height was calculated by assuming that the amount of time from the skate blade leaving the ice to the peak of the jump was the same as that from the peak of the jump to initial blade contact with the ice. Total flight time for each jump was divided in half and applied to the following equation:

$$Height = \frac{1}{2} * g * t^2$$

Where: g is the acceleration due to gravity (9.8 m/s^2)
t is half of the total flight time for one jump

The skaters in this study did not jump as high as those skaters reported in a study of single, double and triple axels (0.68 m single, 0.65 m double, 0.66m triple) (King et al., 1994). King et al.'s (1994) measure of jump height was defined as, "the maximum distance from the ice to the skater's inferior foot measured at the toe." This method assumed that the skater's leg was fully extended at the knee and fully plantarflexed at the toe at the highest point of the jump. Often, skaters do not achieve this position in the air, having some degree of knee flexion and ankle dorsiflexion. Thus, the actual jump heights were most likely lower than those reported by King et al. (1994).

The skaters the study of Miller et al. (1995) also jumped higher (0.35 m single, 0.38 m double) than the skaters here. Their measurement of jump height was calculated as, "the difference between the skaters's centre of gravity position at last contact and the highest position in the flight." Both King et al. (1994), and Miller et al. 1995) studied a different jump (Axel) from the one examined in this project (loop). The axel jump is very different from a loop jump because a skater can transfer more segmental momentum in an axel jump than in a loop jump to attain higher jump heights.

5.3 Peak Ground Reaction Forces

Table 7 summarizes the peak ground reaction forces recorded from the laboratory jump simulations.

Table 7: Laboratory Simulation Peak Ground Reaction Forces (Multiples of Body Weight; $\bar{x}$ (sd))

Subject	Takeoff		Landing	
	Antero-Postero	Vertical	Antero-Postero	Vertical
MK	-0.14 (0.04)	2.12 (0.07)	-0.86 (2.96)	4.34 (0.40)
SM	-0.12 (0.04)	2.19 (0.09)	-1.2 (0.56)	3.65 (0.47)
ES	-0.13 (0.04)	2.21 (0.11)	N/A	4.88 (0.63)

Note: The negative antero-postero sign indicated a force acting in the posterior direction relative to the skater.

Due to equipment malfunction, no force plate information in the antero-postero plane was recorded for ES in the landing condition. Unfortunately, this eliminated this participant's data from the landing kinetic analysis. However, this participant's kinematic data and muscle activity was used for qualitative analysis and comparison.

The vertical ground reaction force tracing of simulated jump takeoffs (Figure 7) yielded a similar shape to the "thrust" period characterized by Miller and Nissinen (1987). Prior to takeoff, the force tracing reached a maximum, then decreased as the body's centre of mass was propelled upward. The magnitude of maximum vertical ground reaction takeoff forces here were considerably smaller than those of gymnasts (n=9) performing a running forward somersault takeoff (peak thrust force= 4.0 ± 0.3 times body weight) (Miller et al., 1987). This was reasonable, because the gymnasts approached their takeoffs from a running start and propelled themselves into the air

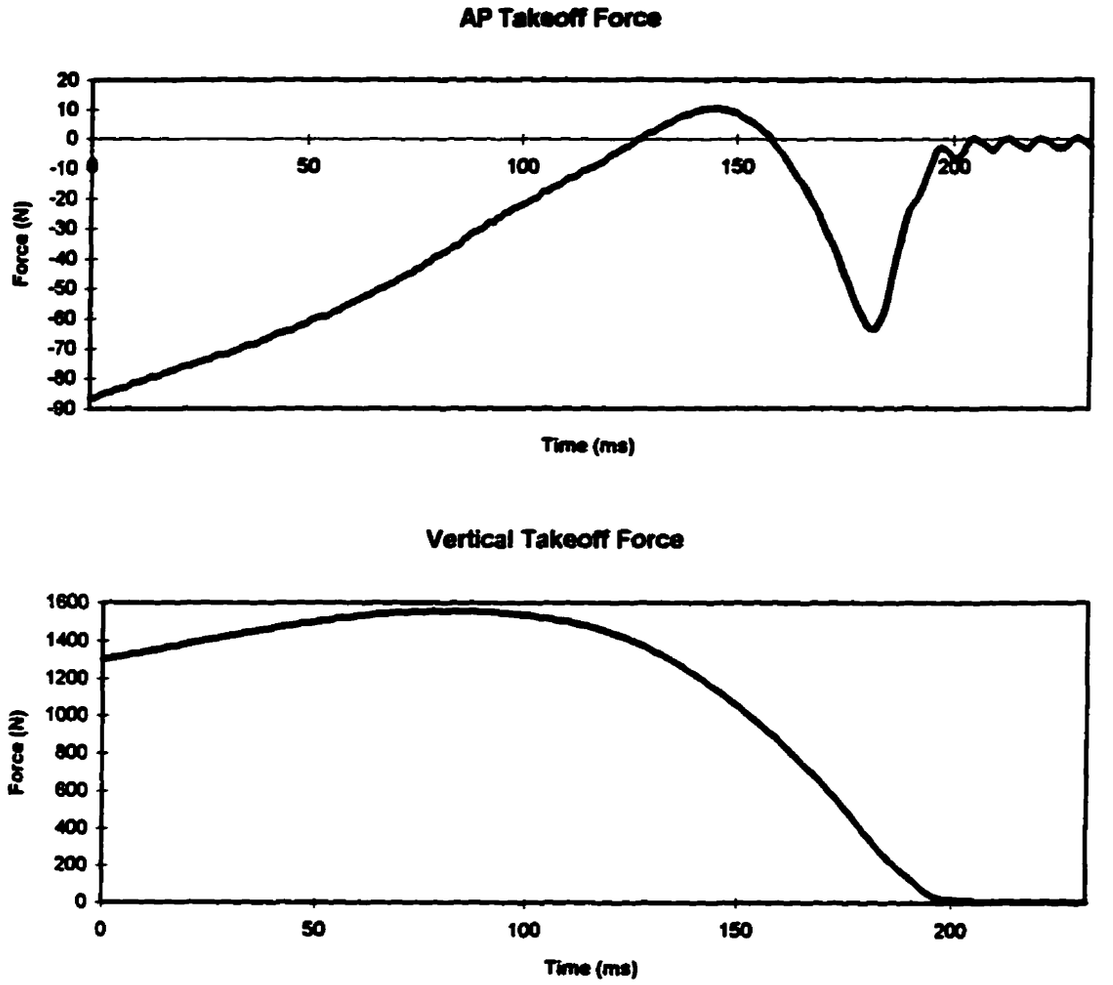

Figure 7: Typical jump takeoff force plate tracings. Takeoff occurs at 200 ms.

with both legs.

The magnitude of peak vertical ground reaction landing forces in this study were similar to those reported by McNitt-Gray (1993) and Foti (1990). Gymnasts (n=6) landing backwards onto a force platform from a 32 cm raised surface experienced peak vertical ground reaction forces of 3.9 times body weight, while recreational athletes (n=6) experienced peak vertical ground reaction forces of 4.2 times body weight under the same conditions (McNitt-Gray, 1993). Skaters (n=10) experienced peak vertical ground reaction forces of 4.1 times body weight in drop landings from a 30 cm raised platform wearing conventional figure skating boots (Foti, 1990).

The vertical ground reaction force tracing of simulated jump landings (Figure 8) exhibited similar characteristics to that found in the drop landing literature (Dufek and Bates, 1990; Dufek and Bates, 1991). This tracing was characterized by 2 distinct peaks after impact, indicative of a toe-heel landing (Dufek and Bates, 1990). Foti (1990) observed the same trends in skaters landing backwards onto a force platform covered by an artificial ice surface. Distinct toe-heel landings were not observed in the vertical ground reaction force tracing of gymnasts by McNitt-Gray (1991), for two possible reasons. First, the force platform in that study was covered by a thin layer of rubber which may have dissipated the impact force. Secondly, the vertical ground reaction forces were reported as a percentage of landing phase (landing phase was defined as the time from initial contact with the force plate to minimum vertical position of the total body centre of gravity), which may have masked the time information of the impact.

In the present study, laboratory force plate data was used as the force input to a link segment model of on-ice skating jump takeoff and landing trials. Post-priori consultation with international level figure skating coaches lent insight into subtle differences between the laboratory simulations and actual on-ice jumps.

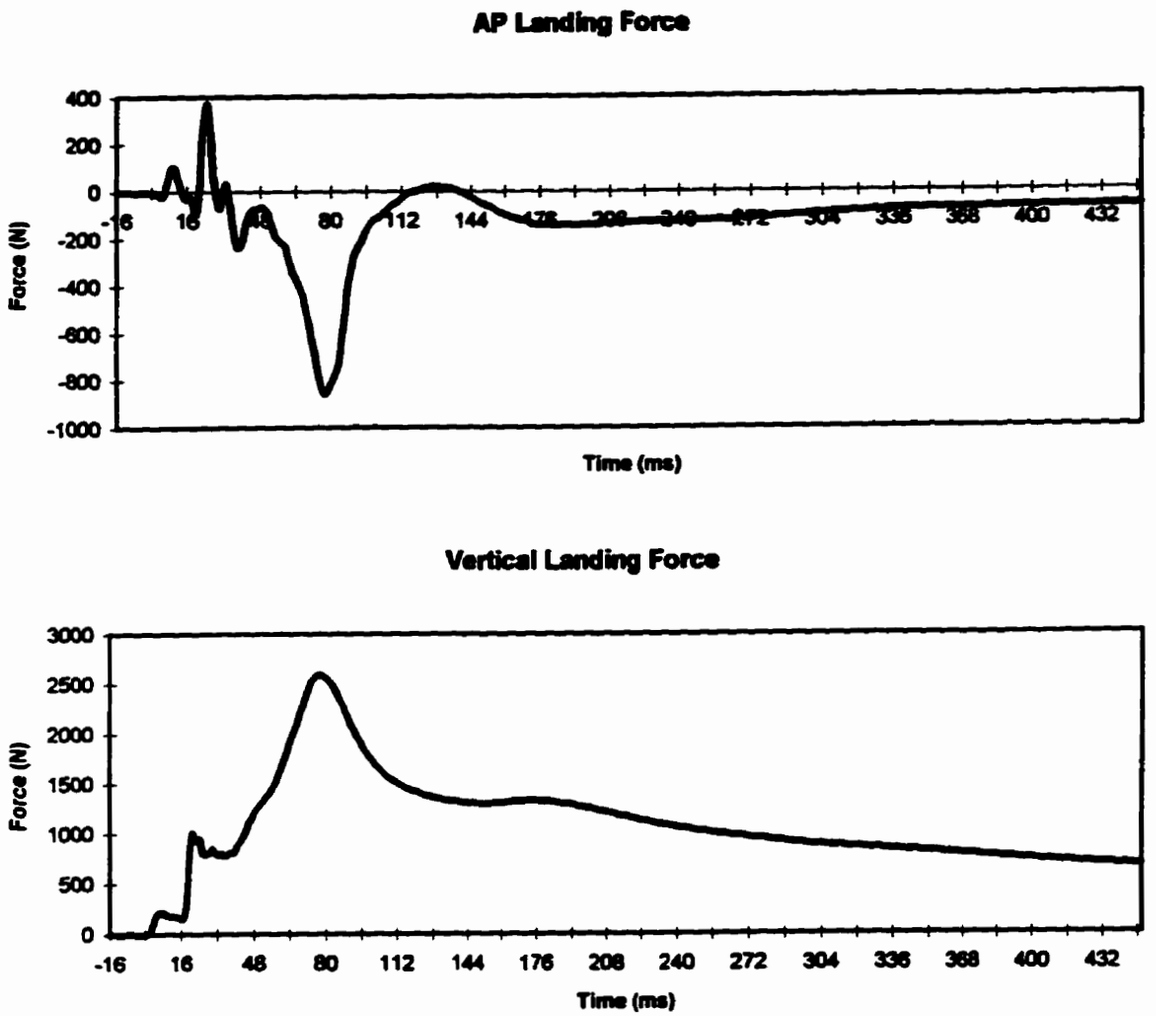

Figure 8: Typical jump landing force plate tracings. Impact occurs at 0 ms.

One obvious difference between the two conditions was the absence of horizontal motion in the laboratory simulations. The vertical ground reaction force vector in simulated landings indicated a toe-heel landing strategy by the skaters. Qualitative video analysis of on-ice jump landings indicated that the skaters preferentially landed on the anterior portion of the blade at the toe pick, then shifted their weight slightly posterior to the anterior third of the skate blade and not to the heel. Foti (1990) reported a similar vertical ground reaction force profile to that of the present study in simulated figure skating jump landings onto a force platform that was covered by artificial ice, thereby permitting the participants to glide backwards after landing.

It was felt that the jump takeoff simulation may have underestimated the true thrust force of on-ice jumps. On-ice, skaters propel themselves into the air by pushing off of the toe pick of the skating blade. The ice yields to the toe pick, allowing the skater to have a solid surface upon which to exert a propulsion force. In the laboratory, the skater was wearing plastic blade guards that protected the skate blade from damaging the force plate and vice versa. This imposed a different propulsion interface than that of the blade-ice interface, so that the propulsive thrust did not come from the toe pick.

5.4 Joint Angles

A great deal of knee flexion and ankle dorsiflexion is required of the skater prior to takeoff in jumping (to take advantage of the stretch-shortening cycle of muscles) and after landing from a jump (to help absorb energy). Comparisons of the extent of this flexion are shown in Table 8, where the minimum joint angles of the knee and ankle are given.

Overall, the skaters' ankle dorsiflexion was greater on-ice than in the laboratory. In laboratory jump takeoffs, peak knee joint flexion angle increased with an accompanying decrease in maximum ankle dorsiflexion compared to that of the on-ice

single loop jump. Compared to the laboratory simulation, SM increased ankle dorsiflexion by an average of 40° and knee flexion by 5° in double loop takeoffs.

Table 8: Minimum Joint Angle
(Degrees; $\bar{x}$ (sd))

Subject	Joint	Takeoff			Landing		
		Laboratory	Single	Double	Laboratory	Single	Double
MK	Ankle	66 (3.8)	57 (4.7)	n/a	55 (1.9)	54 (3.2)	n/a
	Knee	101 (5.9)	116 (2.4)	n/a	101 (4.8)	95 (2.3)	n/a
SM	Ankle	84 (10.9)	62 (5.7)	45 (4.0)	72 (3.4)	52 (3.7)	52 (3.5)
	Knee	115 (7.8)	119 (4.6)	111 (4.2)	118 (2.7)	115 (3.1)	115 (7.2)
ES	Ankle	71 (4.2)	n/a	n/a	60 (2.5)	60 (4.9)	62 (11.1)
	Knee	113 (2.2)	n/a	n/a	127 (3.9)	119 (4.7)	117 (4.3)

The minimum ankle joint dorsiflexion angles in all landing conditions were less than the 80° reported by McNitt-Gray (1991) for drop landings from 0.32 m. The average minimum knee flexion angle of subject MK was similar to that of the gymnasts (95.8°), while SM and ES experienced minimum knee flexion angles comparable to the recreational athletes (108.8°) reported by McNitt-Gray (1990). Ankle dorsiflexion and knee flexion angles did not change substantially between single and double jump landings.

5.5 On-ice Versus Laboratory Muscle Activation Levels

One of the main assumptions of this study was that the laboratory simulations of jump takeoffs and landings were similar to those of on-ice jump takeoffs and landings. In this section, the laboratory and on-ice muscle activation patterns observed within subjects across the takeoff and landing conditions are examined. Ensemble average plots of laboratory versus on-ice muscle activation patterns are found in Figures 9-13.

Comparison of on-ice and laboratory takeoff simulations indicated individual muscle activation strategies in different participants (Figures 9 and 10). In both skaters MK and SM, tibialis anterior activity was minimal compared to that of the other muscle groups. Skater SM exhibited high vastus lateralis (greater than 100% maximum voluntary contraction) and gastrocnemius activation, with lesser contributions from biceps femoris (approximately 60 - 80% maximum voluntary contraction) (Figure 10). Conversely, skater MK demonstrated a high degree of biceps femoris activity (greater than 100% maximum voluntary contraction) with accompanying decreased vastus lateralis and lateral gastrocnemius activation levels (less than 100% maximum voluntary contraction)(Figure 9). These discrepancies may be attributed to different jumping techniques.

Discussions with skating coaches indicated that skater SM, a pairs skater, was highly dependent on his upper body to rotate his jumps, which tended not to have a large horizontal component on the ice, accounting for the greater quadriceps and gastrocnemius activation associated with a predominantly vertical jump. Skater MK may have had increased hamstrings activity as the hip extensors activated to straighten the trunk as he jumped. This skater had a complementary balance of horizontal and vertical components in his jump.

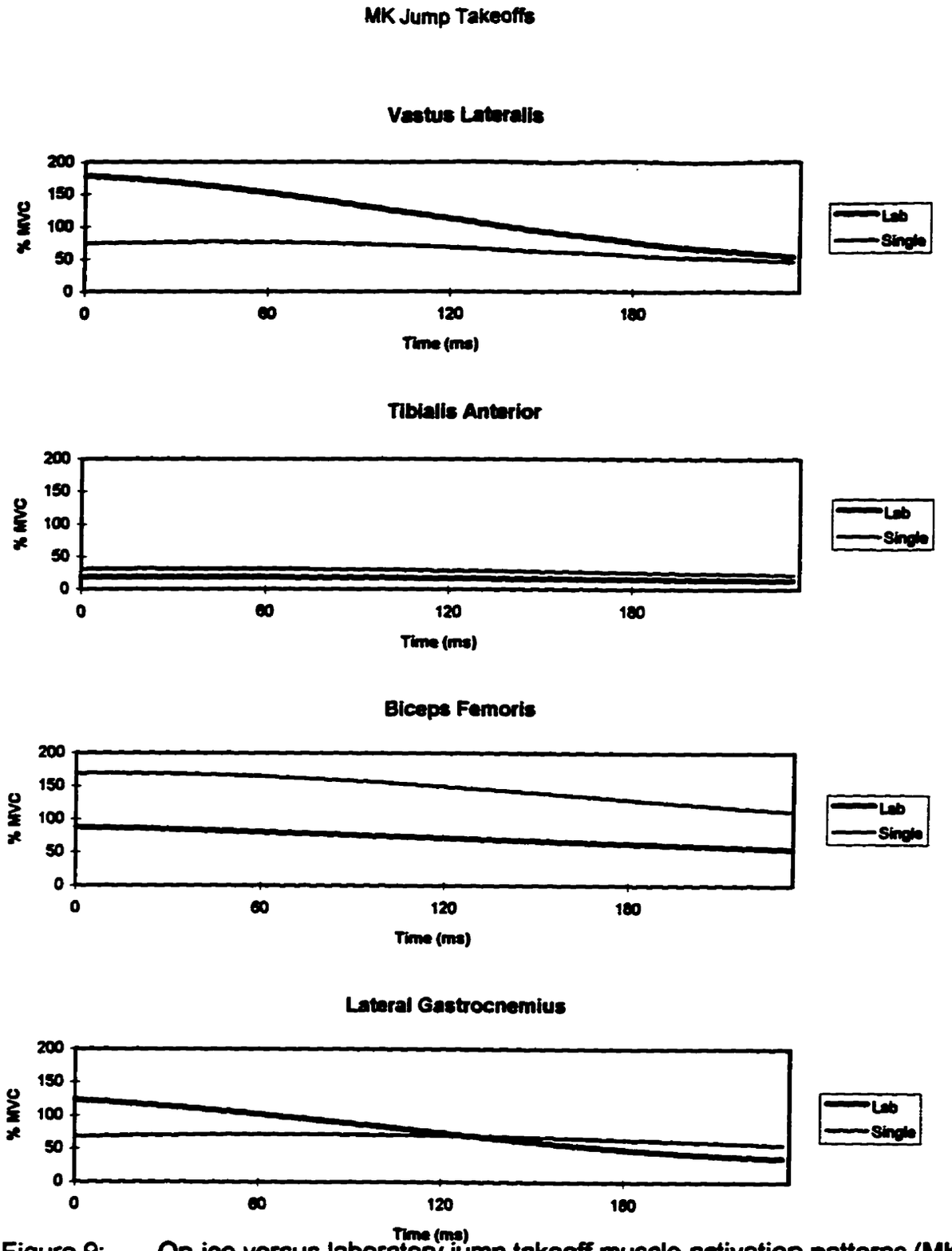

Figure 9: On-ice versus laboratory jump takeoff muscle activation patterns (MK) Takeoff occurs at 200 ms.

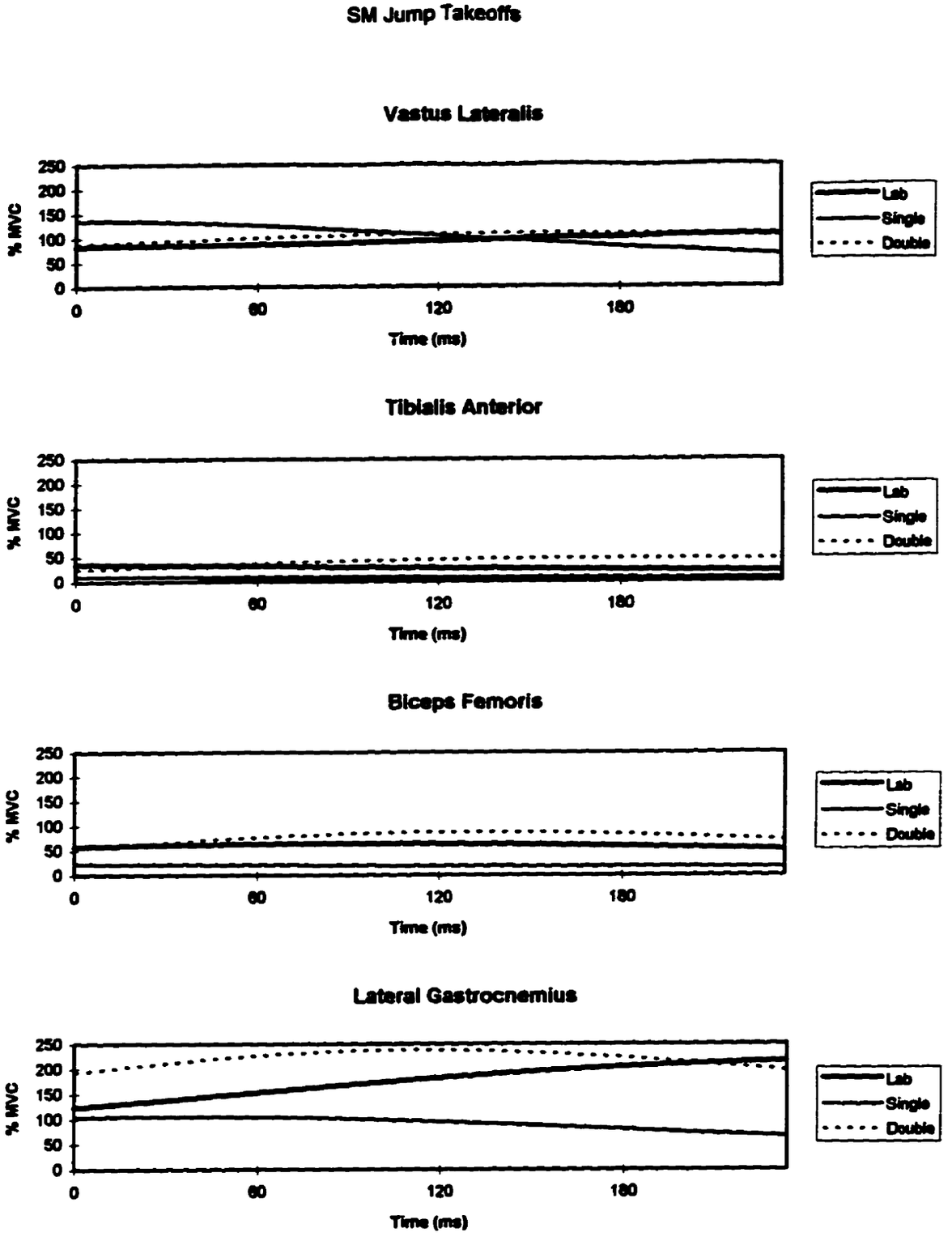

Figure 10: On-ice versus laboratory jump takeoff muscle activation patterns (SM) Takeoff occurs at 200 ms.

As in the double jump takeoffs, double jump landings consistently yielded higher muscle activity than did single jump landings (Figures 11, 12 and 13).

Many of the on-ice muscle activity patterns indicated muscle activation greater than that elicited by the maximal voluntary contraction in the laboratory. Of note were the particularly high activation patterns of biceps femoris in MK (Figures 9 and 11), lateral gastrocnemius in SM (Figures 10 and 12), and overall high muscle activity in ES (Figure 13). A limitation of this study was the use of an anisotonic, isometric muscle contraction as a comparison level of muscle activation for a rapid movement. Figure 14 illustrates the muscle length excursions of one subject during a jump landing and is representative of muscle length excursions of all subjects during landing trials calculated from the anatomical model. Gastrocnemius was consistently lengthened beyond rest length in an eccentric contraction in both jump takeoffs and landings (Figure 15).

Additional factors which may have affected the level of maximal muscle activation included motivation by the participant to produce a maximal contraction, as well as unreported strenuous activity by the participant prior to the testing session.

5.6 Joint Reaction Forces at the Ankle and Knee

Table 9 outlines the peak joint reaction forces at the ankle and knee calculated from the link segment model.

In all subjects, the jump landing joint reaction forces at the ankle and knee were higher than those of jump takeoffs. The magnitude of joint reaction forces at the knee and ankle were similar. The calculated joint reaction forces did not differ greatly between the on-ice and laboratory simulations, indicating that the kinematics of the laboratory simulation and on-ice jumps were similar. The joint reaction forces, however, did not reveal a complete picture of the motions under investigation and

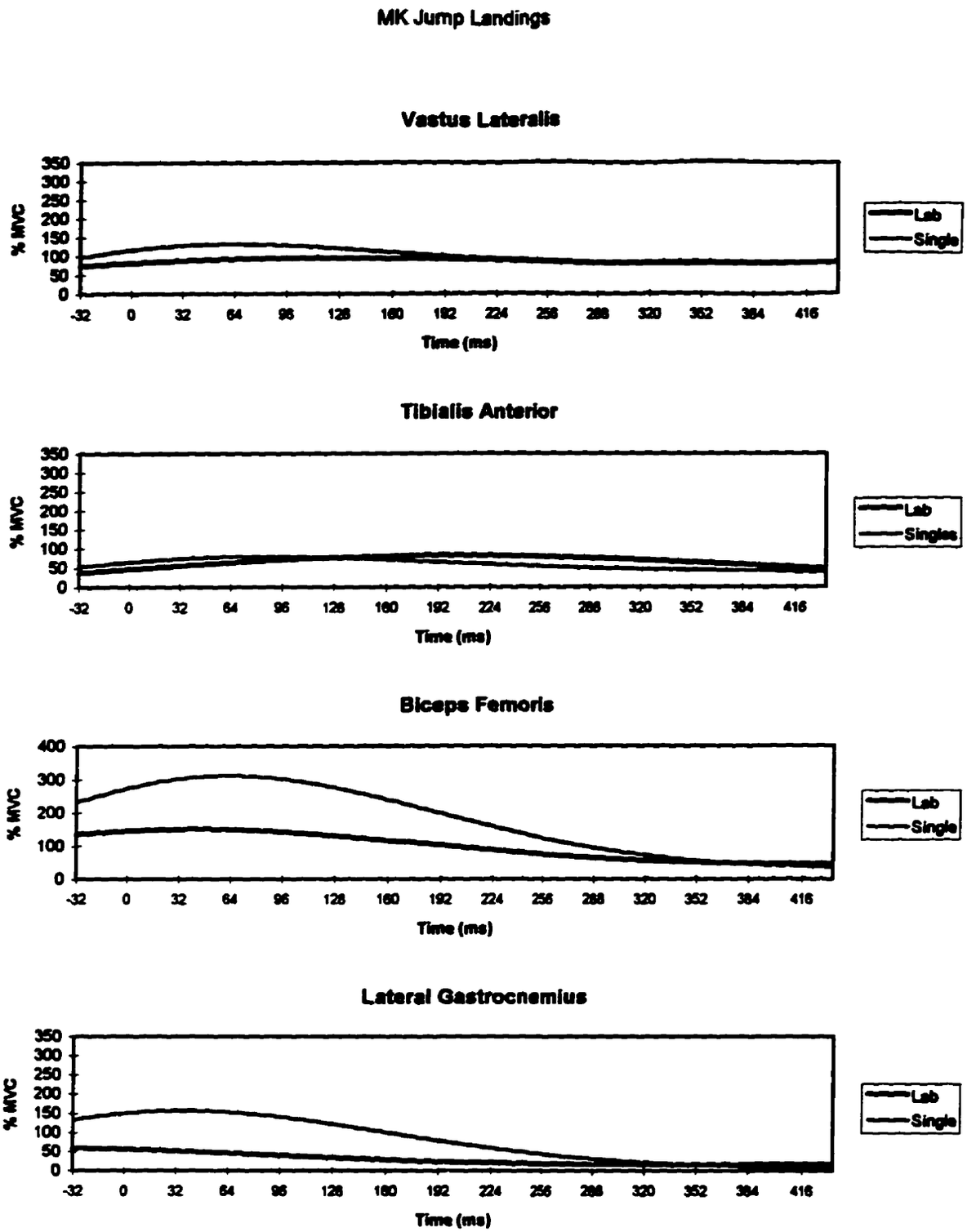

Figure 11: On-ice versus laboratory jump landing muscle activation patterns (MK) Impact occurs at 0 ms.

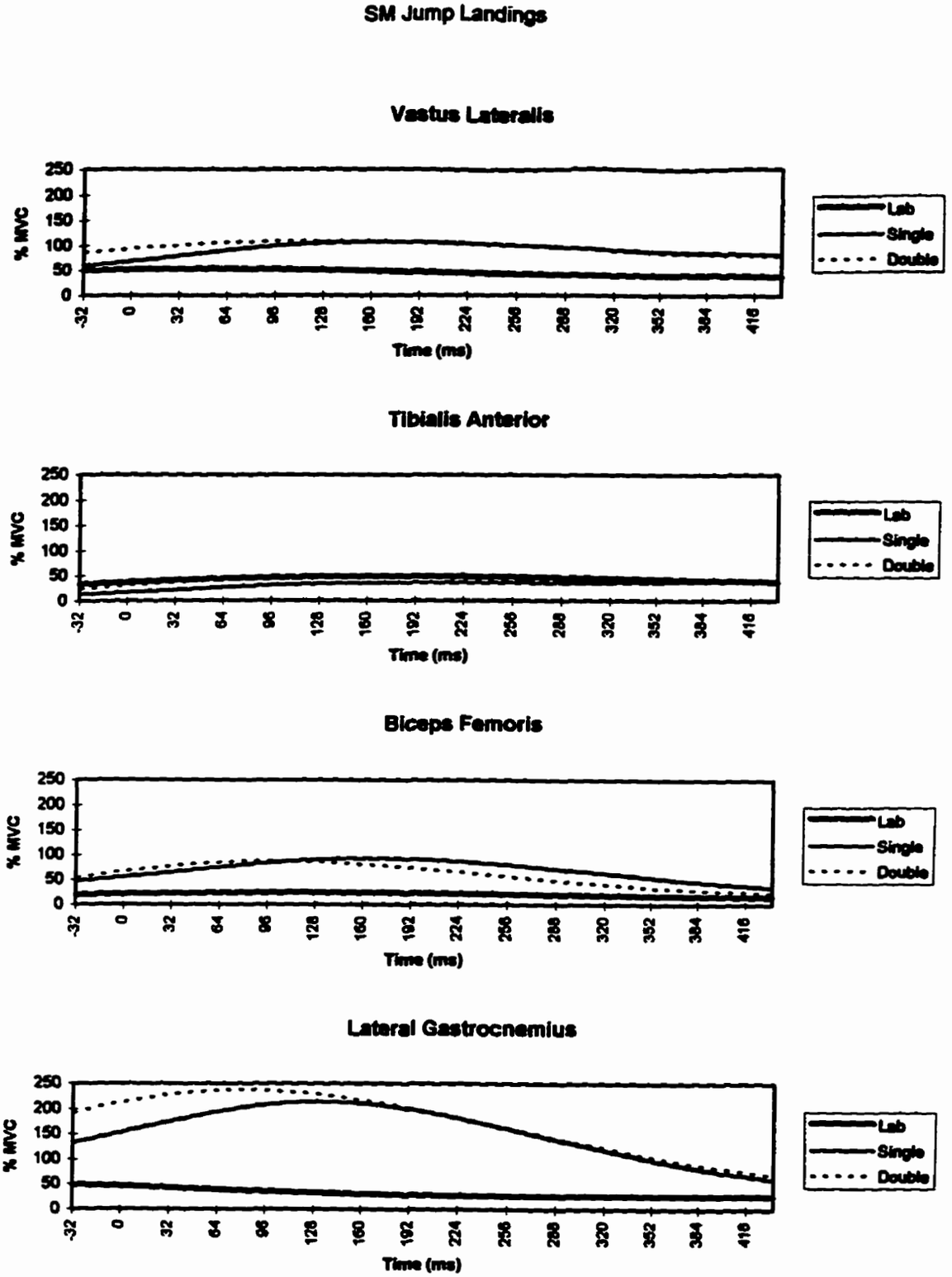

Figure 12: On-ice versus laboratory jump landing muscle activation patterns (SM) Impact occurs at 0 ms.

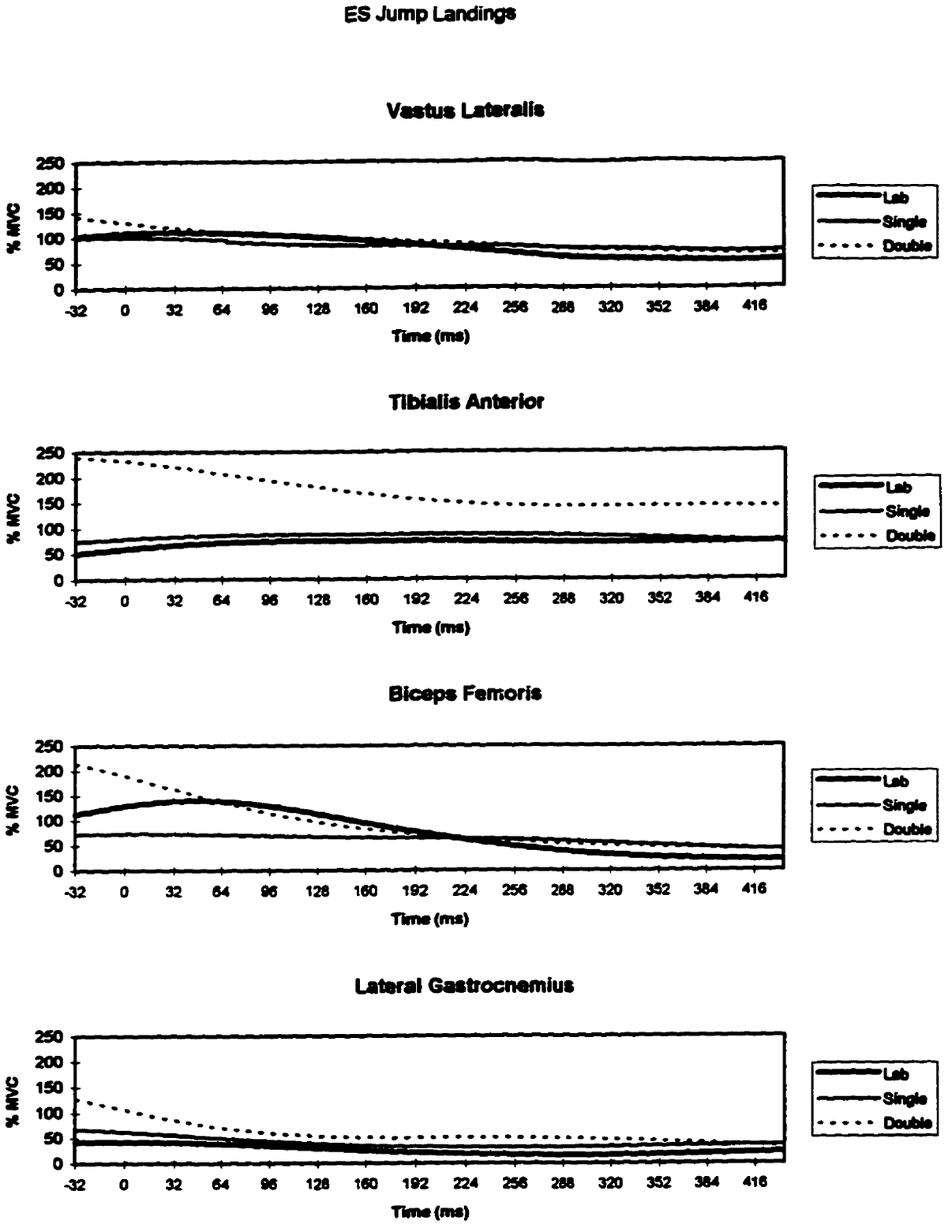

Figure 13: On-ice versus laboratory jump landing muscle activation patterns (ES) Impact occurs at 0 ms.

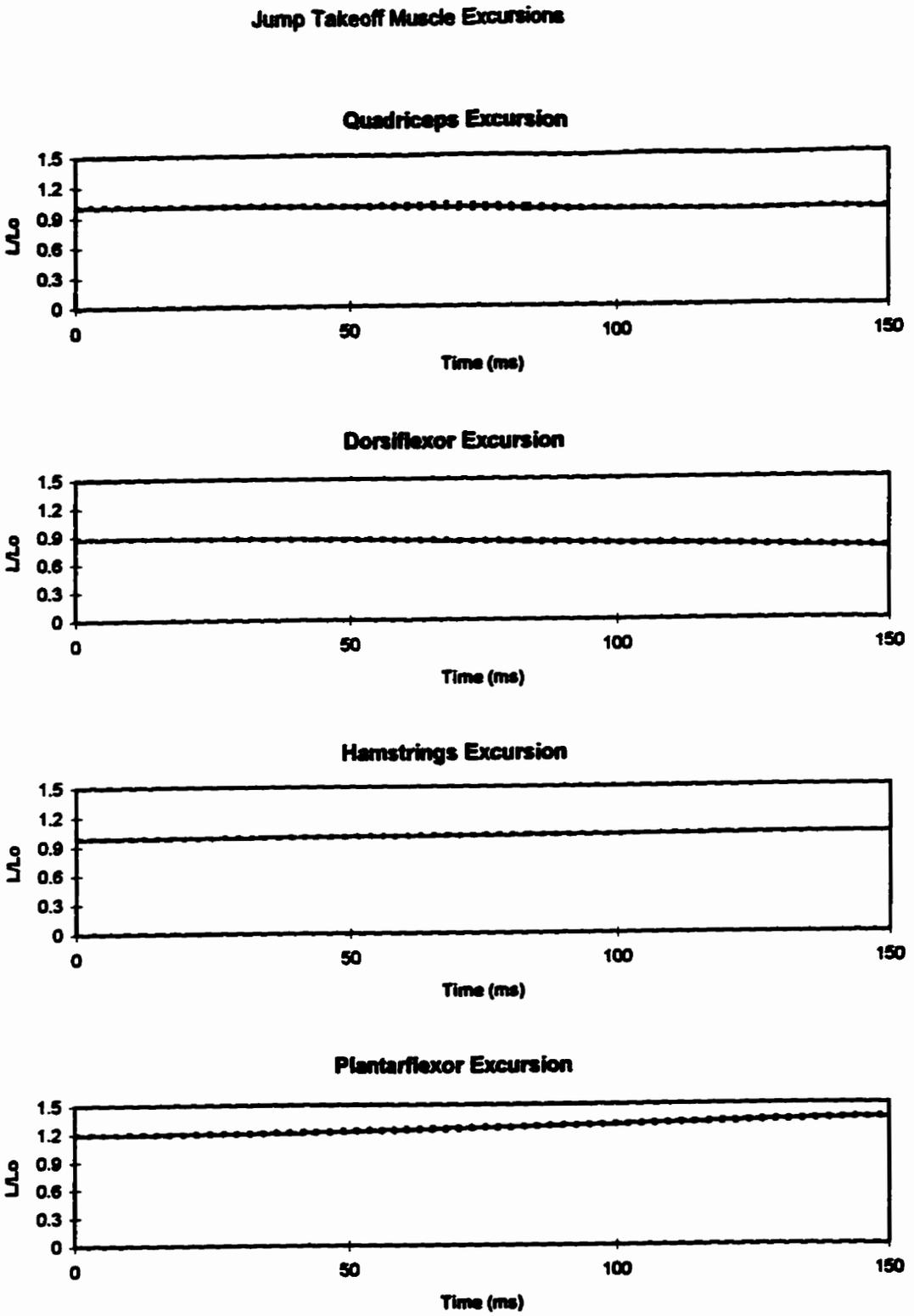

Figure 14: Typical jump takeoff muscle length excursions. Values expressed in terms of rest length (L/Lo) Takeoff occurs at 200 ms.

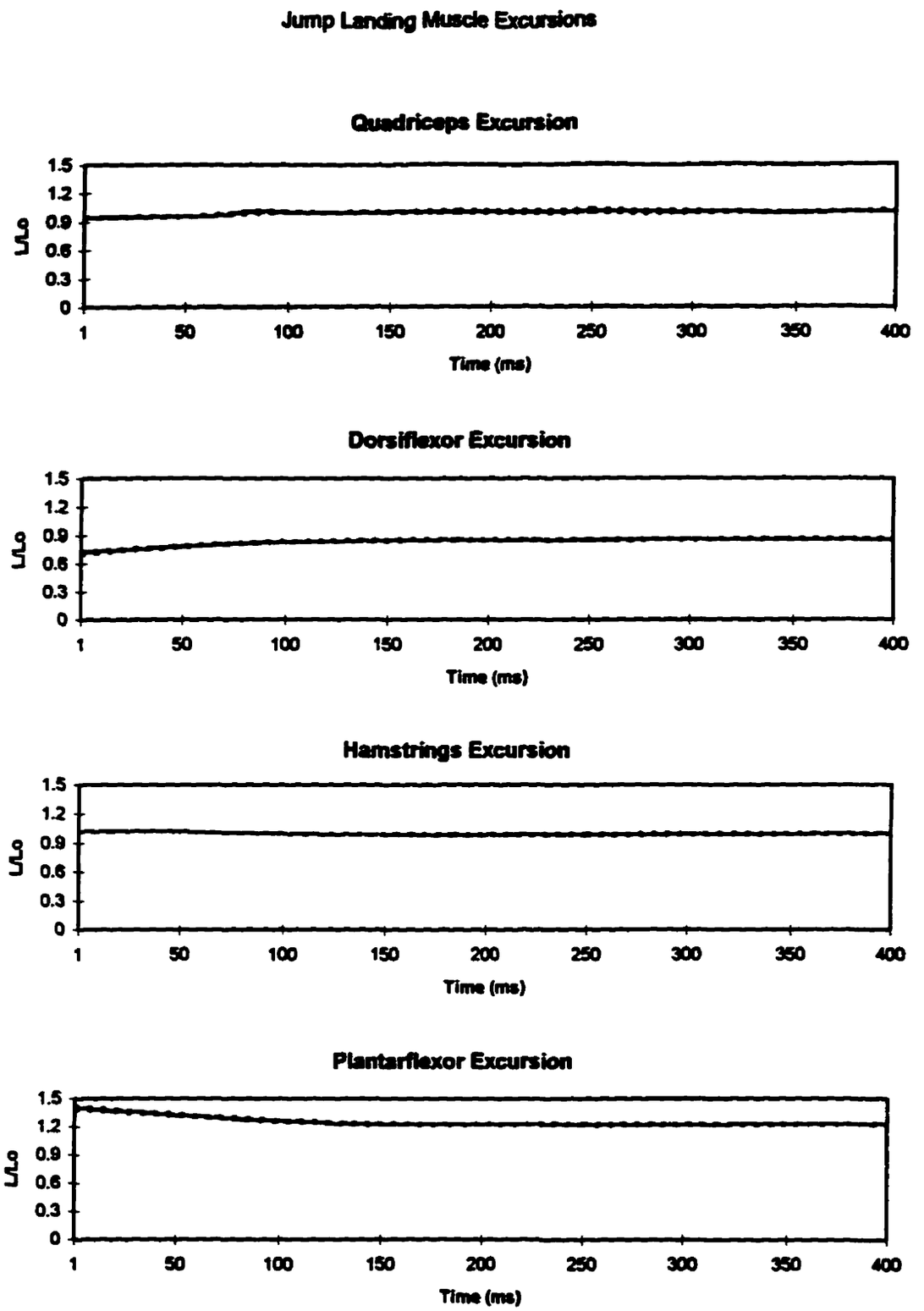

Figure 15: Typical jump landing muscle length excursions. Values expressed in terms of rest length (L/Lo). Impact occurs at 0 ms.

additional insight about the demands on the system was gained by examining the joint moments.

Table 9: Peak Joint Reaction Forces at the Ankle and Knee (Multiples of Body Weight; $\bar{x}$ (sd))

Subject	Joint	Takeoff			Landing		
		Laboratory	Single	Double	Laboratory	Single	Double
MK	Ankle	2.0 (0.08)	2.0 (0.03)	n/a	4.0 (0.53)	3.4 (0.01)	n/a
	Knee	1.9 (0.08)	2.0 (0.02)	n/a	3.9 (0.05)	3.7 (0.03)	n/a
SM	Ankle	2.2 (0.10)	2.4 (0.01)	2.5 (0.05)	4.0 (0.30)	3.6 (0.05)	3.6 (0.04)
	Knee	2.1 (0.10)	2.3 (0.01)	2.6 (0.22)	3.9 (0.31)	3.5 (0.09)	3.4 (0.08)
ES	Ankle	2.1 (0.11)	n/a	n/a	n/a	n/a	n/a
	Knee	2.1 (0.10)	n/a	n/a	n/a	n/a	n/a

5.7 Joint Moments

Figures 16 and 17 illustrate the joint moments of force calculated for each skater in this study. Table 10 summarizes the peak moments of force for each skater. Negative moments about the ankle reflected ankle plantarflexion, and positive moments about the knee reflected knee extension.

During jump takeoffs, the negative moment at the ankle indicated the ankle plantar flexors were active to plantarflex the foot and propel the body into the air. This was consistent with high gastrocnemius activity described in section 5.6. The magnitude of the moment indicated a high degree of involvement of the plantar flexors in generating the force to propel the body upwards. These ankle moments were much larger than those calculated in ballet dancers during relevés en pointe (Galea, 1983).

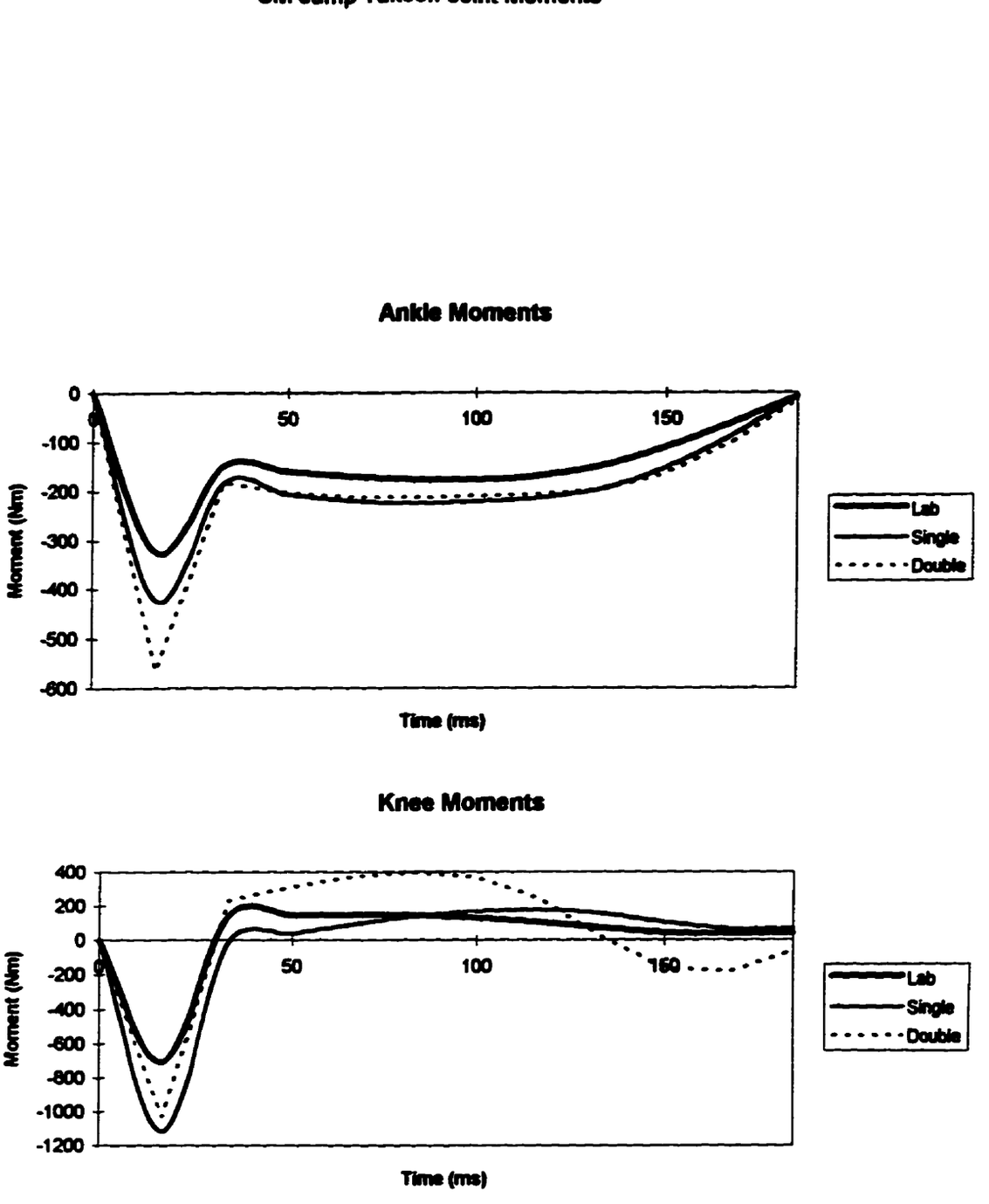

Figure 16: Typical jump takeoff joint moments. Values expressed in Nm. Takeoff occurs at 200 ms.

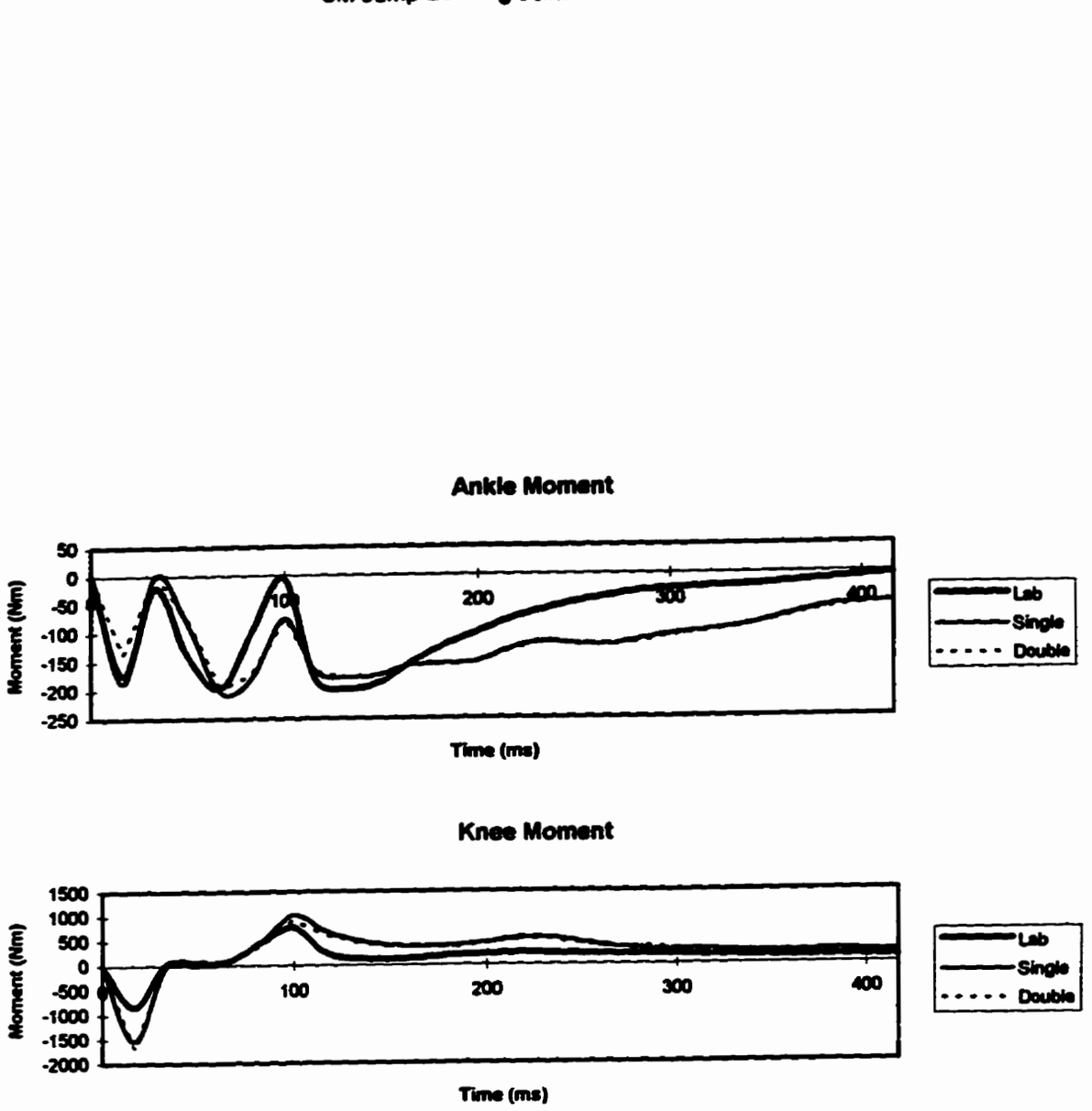

Figure 17: Typical jump landing joint moments. Values expressed in Nm. Impact occurs at 0 ms.

Table 10: Peak Joint Moments of Force at the Ankle and Knee (Nm/kg; $\bar{x}$ (sd))

Subject	Joint	Takeoff			Landing		
		Laboratory	Single	Double	Laboratory	Single	Double
MK	Ankle	-6.1 (1.18)	-5.5 (0.31)	n/a	3.8 (0.55)	4.1 (1.13)	n/a
	Knee	-0.01 (0.79)	-2.8 (0.19)	n/a	14.9 (4.03)	6.1 (0.52)	n/a
SM	Ankle	-4.5 (1.04)	-5.9 (0.82)	-7.8 (1.42)	2.9 (0.23)	2.9 (0.26)	2.7 (0.04)
	Knee	-2.3 (1.24)	-2.5 (0.61)	-6.0 (1.28)	13.1 (2.68)	14.1 (1.10)	12.9 (1.18)
ES	Ankle	-5.9 (0.97)	n/a	n/a	n/a	n/a	n/a
	Knee	-0.7 (0.35)	n/a	n/a	n/a	n/a	n/a

The initial knee flexor moment within the first 40ms of the takeoff phase was characteristic of the last portion of a jumping countermovement prior to takeoff (Figure 16). The hamstrings were active to flex the knee as the skater lowered his body centre of mass prior to jumping. The subsequent positive extensor moment was consistent with increased quadriceps activity (section 5.6) and knee extension.

Plantarflexor moments at the ankle oscillated rapidly during the first 100 ms of jump landing (Figure 17). The oscillation may have been due to impact artifact, however the oscillations corresponded to the fluctuations in the antero-postero force plate tracing and vertical ground reaction force peaks during impact (Figure 8) so it was felt that artifact was not the cause of the oscillatory response. This phenomenon has not been documented in the previous drop landing literature (Schot, Bates, and Dufek, 1994; McNitt-Gray, 1993), where subjects landed on two feet, with a larger base of support for landing than in this study where the skaters were required to land on one leg, on a very thin skate blade. This imposed a precarious balancing act on the ankle

joint.

The magnitude of ankle joint moment also reflected the nature of the one legged landing task. The normalized peak ankle moments in the present study were similar to those reported by Schot et al. (1994) (approximately 2 Nm/kg), and smaller than those of McNitt-Gray (1993) (4.28 Nm/kg). This may be attributable to the stiff skating boot that supports the skater's ankle during landing.

The knee flexor moments noted within the first 35 ms of impact were consistent with the results of gymnastic landings reported by McNitt-Gray (1993). However, knee extensor moments dominated the remainder of the landing phase as the quadriceps muscle group contracted eccentrically to maintain balance and support the body. Joint moments at the knee were considerably larger than those reported in the literature. Peak extensor moments of 2.82 Nm/Kg were experienced by recreational athletes landing from a height of 0.32 m (McNitt-Gray, 1993).

Joint moments of force have given insight to the muscular responses to one foot jump takeoffs and landings. The bone-on-bone forces completed the picture by adding the effect of the active musculature.

5.8 Bone-on-Bone Forces at the Ankle and Knee

Table 11 outlines the peak bone-on-bone forces at the ankle and knee predicted by the muscle model. Standard deviations indicated the variability demonstrated by the participants. Overall, in the laboratory setting, bone-on-bone forces were larger for landings than for takeoffs, while knee bone-on-bone forces were larger than those at the ankle.

Figures 18 - 22 document the calculated bone-on-bone forces in skaters during jump takeoffs and jump landings. While the joint moment of force indicated the net moment

at a joint, individual participants employed different muscle activation strategies to accomplish the same task (Section 5.5).

Similar to the joint reaction forces (Section 5.6), the peak bone-on-bone forces at the ankle and knee were higher in jump landings than in jump takeoffs. However, the calculated joint reaction forces predicted similar forces between the ankle and knee in each condition. The bone-on-bone calculations showed that the knee forces were much higher than the ankle forces.

Table 11: Peak Bone-on-Bone Forces at the Ankle and Knee During Jump Takeoffs and Landings
(Multiples of Body Weight; $\bar{x}$ (sd); [number of trials])

Subject	Joint	Takeoff			Landing		
		Laboratory	Single	Double	Laboratory	Single	Double
MK	Ankle	11.7 (2.43) [8]	7.8 (1.19) [7]	n/a	11.4 (5.33) [20]	17.7 (4.00) [5]	n/a
	Knee	24.7 (22.97)	47.1 (35.89)	n/a	34.5 (12.05)	69.3 (83.48)	n/a
SM	Ankle	8.7 (2.40) [7]	8.1 (1.57) [7]	6.6 (0.51) [6]	9.3 (1.96) [16]	5.8 (0.37) [8]	7.3 (2.46) [5]
	Knee	4.5 (2.37)	22.0 (23.63)	29.7 (27.74)	26.9 (7.85)	23.9 (3.71)	21.5 (7.84)
ES	Ankle	10.5 (3.02) [9]	n/a	n/a	n/a	n/a	n/a
	Knee	29.9 (56.81)	n/a	n/a	n/a	n/a	n/a

Predicted peak bone-on-bone forces at the ankle during jump landings were similar to those forces predicted by Scott and Winter (1990) in running (8.7 - 11.7 times body weight) and less than those predicted in relevés en pointe by Galea (1983) (10 - 14 times body weight).

Ankle bone-on-bone forces during jump takeoffs (Figures 18, 19 and 20) remained fairly stable throughout the takeoff phase of jumping. The bone-on-bone force profile was similar in shape to that of the vertical ground reaction force profile (Figure 10). From the ankle bone-on-bone force profile, it appeared that the three subjects employed different jumping strategies, consistent with the varied muscle activation patterns (Section 5.5). The knee experienced a short duration, high intensity point load during the jump takeoff, consistent with cocontraction at the knee by quadriceps to extend the leg at the knee and by biceps femoris, to extend the trunk at the hip. It appeared that SM experienced more intense knee loading, demonstrated by the sharp peaks in knee bone-on-bone force tracings, than MK, whose knee bone-on-bone peaks were more gradually formed. This was consistent with the discussion of jump technique presented in Section 5.5.

Bone-on-bone forces characterized two features of jump landings (Figures 21 and 22). At the knee, one distinct peak occurred at approximately 100 ms, corresponding to the peak vertical ground reaction force. This peak was out of phase with the two distinct peaks observed at the ankle at 75 and 125 ms. Consistent with the joint moments of force, the ankle bone-on-bone forces were smaller than those at the knee. Combined with the extensor moment, the knee experienced a short duration, high magnitude bone-on-bone force at its articulating surface 100 ms after impact. Similarly, the ankle experienced fairly high bone-on-bone forces approximately 75 ms and 125 ms after impact, however, these forces occurred over a longer duration than those at the knee. The short duration, high intensity forces, especially at the knee, may be one of the factors contributing to the disproportionate number of knee injuries in figure skaters.

The short duration, high intensity point loads experienced during jump takeoffs and landings may be a key factor to understanding more about the injuries that occur at the knee in skaters. Nigg and Bobbert (1990) indicated that excessive load may be

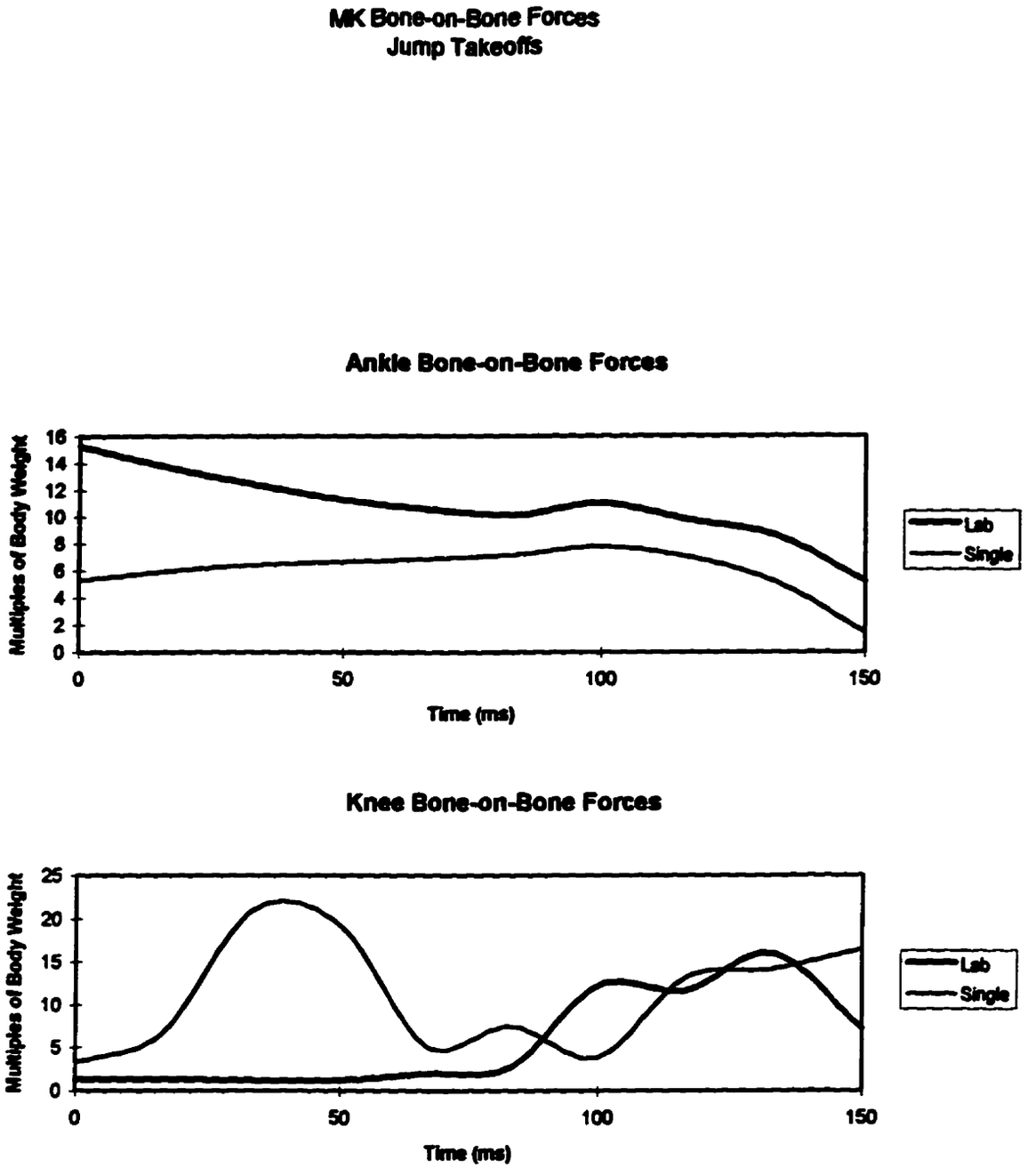

Figure 18: On-ice versus laboratory takeoff bone-on-bone forces (MK) Takeoff occurs at 150 ms.

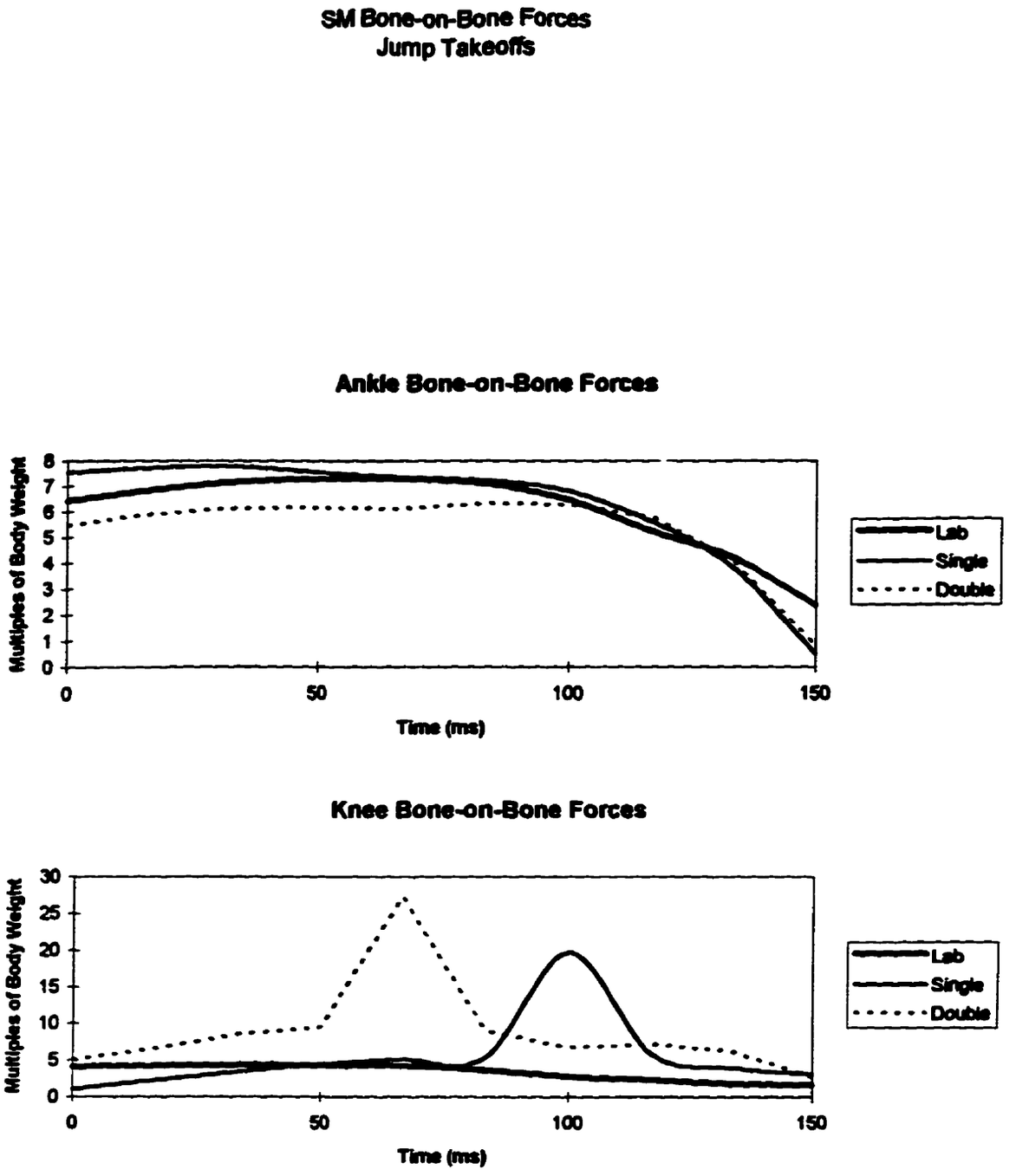

Figure 19: On-ice versus laboratory takeoff bone-on-bone forces (SM) Takeoff occurs at 150 ms.

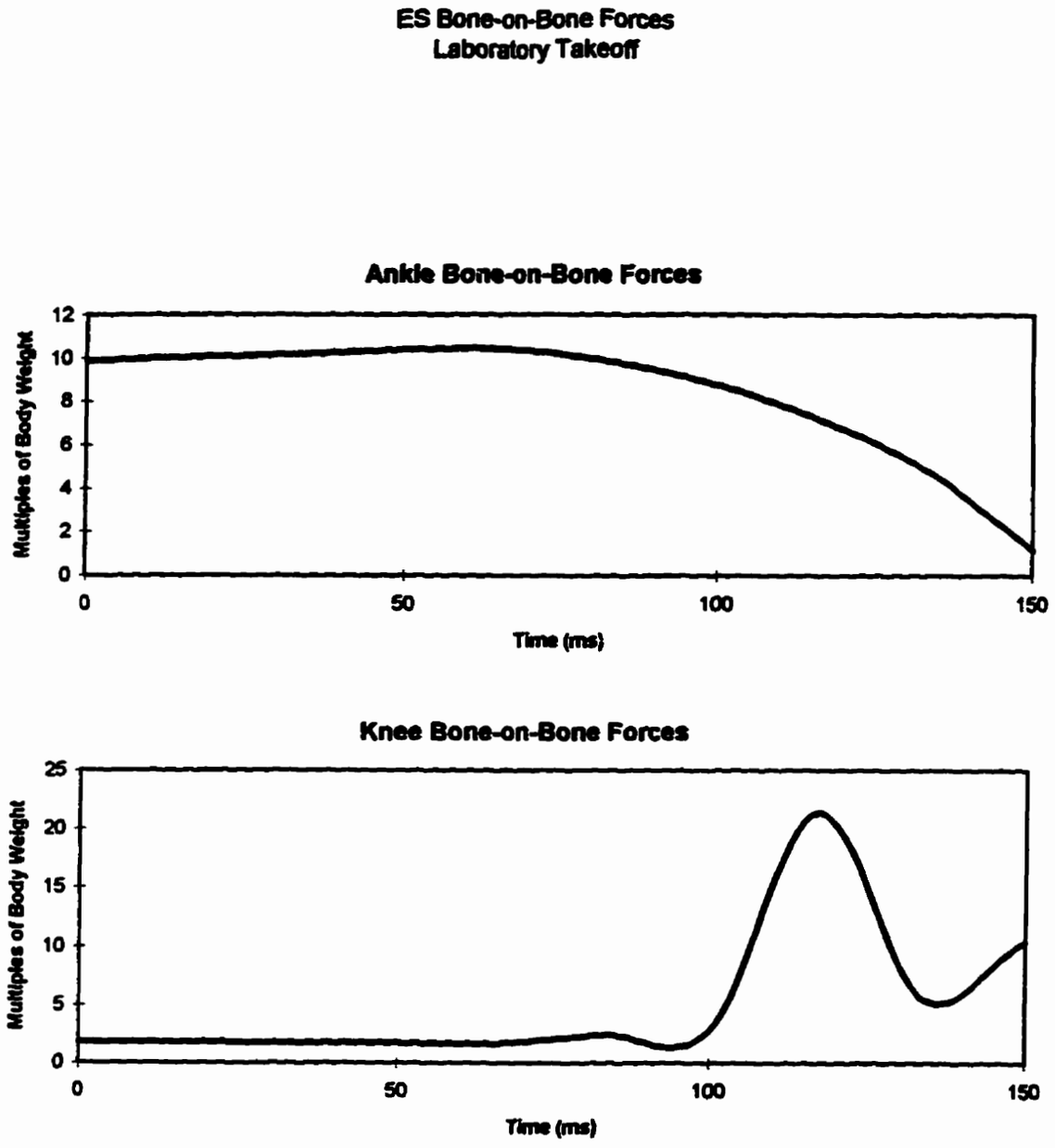

Figure 20: Laboratory takeoff bone-on-bone forces (ES)
Takeoff occurs at 150 ms.

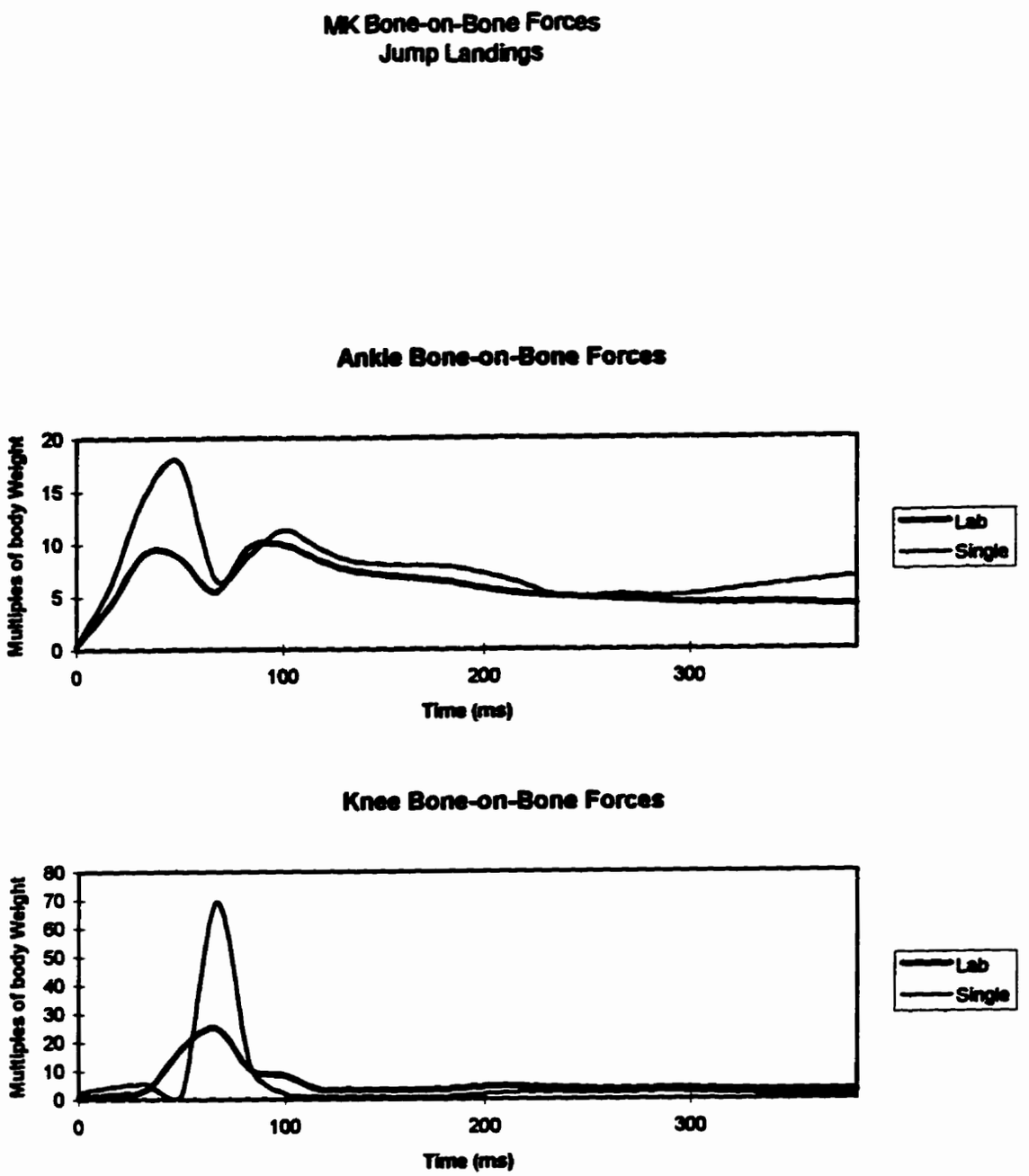

Figure 21: On-ice versus laboratory landing bone-on-bone forces (MK) Impact occurs at 0 ms.

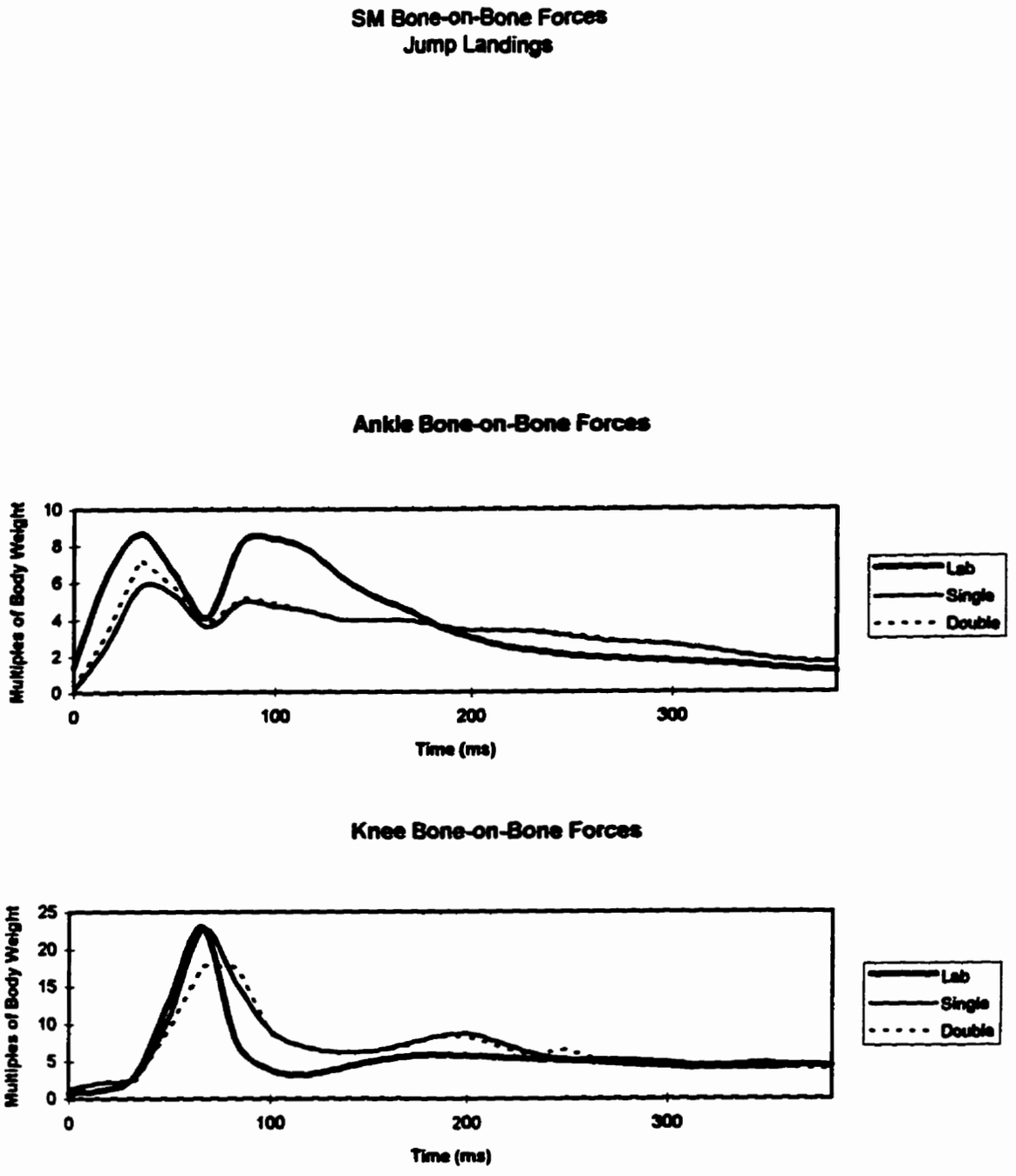

Figure 22: On-ice versus laboratory landing bone-on-bone forces (SM) Impact occurs at 0 ms.

the reason for micro- or macrodamages of anatomical structures. In jump landings, eccentric quadriceps contraction, coupled with the large vertical ground reaction force vector on impact may precipitate patellofemoral pain syndrome. This condition is exacerbated by the compressive component of the quadriceps forcing the patella against the groove and lateral shear as the patella moves relative to the femur during the knee range of motion (Winter and Bishop, 1992). The rapid, eccentric contraction of quadriceps may also be associated with Osgood-Schlatter disease, where the tibial tubercle (quadriceps muscle insertion) is enlarged due to epiphyseal damage (Magee, 1992).

At the ankle, rapid, eccentric contraction of the gastrocnemius created a similar scenario at the calcaneus to that of the tibial tubercle at the knee. While the predicted bone-on-bone force peaks were not as violent as those seen at the knee, they may still precipitate an injury situation to the Achilles tendon.

5.9 Model Discussion

The present link segment model predictions of bone-on-bone forces were reasonable values compared to literature values of similar motions (Scott and Winter, 1990, Galea, 1983). Direct validation of the model was impossible without surgical intervention.

5.9.1 Model Calculations

The model in this study calculated substantial moments and bone-on-bone forces at the ankle and knee joints during jump takeoffs and jump landings. In an effort to further understand the major contributing factors to the model outputs, different model parameters were modified in one representative trial.

It was felt that the filtered kinematic data reduced the impact characteristics of jump landings. Kinematic data filtered at 24 Hz rather than at 6 Hz did not substantially

affect the magnitude of joint moments nor bone-on-bone forces.

The calculated ankle plantarflexor moments in this study were comparable to those of McNitt-Gray (1993), however, it was thought that the skating boot provided support to the bare ankle and that the substantial knee moments in the present study reflected this. To simulate the support of the skating boot, 70% of the support moment generated at the ankle in the link segment model was assigned to the skating boot. This effectively reduced the demands of the ankle musculature to support the landing impact load. The reduced ankle moment was used as an input to the knee support moment. This modification did not greatly reduce the magnitude of the knee landing support moment from the original model iteration, suggesting that the knee extensor musculature plays a crucial role supporting the body upon impact.

The magnitude of knee moments in the present study were substantially larger than those of McNitt-Gray (1991). This may be due to the differences in task demands between studies. Moments about the knee in this study reflected a one-foot landing, thereby reducing the base of support and area of force dissipation, while increasing the balance requirements of the participant, compared to a larger base of support and force dissipation afforded in a two foot landing (McNitt-Gray, 1991). As well, segment endpoints were used to calculate segment centre of mass and radius of gyration in moment calculations. The large knee moments may have been amplified due to large moment arm lengths calculated from segment endpoints.

McNitt-Gray (1991) simulated two foot drop landings from a 0.32 m platform and investigated the contribution of hip moment to landing, noting that the hip moment exhibited an oscillatory pattern out of phase with knee moments during the first 25% of landing. The present study did not examine hip moments; perhaps the hip plays a larger role to offset the large knee moments.

Maximal muscle force in this study was modelled at 50 N/cm^2. The model assumed that all muscles consistently produced this maximal force, scaled to the activation level of the participant, compared to a maximal voluntary contraction. To simulate reduced muscle output, muscle force was reduced to 35 N/cm^2. Calculated bone-on-bone forces decreased accordingly, as the muscle force output was based on muscle cross-sectional area multiplied by the maximum muscle force output.

5.9.2 Model Sources of Error

Potential sources of input error to the model included errors in digitization and data synchronization. Because force plate and EMG data were collected at a different frequency (1000 Hz) than the video data (60 Hz), the data synchronization pulses recorded from the video may have introduced error (15 samples) to the clipped EMG and force plate trial files.

deLooze et al. (1992) documented several sources of error in link segment modelling. Joint centres of rotation, estimated from video data, were used in velocity and acceleration calculations and defined segment endpoints. Noise from digitizing was amplified by double differentiation of joint centre coordinates. This error was cumulative through further calculations (joint accelerations, segmental accelerations, moment of inertia, higher segments in the linkage), resulting in noisy data. In this study, this effect may have been amplified due to the high frequency impact characteristics of the task. Muscle moment arm lengths were also based on joint centres; small changes in moment arm would result in joint moment over- or underestimations. Finally, errors in force plate measurements and estimates of centre of pressure also have a large influence on the magnitude of joint moment of force.

The muscle model output was strongly influenced by the activation level of the muscle compared to a maximal voluntary contraction. Normalization of electromyographic

activity is a problem that has plagued biomechanists (McGill and Norman, 1986; McGill, 1992). The on-ice muscle activation values, as well as some of the laboratory task activation values in this study were considerably higher than the comparison maximal values generated in the laboratory. This may have been due to electrode movement artifact or to different task demands than those of the normalization trial. If the muscle activation levels recorded from the tasks were not as high (up to 350%; resulting in an EMG activation coefficient of 3.5), then the calculated bone-on-bone forces would have been reduced as well. Despite the difficulties scaling muscle activity, the weakness in this approach was overshadowed by its strength, identifying individual muscle activation patterns and approaches to muscle group recruitment (McGill, 1992).

5.9.3 Injury Implications

Very large moments at the knee and ankle were observed in this study. To prevent excessive rotation, structures are required to support the moment imposed by takeoff or landing. In addition to bone and musculo-tendon units, ligaments and articular cartilage are responsible for load support. Neither ligaments nor articular cartilage were considered in this model. The tremendous bone-on-bone forces represented forces at joint articulations, however, muscle groups such as the quadriceps and ankle plantarflexors must contract to support the joint moment, resulting in stress on the musculotendinous units and tendon-bone insertion points.

Butler et al. (1984) calculated that the failure point of the patellar tendon bone unit from young donors (mean age = 26) was approximately 1150 kN. Assuming that the bone-on-bone force calculated at the knee was representative of the stress on the patellar tendon, even the largest calculated bone-on-bone force from this study (69 times BW; 942 kN) was less than that of reported failure values. It was felt that joint forces in this study were probably overestimated due to the maximum muscle stress assigned to the muscles (50 N/cm^2) and high relative activation level of the muscles

during the tasks compared to the normalization level. From this, it is likely that the actual bone-on-bone forces in on-ice loop jumps predicted at the ankle and knee were smaller than those calculated in this study.

The long term effects of repetitive loading on tissues are not known. Van Dijk et al. (1995) examined the joint space characteristics of retired ballet dancers (mean career length 37 years; mean age 59 years; mean training time 45 hours per week) compared to age, weight, and height matched controls. The retired ballet dancers demonstrated significantly smaller joint spaces and signs of arthrosis at the ankle and first metatarsal joints compared to the controls. The dominant "landing leg" in the dancers showed more arthritic changes than did the non-dominant side. This was attributed to the accumulation of microtraumas during the course of a dancer's career. Interestingly, none of the dancers had any complaints about any of the examined joints. Knee joints were not studied in this paper. Compared to a figure skate, the ballet shoe provides no support to the ankle, so it would be expected that the effects of impact in figure skating jump landings would be reduced by the skating boot.

Repetitive loading may be the reason for micro- or macrodamages to the anatomical system (Nigg et al., 1990). While one jump alone may not result in an acute epiphyseal injury, the accumulation of microtrauma due to repetitive jump practice and constant knee flexion/extension cycles incurred as the skater skates between elements ("stroking") may contribute to knee injuries in skaters. The failure point of in-vivo tissue is not known; cadaver material allows a comparison of magnitude of failure force, however, the human body is an incredible piece of machinery. Live tissue may have a considerably higher failure point than that of cadaveric specimens.

Jumping is a part of figure skating necessary for international success. Cessation of jump activity is not an option if the skater's goal is to reach the top of the podium in international competition. Forces experienced by skaters during jumping are of high

intensity, but of short duration. Reduction of knee and ankle injuries, then, are reliant on educated approaches to on-ice and off-ice training.

Chapter 6 - Summary, Conclusions, and Recommendations

6.1 Research Summary

Success in competitive figure skating is dependent upon the number of triple revolution jumps a skater can successfully complete in competition. Compulsory figures were removed from competition in 1991, resulting in a significant change to competitive figure skating training. Rather than spend up to 20 hours per week practising the repetitive tracing of circles on ice, modern day skaters use this time to perfect the double and triple jumps necessary to reach levels of international competition. The price of success was not without its tradeoffs. Figure skating injury studies indicated that the knee and the ankle were the most common injury sites.

To gain insight into potential injury mechanisms, a 2-dimensional, sagittal plane, link segment, inverse dynamic model of the lower limb was created to predict the bone-on-bone forces at the knee and ankle during jump landings and takeoffs. A jump that began and ended on the same leg, the loop jump, was chosen for this study. The study was divided into two components: on-ice and laboratory.

Three male National level figure skating competitors participated in this study. On ice, the skaters were videotaped performing single and double loop jump landings and takeoffs from two different camera angles. During the on-ice jumps, muscle activity of vastus lateralis, tibialis anterior, biceps femoris, and lateral gastrocnemius was recorded with a portable EMG data unit.

An estimate of the location and magnitude of the ground reaction force vector was obtained by laboratory simulations of jump takeoffs and landings. Skaters were asked to perform jump takeoffs and jump landings onto and from a 6-channel force

plate in the laboratory. Jump takeoffs were accomplished by instructing the participant to initiate a jump takeoff on the force plate. A raised platform, representing the maximum on-ice jump height calculated from on-ice video information, was fabricated for each skater. Jump landings were simulated by instructing the skater to jump backwards from the raised platform onto the force plate, landing on one foot, as if on ice. Similar to the on-ice collection, all trials were videotaped and muscle activity recorded. In all of the on-ice and laboratory conditions, the measurement tools (video, force plate, and muscle activity) were synchronized.

Muscle activation was normalized to a static maximal voluntary contraction. Raw electromyographic activity was processed to yield a linear envelope representation of muscle activity. Force plate data was calibrated with manufacturer-supplied shunt values. Video data was manually digitized and scaled to real-life using the Peak Performance video analysis system. Muscle activation, video, and force plate data were used as inputs to an inverse dynamic model of the lower limb.

A 2-dimensional, dynamic, sagittal plane model of the lower limb was programmed in MathCad 6.0 Professional Edition to calculate the bone-on-bone forces at the ankle and knee from the laboratory and on-ice data. An updated version of McGill and Norman's (1986) multiplicative muscle model was incorporated into the lower limb model to account for muscle activation, force/length, force/velocity, and passive elastic contributions to muscle force output. In the absence of on-ice measurements of the ground reaction force vector, representative force plate trials of jump takeoffs and jump landings were used as the kinetic complement to on-ice video and electromyographic information.

On-ice, single loop jump heights ranged from 0.21 to 0.24 m, while double loop jumps were higher, ranging from 0.25 to 0.31m.

Peak vertical ground reaction forces in the laboratory simulations ranged from 2.12 to 2.21 times body weight in jump takeoffs and 3.65 to 4.88 times body weight in jump landings. Post-priori consultation with international figure skating coaches indicated that the vertical ground reaction takeoff force was probably underestimated due to differences in the jump takeoff conditions between the laboratory and the ice.

Muscle activity patterns revealed a high degree of cocontraction on impact in jump landings. Double jump landings produced higher muscle activity levels than single jump landings. Individual muscle activation strategies were identified for each participant. Compared to the laboratory session, muscle activity was often higher in the on-ice jumps.

The plantarflexor muscle group was consistently lengthened beyond rest length in both jump takeoffs and jump landings.

Joint reaction forces at the ankle and knee were larger in jump landings than in jump takeoffs in both laboratory and on-ice trials. Within these conditions, little difference was observed in the magnitude of joint reaction force between the ankle and the knee.

Joint moment analysis indicated that jump takeoffs elicited a plantarflexor moment at the ankle and extensor moment at the knee. Jump landings resulted in an ankle plantarflexor moment and knee extensor moment. In jump landings, the quadriceps contracted eccentrically to support the joint moment.

Peak bone-on-bone forces ranging from 8.7 to 11.7 and 4.5 to 29.9 times body weight at the ankle and knee, respectively, were calculated during jump takeoff simulations. Jump landing simulations resulted in peak bone-on-bone forces ranging from 9.3 to 11.4 and 26.9 to 34.5 times body weight at the ankle and knee, respectively. On-ice,

jump takeoff bone-on-bone forces ranged from 6.6 to 8.1 times body weight at the ankle and 22.0 to 47.1 times body weight at the knee. Jump landings from on-ice trials resulted in peak bone-on-bone forces ranging from 5.8 to 17.3 times body weight at the ankle and 21.5 to 69.3 times body weight at the knee.

Bone-on-bone forces during jump landings were characterized by bimodal peaks at the ankle and a high-intensity, short duration peak, out of phase with the ankle peaks, at the knee. These peaks occurred within the first 125 ms of impact. Bone-on-bone forces at the ankle remained fairly constant throughout jump takeoffs, while a high-intensity, short duration peak was noted at the knee prior to takeoff. These short, explosive periods of force may be a window onto understanding why skaters experience knee and ankle injuries.

The results of this model indicate that very high demands were imposed on the surrounding knee and ankle musculature during jump takeoffs and landings. This model did not account for the stiffness of the skating boot and its contributions to reducing ankle joint moment; the gastrocnemius-soleus complex was modelled as a one-joint muscle responsible for ankle plantarflexion only; muscle force output was assumed to be a constant value (50 N/cm^2).

Jumping is a part of figure skating necessary for international success. Reduction of knee and ankle injuries is dependent on educated approaches to on-ice and off-ice training.

6.2 Conclusions

Based upon the hypotheses in this thesis, the following conclusions were drawn:

1. Hypothesis: *The peak bone-on-bone forces predicted at the knee and ankle*

for jump takeoffs were different than those predicted for jump landings.

Conclusion: Based on the limited sample size in this study, jump landings tended to produce higher bone-on-bone forces at the knee and ankle than did jump takeoffs.

2. Hypothesis: *Double jumps would produce substantially higher peak bone-on-bone forces than single jumps for both takeoffs and landings.*

   Conclusion: Because of the technical limitations in data collection, this hypothesis could not be either supported or rejected. The data from one subject on whom both single and double jump landing bone-on-bone forces were determined was equivocal.

6.3 Recommendations

Based on the results of this study, the following recommendations were made:

1. Based on the large bone-on-bone forces predicted at the ankle and knee in this study, it was recommended that skaters alternate jumping with non-jumping activities during a practice session.
2. Off-ice conditioning programmes should incorporate eccentric training of ankle plantarflexors and knee extensors due to the consistent lengthening contractions in these muscle groups in jumping activities.
2. Static EMG normalization trials did not adequately elicit maximum muscle activity with which to normalize to dynamic actions. In future studies, normalization trials similar to the task demands may provide a better comparison value.

6.4 Future Research Directions

This study used a two-dimensional, sagittal plane model to predict bone-on-bone forces at the ankle and knee during loop jumps. The next natural progression in this area is to conduct a three-dimensional analysis of the jump and include more body segments in the analysis. As well, actual on-ice measurements of forces experienced by skaters during jumps is warranted, providing the data collection system did not interfere with the natural movement patterns of the skater. Post-priori consultation with international level coaches emphasized a need to include the upper torso and arms in the model to determine their effects on the system.

References

Albert, W., and Miller, D.I. (1996). Takeoff characteristics of single and double Axel figure skating jumps. Journal of Applied Biomechanics, (12), 72-87.

Aleshinsky, S. Y. (1986a). Professional service for amateur skaters: What biomechanics can do for figure skating. Skating, November, 10 - 13.

Aleshinsky, S. Y. (1986b). Professional service for amateur skaters: What biomechanics can do for figure skating. Part Two. Skating, December, 11 - 15.

Alexander, R., and Vernon, A. (1975). The dimensions of knee and ankle muscles and the forces they exert. Journal of Human Movement Studies, 1, 115-123.

Bates, B.T., Dufek, J.S., and Davis, H.P. (1992). The effect of trial size on statistical power. Medicine and Science in Sports and Exercise, 24(9), 1059-1068.

Bresler, B., and Frankel, J.P. (1950). The forces and moments in the leg during level walking. Transactions of the ASME, 27-36.

Brock, R.M., and Striowski, C.C. (1986). Injuries in elite figure skaters. The Physician and Sportsmedicine, 14(1), 111-115.

Brown, E.W., and McKeag, D.B. (1987). Training, experience and medical history of pairs skaters. The Physician and Sportsmedicine, 15(4), 100-114.

Brown, J. (1994). An evaluation of the article by Delistraty, D.A., Reisman, E.J., and Snipes, M., "A physiological and nutritional profile of young female figure skaters". Letters to the Editor. The Journal of Sports Medicine and Physical Fitness, 34(2), 199-201.

Butler, D.L., Grood, E.S., Noyes, F.R., Zernicke, R.F., and Brackett, K. (1984). Effects of structure and strain measurement technique on the material properties of young human tendons and fascia. Journal of Biomechanics, 17(8), 579-596.

Butler, D.L., Sheh, M.Y., Stouffer, D.C., Samaranayake, V.A., and Levy, M.S. (1990). Surface strain variation in human patellar tendon and knee cruciate ligaments. Journal of Biomechanical Engineering, 112, 38-45.

Canadian Figure Skating Association. (1995). Official Rules. Gloucester, Ontario : Canadian Figure Skating Association.

Cholewicki, J., McGill, S.M., and Norman, R.W. (1995). Comparison of muscle forces and joint load from an optimization and EMG assisted lumbar spine model : Towards development of a hybrid approach. Journal of Biomechanics, 28(3), 321-331.

Cramer, L.M., and McQueen, C.H. (1990). Overuse injuries in figure skating. in Winter Sports Medicine edited by Casey, M.J., Foster, C., and Hixon, E.G. F.A. Davis Company: Philadelphia.

Crawshaw, A.H., Hastings, G.W., and Dove, J. (1991). The implanted electrical resistance strain gauge : in vitro studies on data integrity. Journal of Medical Engineering Technology, 15(2), 72-77.

Delistraty, D.A., Reisman, E.J., and Snipes, M. (1992). A physiological and nutritional profile of young female figure skaters. The Journal of Sports Medicine and Physical Fitness, 32,(2), 149-155.

de Looze, M.P., Kingma, I., Bussmann, J.B.J., and Toussaint, H.M. (1992). Validation of a dynamic linked segment model to calculate joint moments in lifting. Clinical Biomechanics, 7, 161 -169.

Deng, Y.C., and Goldsmith W. (1987). Response of a human head/neck/upper-torso replica to dynamic loading --II. Analytical/numerical model. Journal of Biomechanics, 20(5), 487-497.

Dufek, J.S. and Bates, B.T. (1991). Dynamic performance assessment of selected sport shoes on impact forces. Medicine and Science in Sports and Exercise, 23(9), 1062-1067.

Dufek, J.S. and Bates, B.T. (1991). Biomechanical factors associated with injury during landing in jump sports. Sports Medicine, 12(5), 326-337.

Dufek, J.S. and Bates, B.T. (1991). The evaluation and prediction of impact forces during landings. Medicine and Science in Sports and Exercise, 22(3), 370-377.

Fernandez-Palazzi, F., Rivas, A., and Mujica, P. (1990). Achilles tendinitis in ballet dancers. Clinical Orthopaedics, 257, 257-261.

Fitness Canada. (1986). Canadian Standardized Test of Fitness Operations Manual. Government of Canada Fitness and Amateur Sport. Ottawa.

Foti, T.A. (1990). The Biomechanical Evaluation of Landings in an Articulated Boot Figure Skate. Unpublished master's thesis, University of Delaware.

Fukashiro, S., Komi, P.V., Jarvinen, M., and Miyashita, M. (1993). Comparison between the directly measured Achilles tendon force and the tendon force calculated from the ankle joint moment during vertical jumps. Clinical Biomechanics, 8, 25 - 30.

Fukunage, T., Roy, R.R., Shellock, F.G., Hodgson, J.A., Kay, M.K., Lee, P.L., Kwong-Fu, H., and Edgerton, V.R. (1992). Physiological cross sectional area of human leg muscles based on magnetic resonance imaging. Journal of Orthopaedic Research, 10, 926-934.

Galea, V. (1983). Bone-on-Bone and Muscle Forces in the First Metarsophalangeal and Talocrural Joints During Releves on Pointe. Unpublished master's thesis, University of Waterloo, Waterloo, Ontario.

Garrick, J.G. (1985). Characterization of the patient population in a sports medicine facility. The Physician and Sportsmedicine, 13(10), 73-77.

Gordon, A.M., Huxley, A.F., and Julian, F.J. (1966). The variation in isometric tension with sarcomere length in vertebrate muscle fibres. Journal of Physiology, (184), 170-192.

Hagberg, M., Silverstein, B., Wells, R., Smith, M.J., Hendrick, H.W., Carayon, P., and Pérusse, M. (1995). Work Related Musculoskeletal Disorders (WMSDs): A Reference Book for Prevention. Bristol. PA : Taylor and Francis, Inc.

Hill, A.V. (1938). The heat of shortening and the dynamic constants in muscle. Proceedings of the Royal Society, B-126, 136-195.

International Skating Union. (1994). Regulations 1994. (Available from the Canadian Figure Skating Association, Gloucester, Ontario).

Kjaer, M. and Larsson, B. (1992). Physiological profile and incidence of injuries among elite figure skaters. Journal of Sports Sciences, (10), 29-36.

King, D.L., Arnold, A.S., and Smith, S.L. (1994). A kinematic comparison of single, double, and triple axels. Journal of Applied Biomechanics, 10, 51-60.

Lieber, R.C., and Bodine-Fowler, S.C. (1993). Skeletal muscle mechanics : Implications for rehabilitation. Physical Therapy, 73(12), 844-855.

Magee, D.J. (1992). Orthopedic Physical Assessment (Second Edition). Toronto : W.B. Saunders Company.

McGill, S.M. (1992). A myoelectrically based dynamic three-dimensional model to predict loads on lumbar spine tissues during lateral bending. Journal of Biomechanics, 25(4), 395-414.

McGill, S.M., and Norman, R.W. (1986). Partitioning of the L4-L5 dynamic moment into disc, ligamentous, and muscular components during lifting. Spine, 11(7), 666-678.

McGill, S.M., Thorstensson, A., and Norman, R.W. (1989). Non-rigid response of the trunk to dynamic axial loading: an evaluation of current modelling assumptions. Clinical Biomechanics, 4, 45-50.

McNitt-Gray, J., Yokoi, T., and Millward, C. (1994). Landing strategies used by gymnasts on different surfaces. Journal of Applied Biomechanics, (10), 237-252.

McNitt-Gray, J., Yokoi, T., and Millward, C. (1994). Landing strategies adjustments made by female gymnasts in response to drop height and mat composition. Journal of Applied Biomechanics, (9), 173-190.

McNitt-Gray, J. (1993). Kinetics of the lower extremities during drop landings from three heights. Journal of Biomechanics, 26(9), 1037-1046.

McNitt-Gray, J. (1991a). Kinematics and impulse characteristics of drop landings from three heights. International Journal of Sport Biomechanics, 7, 201-224.

McNitt-Gray, J. (1991b). Kinetics of the lower extremities during drop landings from three heights. Journal of Biomechanics, 26(9), 1037-1046.

Miller, D.I., and Albert, W.J. (1995). Assessing axel performance of Canadian figure skaters: Final Report to Sport Canada.

Miller, D. I, and Albert, W.J. (1994). Angular momentum stategies in axel jumping. Conference Proceedings of the American Society of Biomechanics, October 1994, Ohio State University, Columbus, Ohio, 13 -14.

Miller, D. I. and Nissinen, M.A. (1987). Critical examination of ground reaction force in the running forward somersault. International Journal of Sport Biomechanics, (3), 189-206.

Morlock, M., and Nigg, B.M. (1991). Theoretical considerations and practical results on the influence of the representation of the foot for the estimation of internal forces with models. Clinical Biomechanics, 6, 3-13.

Narici, M.V., Landoni, L., and Minetti, A.E. (1992). Assessment of human knee extensor muscles stress from in vivo physiological cross-sectional area and strength measurements. European Journal of Applied Physiology, 65, 438-444.

Nash, H.L. (1988). US Olympic figure skaters: honing their performances. The Physician and Sportsmedicine, 16(2), 180 - 185.

Niek van Dijk, C., Lim, L.S.L., Poortman, A., Strubbe, E.H., and Marti, R.K. (1995). Degenerative joint disease in female ballet dancers. The American Journal of Sports Medicine, 23(3), 295-300.

Nigg, B.M. and Bobbert, M. (1990). On the potential of various approaches in load analysis to reduce the frequency of sports injuries. Journal of Biomechanics Supplemental, 23(1), 3-12.

Niinimaa, V. (1982). Figure skating: What do we know about it? The Physician and Sportsmedicine, 10(1), 51-56.

Niinimaa, V., Woch, Z.T., Shephard, R.J. (1979). Intensity of physical effort during a free figure skating programme. in Terauds, J. Gross, H.J. (eds) Science in Skiing, Skating, and Hockey. Del Mar, Academic Publishers.

Norman, R.W.K. (1977). The Use of Electromyography in the Calculation of Dynamic Joint Torque. Unpublished doctoral dissertation, Pennsylvania State University at University Park, Pennsylvania.

Norman, R.W. (1989). A barrier to understanding human motion mechanism: A commentary. In Future Directions in Exercise and Sport Science Research (pp 151-161). Champaign, Illinois : Human Kinetics Publishers.

Panzer, V.P. (1987). Lower Extremity Loads in Landings of Elite Gymnasts. Unpublished doctoral dissertation, University of Oregon, Oregon.

Pearsall, D.J., and Reid, J.G. (1994). The study of human body segment parameters in biomechanics: An historical review and current status report. Sports Medicine, 18(2),126-140.

Pecina, M., Bojanic, I., and Dubravcic, S. (1990). Stress fractures in figure skaters. The American Journal of Sports Medicine, 18(3), 277-279.

Pezzack, J.C., and Norman, R.W. (1981). A validation of the joint reaction force and resultant moment output of an 'n' link plane motion model of the human. In Morecki, A.,

Plagenhoef, S., Evans, F.G., and Abdelnour, T. (1983). Anatomical data for analyzing human motion. Research Quarterly for Exercise and Sport, 54(2), 169-178.

Podolsky, A., Kaufman, K.R., Cahalan, T.D., Aleshinsky, S.Y., and Chao, E.Y.S. (1990). The relationship of strength and jump height in figure skaters. The American Journal of Sports Medicine, 18,(4), 400-405.

Roi, G.S., Mevio, M., Occhi, G., Gemma, S., and Facchini, R. (1989). Functional assessment of high level ice-dancing. The Journal of Sports Medicine and Physical Fitness, 29(2), 189-193.

Schot, P., Bates, B., and Dufek, J.S. (1994). Bilateral performance summetry during drop landing: a kinetic analysis. Medicine and Science in Sports and Exercise, 26(9), 1153-1159.

Scott, S.H., and Winter, D.A. (1990). Internal forces at chronic running injury sites. Medicine and Science in Sports and Exercise, 22(3), 357-369.

Simonsen, E.B., Dyhre-Poulsen, P., Voigt, M., Aagaard, P., Sjøgaard, G., and Bojsen-Møller. (1995). Bone-on-bone forces during loaded and unloaded walking. Acta Anatomica, 152, 133-142.

Slemenda, C.W., and Johnston, C.C. (1993). High intensity activities in young women: site specific bone mass effects among female figure skaters. Bone and Mineral, 20, 125-132.

Smith, A.D. (1990). Foot and ankle injuries in figure skaters. The Physician and Sportsmedicine, 18(3), 73-86.

Smith, A.D., and Micheli, L.J. (1982). Injuries in competitive figure skaters. The Physician and Sportsmedicine, 10(1), 36 - 47.

Smith, A.D., and Ludington, R. (1989). Injuries in elite pair skaters and ice dancers. The American Journal of Sports Medicine, 17,(4), 482-488.

Speer, D.P. and Braun, J.K. (1985). The biomechanical basis of growth plate injuries. The Physician and Sportsmedicine, 12(7), 72 - 78.

Sprigings, E.J. (1987). Sport biomechanics: Data collection, modelling, and implementation stages of development. Canadian Journal of Sport Sciences, 13(1), 3-7.

Sutarno, C.G., and McGill, S.M. (1995). Isovelocity investigation of the lengthening behaviour of the erector spinae muscles. European Journal of Applied Physiology, 70, 146-153.

Wells, R.P. (1981). The projection of ground reaction force as a predictor of internal joint moments. Bulletin of Prosthetic Research, 18, 15-19.

Wickiewicz, T.L., Roy, R.R., Powell, P.L., and Edgerton, V.R. (1983). Muscle architecture of the human lower limb. Clinical Orthopaedics and Related Research, 179, 275-283.

Winter, D.A. (1990). Biomechanics and Motor Control of Human Movement (Second Edition). Toronto : Wiley Interscience.

Winter, D.A., and Bishop, P.J. (1992). Lower extremity injury : Biomechanical factors associated with chronic injury to the lower extremity. Sports Medicine, 14(3), 149-156.

Xu, W.S., Butler, D.L., Stouffer, D.C., Grood, E.S., and Glos, D.L. (1992). Theoretical analysis of an implantable force transducer for tendon and ligament structures. Journal of Biomechanical Engineering, 114, 170-177.

Zipp, P. (1982). Recommendations for the standardization of lead positions in surface electromyography. European Journal of Applied Physiology, 50, 41-54.

APPENDIX A

MathCad Computer Programme

A 2-Dimensional, 2-Segment Dynamic Link Segment Model of the Ankle and Knee

Michelle Kho, May, 1996

Based on KINETIC.MCD by John Pezzack and Richard Wells, May 1996

Introduction

This model of the lower limb calculates the bone-on-bone forces at the knee and ankle of dynamic motion. A sagittal view of the subject is digitized.

Filtered co-ordinate data from PeakPerformance is synchronized with force plate data.

Required Input

General constants:

$\pi = 3.142$	pi	**Note:** All units are m, kg, s based
g := 9.81	gravitational constant	
cleg := 0.841	length of cadaver leg	
Ficks := 50	Fick's constant	

Physiological Cross Sectional Areas from Literature:

qcsa1 := 280.1	**Quadriceps** (Narici, Landoni, and Minetti, 1992)
qcsa := qcsa1·Ficks	
hcsa1 := 115	**Hamstrings**
hcsa := hcsa1·Ficks	
dfcsa1 := 18.2	**Dorsiflexors** (Fukunaga, Roy, Shellock, Hodgson, Day, Lee, Kwong-Fu, and Edgerton, 1992)
dfcsa := dfcsa1·Ficks	
pfcsa1 := 326.1	**Plantarflexors** (Fukunaga et al., 1992)
pfcsa := pfcsa1·Ficks	

Hill's Constants: (McGill and Norman, 1988)

Aq := 0.25·qcsa	**Individual muscle constants**
Ah := 0.25·hcsa	
Ad := 0.25·dfcsa	
Ap := 0.25·pfcsa	
BHill := 0.25·3.6	**Hill's constant; Vmax is 3.6 Lo/s**
nonlinear := 1.3	(Cholewicki, McGill, and Norman, 1995)

Data specific constants:

jselected := 1 **frame of interest**

$$skate := \frac{14.246 - 0.0028}{g} \qquad skate = 1.452$$ **Mass of 1 skate**

$$\Delta t := \frac{1}{60}$$ **time between data frames**

nseg := 4 **number of segments being modelled**

npts := nseg + 1 **number of body markers required**

njnts := nseg - 1 **number of body joints modelled**

Anthropometric constants: **(Plagenhof, Evans, and Abdelnour, 1983)**

$$mass := \frac{723.5572 + 5.6944}{g} - 2 \cdot skate$$ **subject's total body mass**

mass = 71.434

subscripts denote segment number where:
2 is the thigh; 3 is the leg; 4 is the foot

segment mass proportion of total body mass

$mp_2 := .105$ $mp_3 := .0475$ $mp_4 := .0143$

proximal proportion of segment length to segment centre of mass

$rp_2 := .433$ $rp_3 := .434$ $rp_4 := .5$

radius of gryration proportion of segment length with respect to proximal

$kp_2 := .54$ $kp_3 := .529$ $kp_4 := .69$

The Link Segment Model

Read the Peak Performance .cda data processed to a .prn file by the peaktabl.bas program (peaktabl.bas program written by John Pezzack, May 1996)

$M := READPRN(small v09)$ — read video data file test.prn into the matrix M

$M := M^T$ — transpose the matrix to suit the application design

$M := M \cdot .01$ — convert coordinates into metres from centimetres

$frames := cols(M)$ $\quad j := 1 .. frames$ — determine number of frames of video data

$time_j := (j - 1) \cdot \Delta t$ — time of frame in seconds

Read the corresponding .prn file of the force plate data for the above video data:

$N := READPRN(sm2lf005)$

Extract the columns of information required:

$$\Delta t2 := \frac{1}{1000}$$

$ftime := rows(N)$ — time array is equal to the number of rows of data

$k := 1 .. ftime$ — determine number of samples of force data

$Time_k := (k - 1) \cdot \Delta t2$ $\quad \Delta t2 = 0.001$

$Fap := N^{<6>}$ — horizontal force is column 6

$Fv := N^{<7>}$ — vertical force is column 7 $\quad Mx := N^{<2>}$

$$CPap_k := if\left(Fv_k > 0, \frac{Mx_k}{Fv_k}, 0\right)$$ — centre of pressure is calculated by dividing the moment by the vertical force; set centre of pressure to zero if Mx or Fv is zero

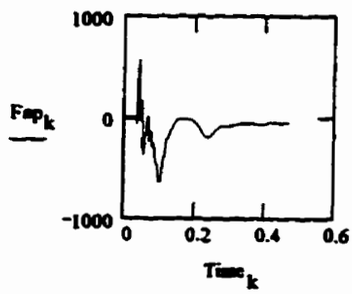

Antero-Postero Force Plate Tracing

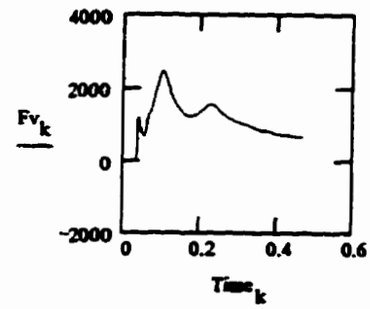

Vertical Force Plate Tracing

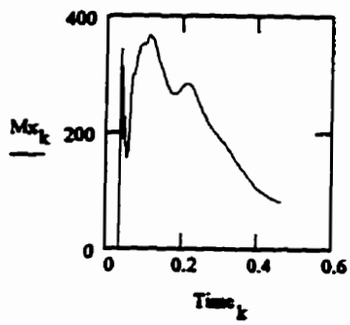

Moment about the x-axis

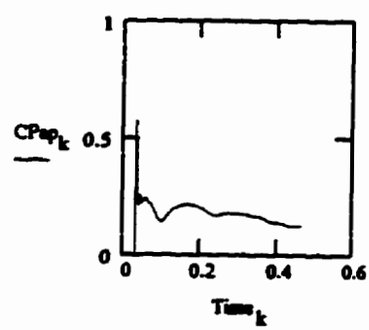

Plot of Centre of Pressure WRT Origin of Force Plate

External force data to be applied to the link segment model (force plate):

$Gx_j := linterp(Time, Fap, time_j)$

$Gy_j := linterp(Time, Fv, time_j)$

$cpx_j := linterp(Time, CPap, time_j)$

linear interpolation is used to estimate the force and centre of pressure at the time of the frame. This is required because the force data was collected at a different sample rate (1000 Hz) than the video (60 Hz).

Filtered (x,y) coordinate data for subject markers centred on the j-th frame

body marker location subscripts:

1 - Shoulder; 2 - hip; 3 - knee; 4 - ankle; 5 - metatarsal

Each frame is extracted from the M matrix of all frames and deposited into the x and y matrices:

$x_{1,j} := M_{1,j}$ $y_{1,j} := M_{2,j}$ **Shoulder marker**

$x_{2,j} := M_{3,j}$ $y_{2,j} := M_{4,j}$ **Hip marker**

$x_{3,j} := M_{5,j}$ $y_{3,j} := M_{6,j}$ **Knee Marker**

$x_{4,j} := M_{7,j}$ $y_{4,j} := M_{8,j}$ **Ankle Marker**

$x_{5,j} := M_{9,j}$ $y_{5,j} := M_{10,j}$ **Metatarsal Marker**

$cpy_j := M_{12,j}$ **Set y-coordinate of CofP to correspond to impact on plate**

$smcpxl := READPRN(smcpxl)$ **Read a matrix that scales CofP from the force plate data with respect to the origin and ankle marker**

$cpx_j := smcpxl_j + x_{4,j}$ **Set x-coordinate of Cof P to scaled value with respect to the ankle marker**

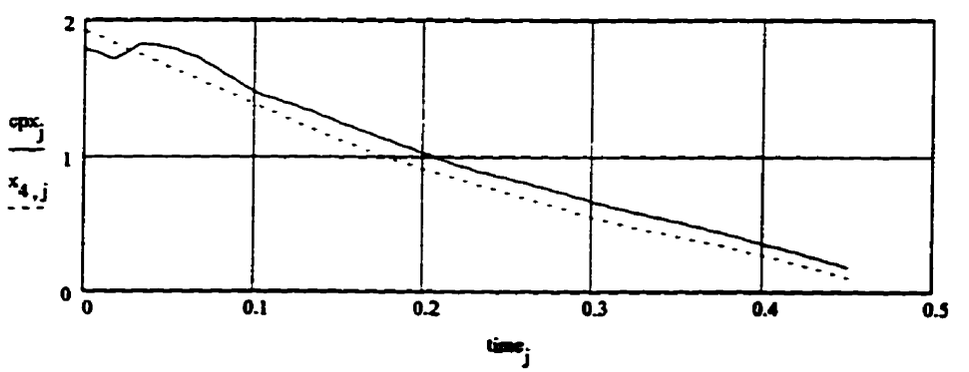

Stick Figure Plot of the Subject every 5 Frames

i := 1 .. npts j := jselected (Frame 1)

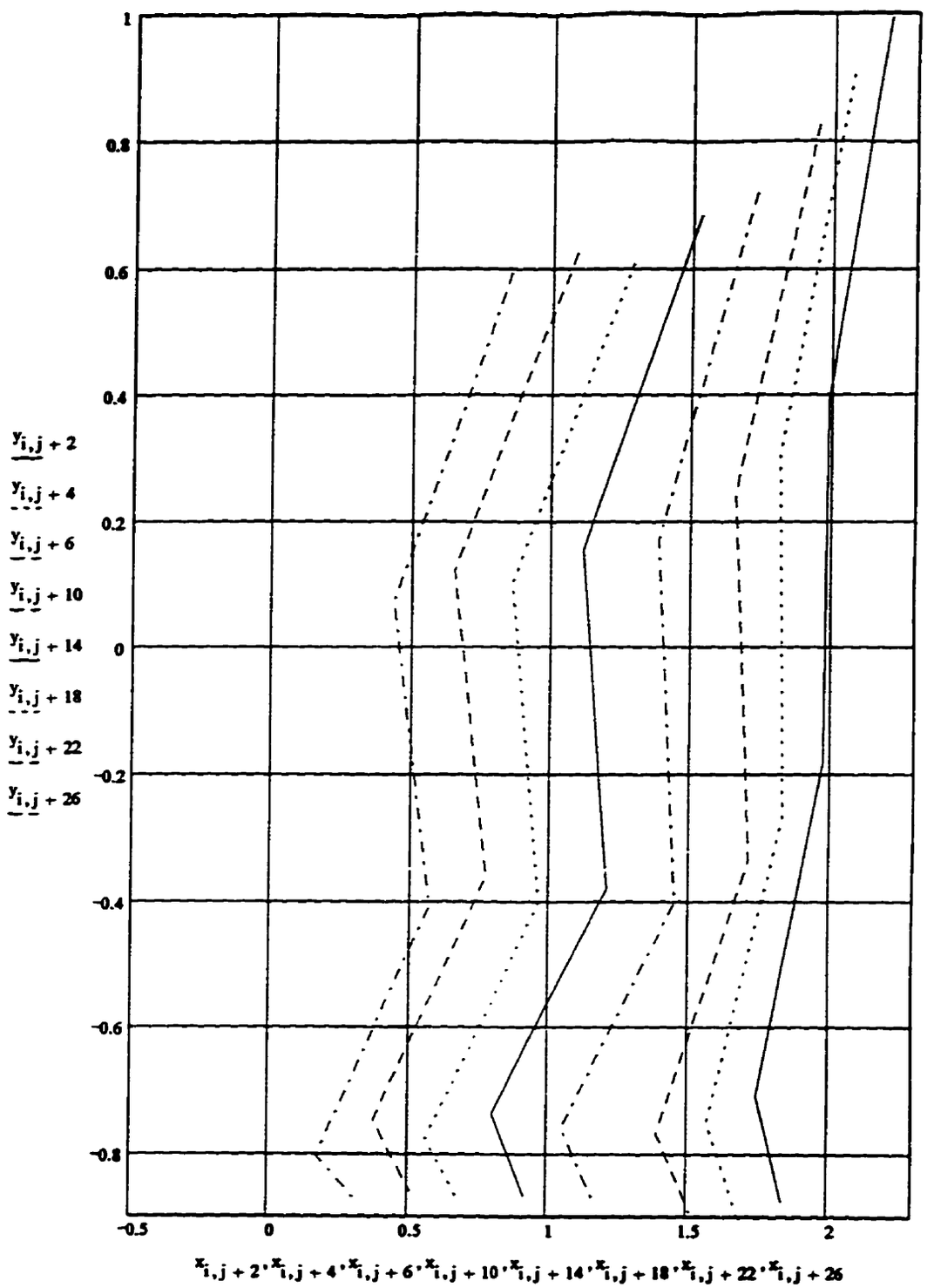

Calculate Marker Kinematics

Calculate the linear velocity (vx,vy) of each body marker (Winter, 1990)

$i := 1 .. npts \quad j := 2 .. frames - 1$

$$vx_{i,j} := \frac{x_{i,j+1} - x_{i,j-1}}{2 \cdot \Delta t} \qquad vy_{i,j} := \frac{y_{i,j+1} - y_{i,j-1}}{2 \cdot \Delta t}$$

Calculate the linear acceleration (ax,ay) of each body marker (Winter, 1990)

$i := 1 .. npts$

$$ax_{i,j} := \frac{x_{i,j+1} - 2 \cdot x_{i,j} + x_{i,j-1}}{\Delta t^2} \qquad ay_{i,j} := \frac{y_{i,j+1} - 2 \cdot y_{i,j} + y_{i,j-1}}{\Delta t^2}$$

Resulting linear kinematics for each body marker

$j := jselected + 2$ **(impact)**

i	$x_{i,j}$	$y_{i,j}$	$vx_{i,j}$	$vy_{i,j}$	$ax_{i,j}$	$ay_{i,j}$
1.000	2.198	0.995	-4.166	-2.736	7.4030	$-4.6800 \cdot 10^{-3}$
2.000	1.984	0.391	-5.221	-2.644	5.5638	7.4070
3.000	1.971	-0.179	-4.768	-2.993	29.0059	16.0459
4.000	1.746	-0.709	-5.390	-1.589	4.9331	17.8988
5.000	1.837	-0.876	-4.367	-1.476	-8.0222	48.7649

Calculate the Absolute Angular Kinematics for each Segment

2 = Thigh; 3 = Shank; 4 = Foot

$i := 2..nseg \qquad j := 2..frames$

Note: All of these values are for each segment WRT horizontal.

$\theta_{i,j} := angle\left(x_{i,j} - x_{i+1,j}, y_{i,j} - y_{i+1,j}\right)$ **Theta for all 3 frames**

$d_{i,j} := \theta_{i,j} \cdot \frac{180}{\pi}$ **Angle in degrees**

$j := 2..frames - 1$

$\omega_{i,j} := \frac{\theta_{i,j+1} - \theta_{i,j-1}}{2 \cdot \Delta t}$ **Omega and Alpha for the j-th frame**

$\alpha_{i,j} := \frac{\theta_{i,j+1} - 2 \cdot \theta_{i,j} + \theta_{i,j-1}}{\Delta t^2}$

$j := 3..frames - 1$

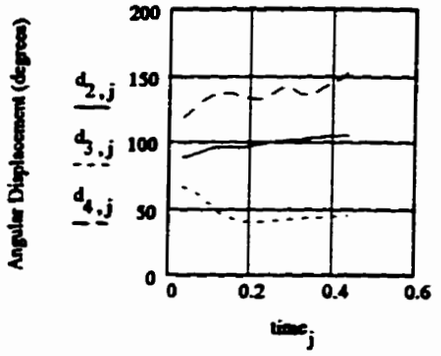

Angular Displacement

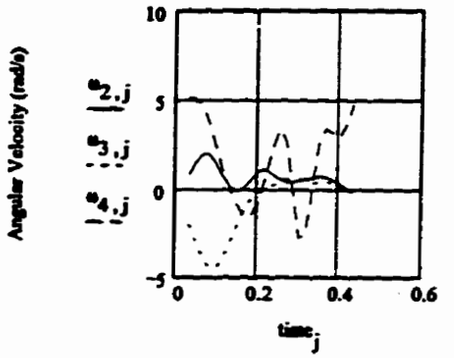

Angular Velocity

d2 = thigh; d3 = shank; d4 = foot

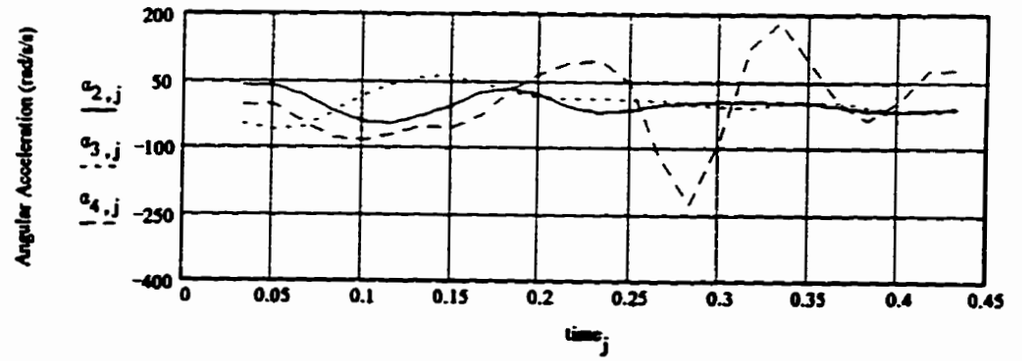

Angular Acceleration

Calculate the Relative Angular Kinematics for each Joint

$i := 1 .. njnts - 1$ **where subscripts indicate: 1 - Knee; 2 - Ankle**

$j := 2 .. frames - 1$

$$r\theta_{1,j} := \pi - \left(\theta_{2,j} - \theta_{3,j}\right) \qquad r\theta_{2,j} := \theta_{4,j} - \theta_{3,j} - \frac{\pi}{2} + 30 \cdot \frac{\pi}{180}$$

$$r\omega_{1,j} := \omega_{2,j} - \omega_{3,j} \qquad r\omega_{2,j} := \omega_{4,j} - \omega_{3,j}$$

$$r\alpha_{1,j} := \alpha_{2,j} - \alpha_{3,j} \qquad r\alpha_{2,j} := \alpha_{4,j} - \alpha_{3,j}$$

$$dr\theta_{1,j} := \left[\pi - \left(\theta_{2,j} - \theta_{3,j}\right)\right] \cdot \frac{180}{\pi} \qquad dr\theta_{2,j} := \left(\theta_{4,j} - \theta_{3,j} - \frac{\pi}{2} + 30 \cdot \frac{\pi}{180}\right) \cdot \frac{180}{\pi}$$

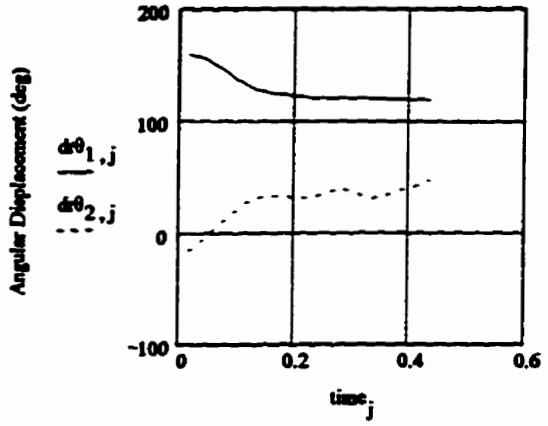

Angular Displacement

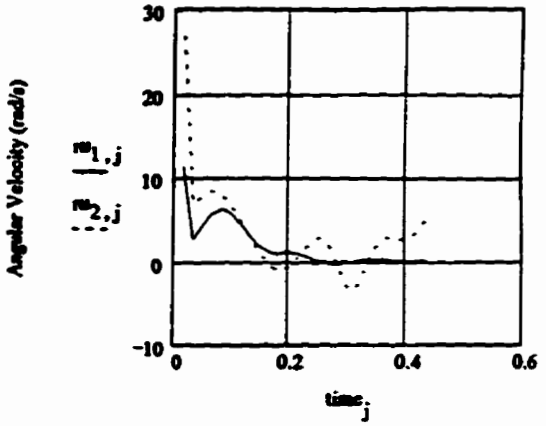

Angular Velocity

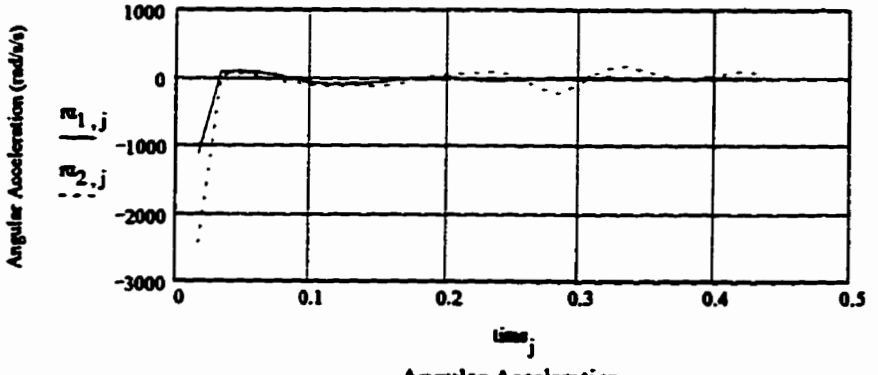

Angular Acceleration

Anthropometric Calculations for each Body Segment

$i := 2..nseg$

$m_i := mp_i \cdot mass$ — **Segment mass** $m_4 = 1.022$

$m_4 := m_4 + skate$ — **Foot and skate mass** $m_4 = 2.473$

$l_i := \sqrt{(x_{i+1,j} - x_{i,j})^2 + (y_{i+1,j} - y_{i,j})^2}$ — **Segment length**

$r_i := rp_i \cdot l_i$ — **Radius to segment centre from proximal end**

$\rho_i := kp_i \cdot l_i$ — **Radius of gyration with respect to the proximal end of the segment**

$dc_2 := l_2 \cdot (kp_2 - .433)$ — **Distance correction for radius of gyration for thigh (2), shank (3), and foot (4)**

$dc_3 := l_3 \cdot (kp_3 - .434)$

$dc_4 := l_4 \cdot (kp_4 - .5)$

$I_i := m_i \cdot (\rho_i)^2$ — **Moment of inertia about proximal end of segment**

$Icorr_i := I_i - m_i \cdot (dc_i)^2$ — **Corrected moment of inertia wrt Centre of Mass**

Table of body segment anthropometric values:

2 = thigh; 3 = shank; 4 = foot and skate

i	m_i	mp_i	l_i	r_i	rp_i	ρ_i	kp_i	$Icorr_i$
2.000	7.501	0.105	0.499	0.216	0.433	0.269	0.540	0.523
3.000	3.393	0.048	0.557	0.242	0.434	0.295	0.529	0.286
4.000	2.473	0.014	0.169	0.085	0.500	0.117	0.690	0.031

Calculation of Body Segment Centres of Mass and their Kinematics

Segment centre of mass position:

$j := 1 .. frames$

$$xcm_{i,j} := x_{i,j} + rp_i \cdot (x_{i+1,j} - x_{i,j}) \qquad ycm_{i,j} := y_{i,j} + rp_i \cdot (y_{i+1,j} - y_{i,j})$$

Segment centre of mass linear velocity:

$j := 2 .. frames - 1$

$$vxcm_{i,j} := \frac{xcm_{i,j+1} - xcm_{i,j-1}}{2 \cdot \Delta t} \qquad vycm_{i,j} := \frac{ycm_{i,j+1} - ycm_{i,j-1}}{2 \cdot \Delta t}$$

Segment centre of mass linear acceleration:

$$axcm_{i,j} := \frac{xcm_{i,j+1} - 2 \cdot xcm_{i,j} + xcm_{i,j-1}}{\Delta t^2} \quad aycm_{i,j} := \frac{ycm_{i,j+1} - 2 \cdot ycm_{i,j} + ycm_{i,j-1}}{\Delta t^2}$$

Table of body segment centre of mass kinematics:

j = jselected + 2

i	$xcm_{i,j}$	$ycm_{i,j}$	$vxcm_{i,j}$	$vycm_{i,j}$	$axcm_{i,j}$	$aycm_{i,j}$
2.000	1.979	0.144	-5.025	-2.795	15.714	11.148
3.000	1.874	-0.409	-5.038	-2.384	18.558	16.850
4.000	1.792	-0.793	-4.878	-1.533	-1.545	33.332

Calculation of the centre of mass of the linkage system

$$X = \frac{\sum_i xcm_{i,j} \cdot m_i}{\sum_i m_i} \qquad Y = \frac{\sum_i ycm_{i,j} \cdot m_i}{\sum_i m_i}$$

Linkage system centre of mass:

X = 1.917 Y = -0.170

Calculation of Joint Reaction Forces and Moments

$i := nseg \qquad j := 2 .. frames - 1 \qquad i = 4.000$ **For the proximal end of each segment**

$$Rx_{i,j} := m_i \cdot axcm_{i,j} - Gx_j$$

$$Ry_{i,j} := m_i \cdot aycm_{i,j} + m_i \cdot g - Gy_j$$

Foot dealing with ground reaction forces –must be special

$$JM_{i,j} := Icorr_i \cdot \alpha_{i,j} + Gx_j \cdot (cpy_j - ycm_{i,j}) - Gy_j \cdot (cpx_j - xcm_{i,j}) + Rx_{i,j} \cdot (y_{i,j} - ycm_{i,j}) - Ry_{i,j} \cdot (x_{i,j} - xcm_{i,j})$$

$i := nseg - 1 .. 1$ **For the balance of the segments, from 2nd segment to first, ie up to knee**

$$Rx_{i,j} := m_i \cdot axcm_{i,j} + Rx_{i+1,j}$$

$$Ry_{i,j} := m_i \cdot aycm_{i,j} + Ry_{i+1,j} + m_i \cdot g$$

$$JM_{i,j} := Icorr_i \cdot \alpha_{i,j} - Rx_{i+1,j} \cdot (y_{i+1,j} - ycm_{i,j}) + Ry_{i+1,j} \cdot (x_{i+1,j} - xcm_{i,j}) + Rx_{i,j} \cdot (y_{i,j} - ycm_{i,j}) - Ry_{i,j} \cdot (x_{i,j} - x$$

Net Joint Reaction Force

$j := 2 .. frames - 1$

$i := 2 - nseg .. 1$

$$Rxy_{3,j} := \sqrt{(Rx_{3,j})^2 + (Ry_{3,j})^2} \qquad Rxy_{4,j} := \sqrt{(Rx_{4,j})^2 + (Ry_{4,j})^2}$$

Joint Reaction Forces WRT BW

$$Rxybw_{3,j} := \frac{Rxy_{3,j}}{mass \cdot g} \qquad Rxybw_{4,j} := \frac{Rxy_{4,j}}{mass \cdot g}$$

Graphs of Joint Reaction Forces and Moments

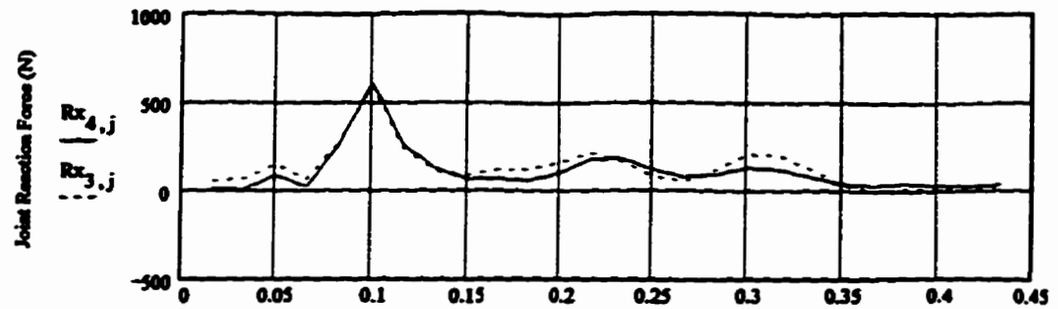

Joint Reaction Force (X)

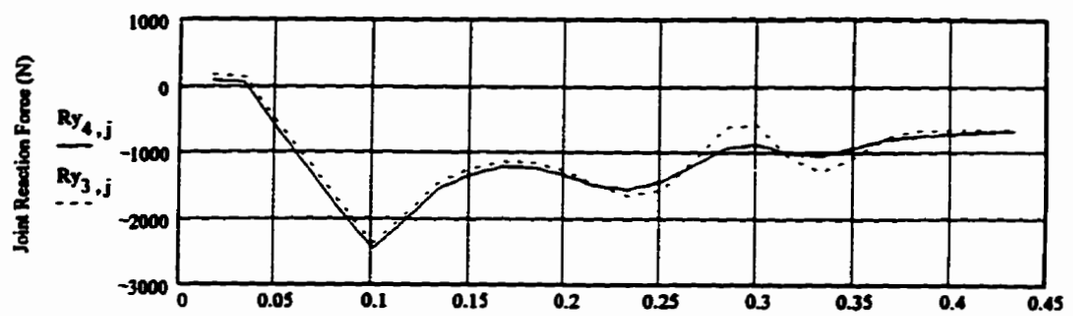

Joint Reaction Force (Y)

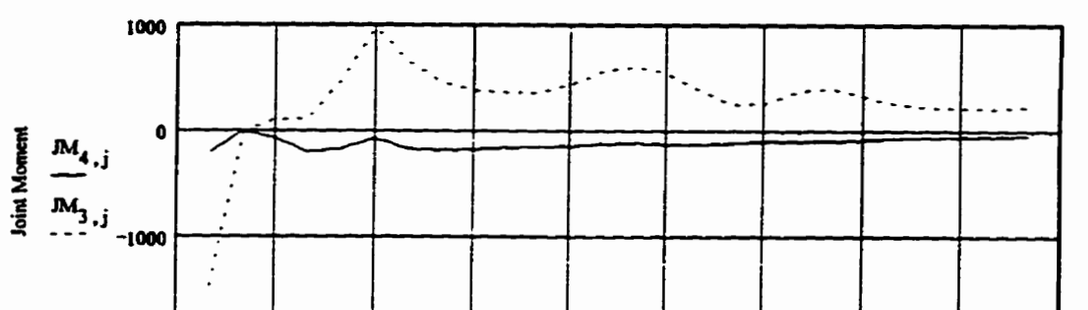

Joint Moment (Nm)

Graphs of Resultant Joint Reaction Forces and Moments

j = jselected

i = 1.. npts

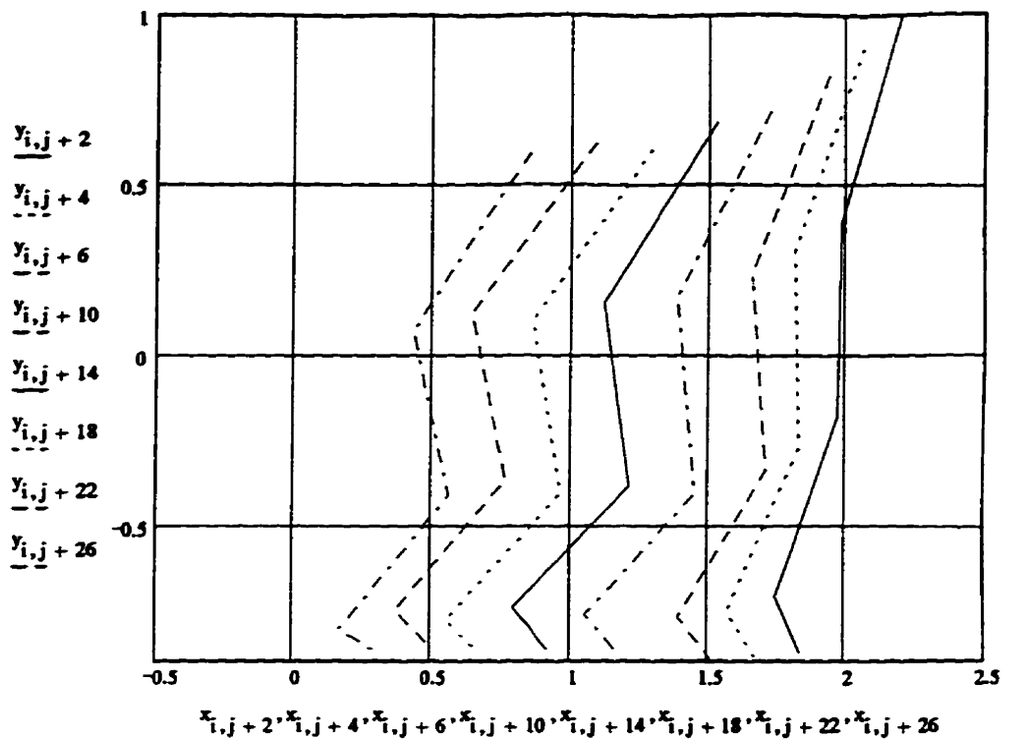

j := 2.. frames - 1

i := nseg

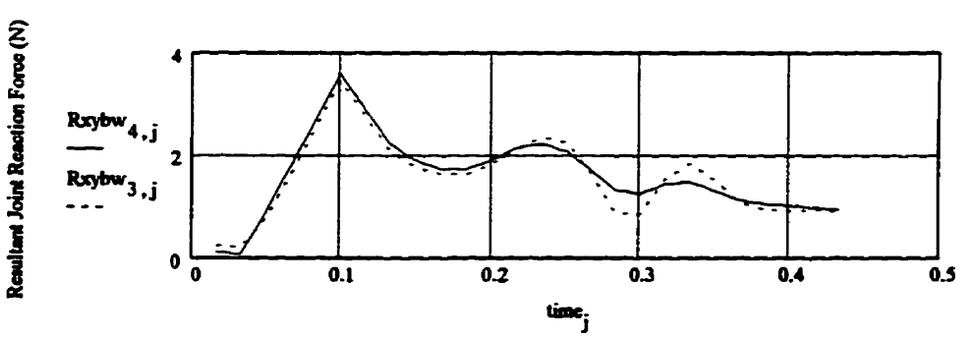

Resultant Joint Reaction Force (wrt BW)

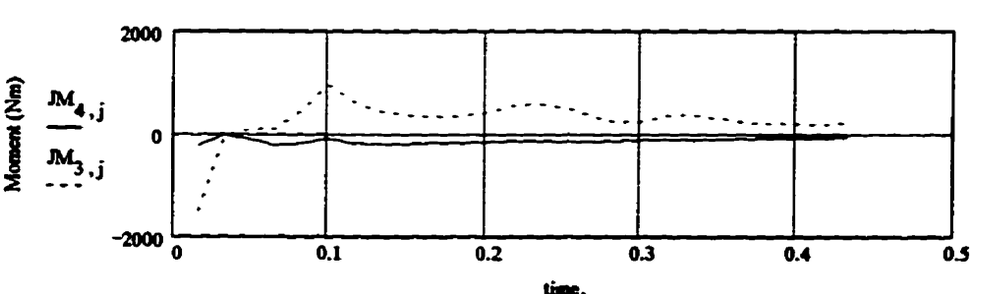

Joint Moment (4 = ankle; 3 = knee)

Now, we're on our way to calculating bone-on-bone forces.....

The Anatomical Model

1. Relate joint position to individual muscle group moment arm lengths:

$Q := READPRN(quads)$

$d := rows(Q)$

$da := 1..d \qquad qangle := Q^{<3>} \qquad qarm := Q^{<2>} \cdot .01 \qquad qmal_j := linterp(qangle, qarm, r\theta_{1,j})$

$B := READPRN(biceps)$

$h := rows(B) \qquad h = 19.000$

$ha := 1..h \qquad bangle := B^{<3>} \qquad barm := B^{<2>} \cdot .01 \qquad bmal_j := linterp(bangle, barm, r\theta_{1,j})$

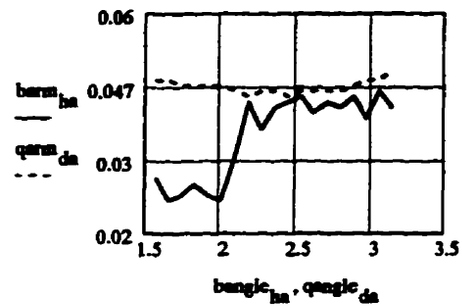

Moment Arms changing with respect to knee angle (rads) (measured from cadaver)

Note: Biceps moment arm changes confirmed on cadaver.

$T := READPRN(tibant)$

$t := rows(T) \qquad t = 15.000$

$ta := 1..t \qquad tangle := T^{<4>} \qquad tarm := T^{<3>} \cdot .01 \qquad tmal_j := linterp(tangle, tarm, r\theta_{2,j})$

$G := READPRN(gastrocs)$

$g := rows(G) \qquad g = 15.000$

$ga := 1..g \qquad gangle := G^{<4>} \qquad garm := G^{<3>} \cdot .01 \qquad gmal_j := linterp(gangle, garm, r\theta_{2,j})$

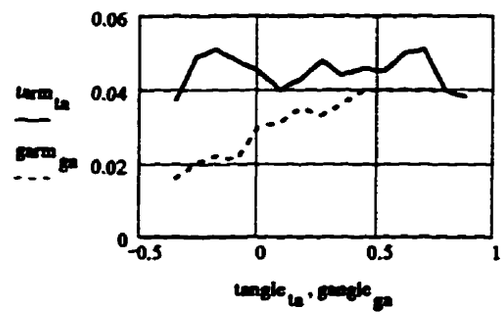

Moment Arms changing with respect to ankle angle (measured from cadaver)

2. Express moment arm lengths scaled to the subject as a function of leg length (femur + fibula):

$sleg := l_2 + l_3$ $\quad sleg = 1.056$

$tmal_j := \frac{tmal_j}{cleg} \cdot (sleg)$ $\quad gmal_j := \frac{gmal_j}{cleg} \cdot (sleg)$ $\quad qmal_j := \frac{qmal_j}{cleg} \cdot (sleg)$ $\quad bmal_j := \frac{bmal_j}{cleg} \cdot (sleg)$

Plot of Changing Moment Arm Lengths during trial:

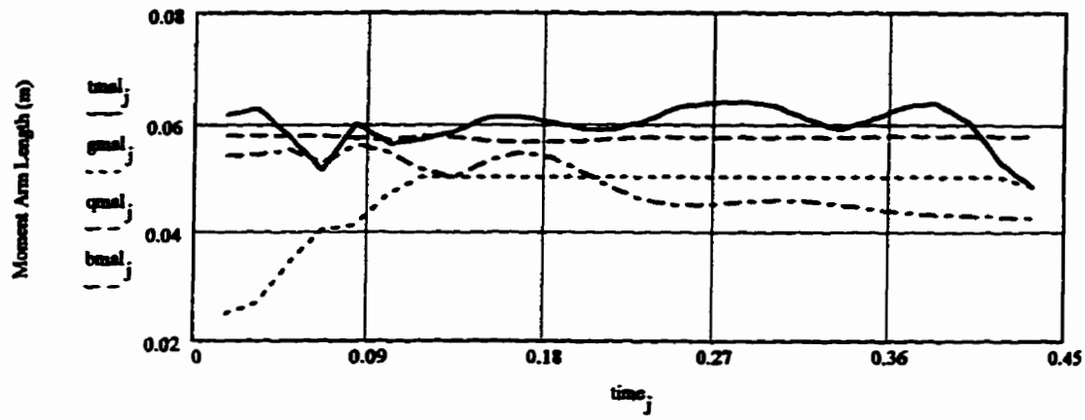

Scaled Moment Arm Excursions

3. Muscle Origin-Insertion Co-ordinates:

a) Biceps Femoris - Representative of Hamstrings

HamOx := 0.081·sleg·(-1) $\quad$ HamOy := 0.069·sleg·(-1)

HamKx := 0.034·sleg·(-1) $\quad$ HamKy := 0

HamIx := 0.054·sleg·(-1) $\quad$ HamIy := 0.036·sleg·(-1)

b) Vastus Lateralis - Representative of Quadriceps

QuadOx := 0.03·sleg $\quad$ QuadOy := 0

QuadKx := 0.054·sleg $\quad$ QuadKy := 0

QuadIx := 0.054·sleg $\quad$ QuadIy := 0.063·sleg·(-1)

c) Tibialis Anterior - Representative of Ankle Dorsi Flexors

TibOx := 0 $\quad$ TibOy := 0.099·sleg·(-1)

TibAx := 0.042·sleg $\quad$ TibAy := 0.044·sleg

TibIx := 0 $\quad$ TibIy := 0.068·sleg·(-1)

d) Lateral Gastrocnemius - Representative of Ankle Plantar Flexors and Knee Flexors

GasOx := 0.027·sleg·(-1) $\quad$ GasOy := 0.036·sleg

GasAx := 0.034·sleg·(-1) $\quad$ GasAy := 0

GasIx := 0.061·sleg·(-1) $\quad$ GasIy := 0.019·sleg·(-1)

4. Rotate the coordinates to account for segment angle:

$\psi_{2,j} := \theta_{2,j} - \frac{\pi}{2}$ $\psi_{3,j} := \theta_{3,j} - \frac{\pi}{2}$ $\psi_{4,j} := \theta_{4,j} - \frac{\pi}{2}$ **Correct point to vertical wrt segment angle**

a) **Biceps Femoris**

$RHamOx_j := HamOx \cdot \cos(\psi_{2,j}) - HamOy \cdot \sin(\psi_{2,j})$ $RHamOy_j := HamOx \cdot \sin(\psi_{2,j}) + HamOy \cdot \cos(\psi_{2,j})$

$RHamKx_j := HamKx \cdot \cos(\psi_{2,j}) - HamKy \cdot \sin(\psi_{2,j})$ $RHamKy_j := HamKx \cdot \sin(\psi_{2,j}) + HamKy \cdot \cos(\psi_{2,j})$

$RHamIx_j := HamIx \cdot \cos(\psi_{3,j}) - HamIy \cdot \sin(\psi_{3,j})$ $RHamIy_j := HamIx \cdot \sin(\psi_{3,j}) + HamIy \cdot \cos(\psi_{3,j})$

b) **Vastus Lateralis**

$RQuadOx_j := QuadOx \cdot \cos(\psi_{2,j}) - QuadOy \cdot \sin(\psi_{2,j})$ $RQuadOy_j := QuadOx \cdot \sin(\psi_{2,j}) + QuadOy \cdot \cos(\psi_{2,j})$

$RQuadKx_j := QuadKx \cdot \cos(\psi_{3,j}) - QuadKy \cdot \sin(\psi_{3,j})$ $RQuadKy_j := QuadKx \cdot \sin(\psi_{3,j}) + QuadKy \cdot \cos(\psi_{2,j})$

$RQuadIx_j := QuadIx \cdot \cos(\psi_{3,j}) - QuadIy \cdot \sin(\psi_{3,j})$ $RQuadIy_j := QuadIx \cdot \sin(\psi_{3,j}) + QuadIy \cdot \cos(\psi_{3,j})$

c) **Tibialis Anterior**

$RTibOx_j := TibOx \cdot \cos(\psi_{3,j}) - TibOy \cdot \sin(\psi_{3,j})$ $RTibOy_j := TibOx \cdot \sin(\psi_{3,j}) + TibOy \cdot \cos(\psi_{3,j})$

$RTibMx_j := TibAx \cdot \cos(\psi_{4,j}) - TibAy \cdot \sin(\psi_{4,j})$ $RTibMy_j := TibAx \cdot \sin(\psi_{4,j}) + TibAy \cdot \cos(\psi_{4,j})$

$RTibIx_j := TibIx \cdot \cos(\psi_{4,j}) - TibIy \cdot \sin(\psi_{4,j})$ $RTibIy_j := TibIx \cdot \sin(\psi_{4,j}) + TibIy \cdot \cos(\psi_{4,j})$

d) **Lateral Gastrocnemius**

$RGasOx_j := GasOx \cdot \cos(\psi_{2,j}) - GasOy \cdot \sin(\psi_{2,j})$ $RGasOy_j := GasOx \cdot \sin(\psi_{2,j}) + GasOy \cdot \cos(\psi_{2,j})$

$RGasAx_j := GasAx \cdot \cos(\psi_{3,j}) - GasAy \cdot \sin(\psi_{3,j})$ $RGasAy_j := GasAx \cdot \sin(\psi_{3,j}) + GasAy \cdot \cos(\psi_{3,j})$

$RGasIx_j := GasIx \cdot \cos(\psi_{4,j}) - GasIy \cdot \sin(\psi_{4,j})$ $RGasIy_j := GasIx \cdot \sin(\psi_{4,j}) + GasIy \cdot \cos(\psi_{4,j})$

5. Transform to Global Co-ordinate system:

a) **Biceps Femoris**

$FHamOx_j := x_{2,j} + RHamOx_j$ $FHamOy_j := y_{2,j} + RHamOy_j$

$FHamKx_j := x_{3,j} + RHamKx_j$ $FHamKy_j := y_{3,j} + RHamKy_j$

$FHamIx_j := x_{3,j} + RHamIx_j$ $FHamIy_j := y_{3,j} + RHamIy_j$

b) **Vastus Lateralis**

$FQuadOx_j := x_{2,j} + RQuadOx_j$ $FQuadOy_j := y_{2,j} + RQuadOy_j$

$FQuadKx_j := x_{3,j} + RQuadKx_j$ $FQuadKy_j := y_{3,j} + RQuadKy_j$

$FQuadIx_j := x_{3,j} + RQuadIx_j$ $FQuadIy_j := y_{3,j} + RQuadIy_j$

c) Tibialis Anterior

$FTibOx_j := x_{3,j} + RTibOx_j$ $\quad FTibOy_j := y_{3,j} + RTibOy_j$

$FTibMx_j := x_{4,j} + RTibMx_j$ $\quad FTibMy_j := y_{4,j} + RTibMy_j$

$FTibIx_j := x_{4,j} + RTibIx_j$ $\quad FTibIy_j := y_{4,j} + RTibIy_j$

d) Lateral Gastrocnemius

$FGasOx_j := x_{3,j} + RGasOx_j$ $\quad FGasOy_j := y_{3,j} + RGasOy_j$

$FGasAx_j := x_{3,j} + RGasAx_j$ $\quad FGasAy_j := y_{3,j} + RGasAy_j$

$FGasIx_j := x_{4,j} + RGasIx_j$ $\quad FGasIy_j := y_{4,j} + RGasIy_j$

6. Normalize Muscle Length to Rest Length (Lo):

Read Measured Cadaver Muscle Lengths and scale to Subject:

i) Quadriceps Length:

QL := READPRN(lquads) $\quad$ q := rows(QL) $\quad$ qa := 1 .. q

$qangle := QL^{<3>}$ $\quad qlength := \frac{QL^{<2>} \cdot .01}{cleg} \cdot sleg$

ii) Hamstrings Length:

HL := READPRN(lhams) $\quad$ $hangle := HL^{<3>}$ $\quad hlength := \frac{HL^{<2>} \cdot .01}{cleg} \cdot sleg$

iii) Tibialis Anterior Length:

TL := READPRN(ltibant)

$tangle := TL^{<3>}$ $\quad tlength := \frac{TL^{<2>} \cdot .01}{cleg} \cdot sleg$

iv) Gastrocnemius Length:

GAL := READPRN(lgasta)

$gaangle := GAL^{<3>}$ $\quad galength := \frac{GAL^{<2>} \cdot .01}{cleg} \cdot sleg$

Gastrocnemius length with knee angle fixed at 130 degrees and changing ankle angle

GKL := READPRN(lgastk)

$gkangle := GKL^{<3>}$ $\quad gklength := \frac{GKL^{<2>} \cdot .01}{cleg} \cdot sleg$

Gastrocnemius length with ankle angle fixed at 140 degrees and changing knee angle

Determine Rest Length of Muscle:

Rest Lengths based on knee angle (quadriceps and hamstrings) and ankle angle (tibialis anterior and gastrocnemius), Galea, 1983

LoQuads := linterp(qangle, qlength, 131·deg) $\quad$ LoQuads = 0.698

LoHams := linterp(hangle, hlength, 131·deg) $\quad$ LoHams = 0.503

LoGas := linterp(gkangle, gklength, 140·deg) $\quad$ LoGas = 0.509

LoTib := linterp(tangle, tlength, 140·deg) $\quad$ LoTib = 0.476

Interpolated Muscle Lengths as a function of Rest Length through Joint Range of Motion:

$$IQuads_j := linterp\left(qangle, \frac{qlength}{LoQuads}, r\theta_{1,j}\right)$$

$$IHams_j := linterp\left(hangle, \frac{hlength}{LoHams}, r\theta_{1,j}\right)$$

$$ITib_j := linterp\left(tangle, \frac{tlength}{LoTib}, r\theta_{2,j}\right)$$

$$IGask_j := linterp\left(gkangle, gklength, r\theta_{1,j}\right)$$

$$IGasa_j := linterp\left(gaangle, galength, r\theta_{2,j}\right)$$

$$\Delta Gas_j := \left|IGasa_j - LoGas\right| - \left|IGask_j - LoGas\right|$$

$$IGas_j := \frac{LoGas + \Delta Gas_j}{LoGas}$$

Muscle Velocities as a function of Rest Length:

$j := 2 .. frames - 2$

$$vQuads_j := \frac{IQuads_{j+1} - IQuads_{j-1}}{2 \cdot \Delta t}$$

$$vHams_j := \frac{IHams_{j+1} - IHams_{j-1}}{2 \cdot \Delta t}$$

$$vGas_j := \frac{IGas_{j+1} - IGas_{j-1}}{2 \cdot \Delta t}$$

$$vTib_j := \frac{ITib_{j+1} - ITib_{j-1}}{2 \cdot \Delta t}$$

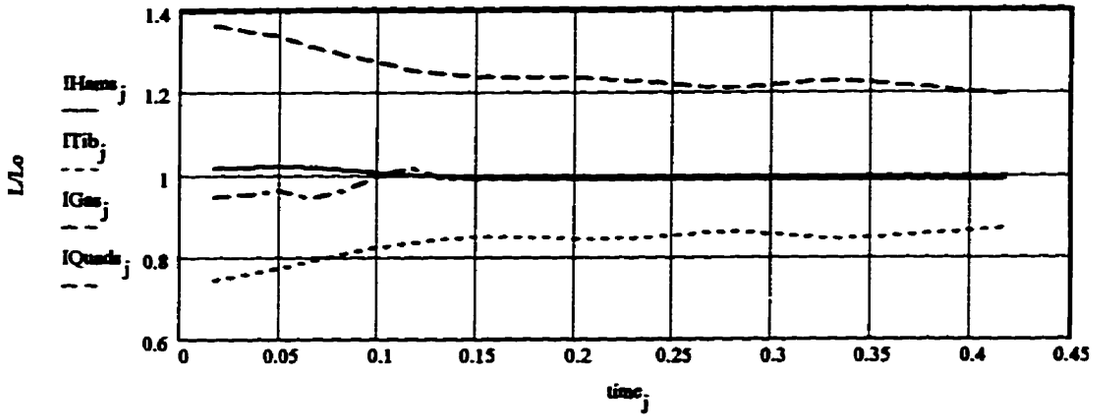

Muscle Excursion Lengths Over Time

$j := 3 .. frames - 2$

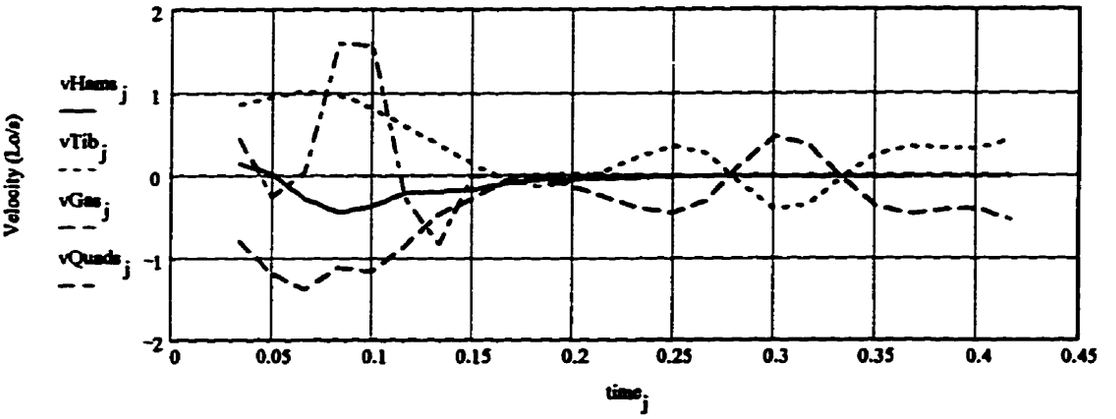

Muscle Velocities

The Muscle Model

(McGill and Norman, 1986; updated 1995)

1. Read processed and filtered EMG files (normalized to % MVC)

$M := READPRN(smsle009)$

$mtime := rows(M)$ $\quad mtime = 467.000$

$vastus := M^{\langle 2 \rangle}$ $\quad tibant := M^{\langle 3 \rangle}$ $\quad biceps := M^{\langle 4 \rangle}$ $\quad gastrocs := M^{\langle 5 \rangle}$

$vastus_j := linterp(Time, vastus, time_j)$ $\quad biceps_j := linterp(Time, biceps, time_j)$

$tibant_j := linterp(Time, tibant, time_j)$ $\quad gastrocs_j := linterp(Time, gastrocs, time_j)$

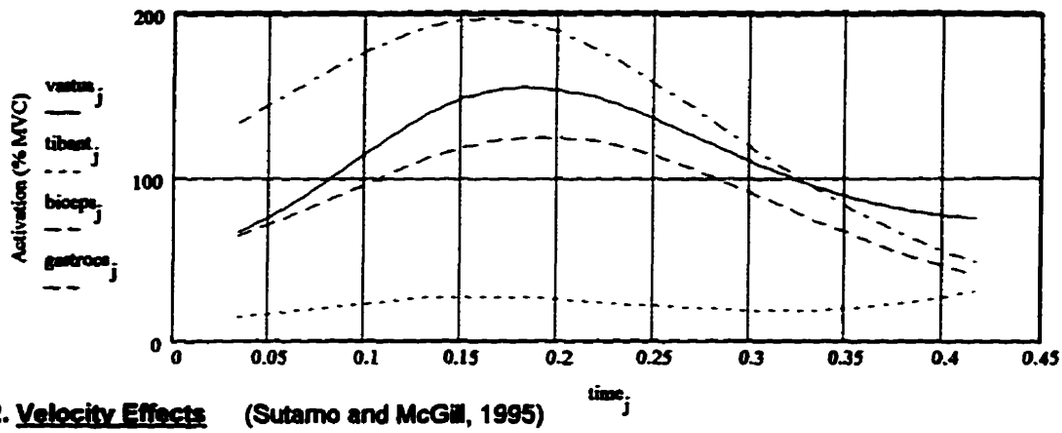

2. Velocity Effects (Sutamo and McGill, 1995)

a) Quadriceps

$$\beta q_j = \frac{qcsa \cdot BHill - (|vQuads_j| \cdot Aq)}{(|vQuads_j| + BHill) \cdot qcsa}$$

The β value is calculated for all velocities, but only used if the muscle is less than 60% active.

$$velaugq_j = \begin{cases} 1.6 \cdot vQuads_j + 1 & \text{if } vastus_j > 80 \text{ and } vQuads_j < 0.125 \\ 1.2 & \text{if } vastus_j > 80 \text{ and } vQuads_j \geq 0.125 \\ \left(\beta q_j + \frac{1 - \beta q_j}{2}\right) & \text{if } vastus_j \leq 60 \\ \beta q_j & \text{if } vQuads_j < 0 \\ 1 & \text{otherwise} \end{cases}$$

b. Tibialis Anterior

$$\beta d_j = \frac{dfcsa \cdot BHill - |vTib_j| \cdot Ad}{(|vTib_j| + BHill) \cdot dfcsa}$$

$$velaugd_j = \begin{cases} 1.6 \cdot vTib_j + 1 & \text{if } tibant_j > 80 \text{ and } vTib_j < 0.125 \\ 1.2 & \text{if } tibant_j > 80 \text{ and } vTib_j \geq 0.125 \\ \left(\beta d_j + \frac{1 - \beta d_j}{2}\right) & \text{if } tibant_j \leq 60 \\ \beta d_j & \text{if } vTib_j < 0 \\ 1 & \text{otherwise} \end{cases}$$

c. Biceps Femoris

$$\beta h_j := \frac{hcsa \cdot BHill - |vHams_j| \cdot Ah}{(|vHams_j| + BHill) \cdot hcsa}$$

$$velaugh_j := \begin{cases} 1.6 \cdot vHams_j + 1 \text{ if } \begin{cases} biceps_j > 80 \\ vHams_j < 0.125 \end{cases} \\ 1.2 \text{ if } \begin{cases} biceps_j > 80 \\ vHams_j \geq 0.125 \end{cases} \\ \left(\beta h_j + \frac{1 - \beta h_j}{2}\right) \text{ if } biceps_j \leq 60 \\ \beta h_j \text{ if } vHams_j < 0 \\ 1 \text{ otherwise} \end{cases}$$

d. Lateral Gastrocnemius

$$\beta p_j := \frac{pfcsa \cdot BHill - |vGas_j| \cdot Ap}{(|vGas_j| + BHill) \cdot pfcsa}$$

$$velaugp_j := \begin{cases} 1.6 \cdot vGas_j + 1 \text{ if } \begin{cases} gastrocs_j > 80 \\ vGas_j < 0.125 \end{cases} \\ 1.2 \text{ if } \begin{cases} gastrocs_j > 80 \\ vGas_j \geq 0.125 \end{cases} \\ \left(\beta p_j + \frac{1 - \beta p_j}{2}\right) \text{ if } gastrocs_j \leq 60 \\ \beta p_j \text{ if } vGas_j < 0 \\ 1 \text{ otherwise} \end{cases}$$

3. Length Effects

a) Quadriceps

$$lenaugq_j := \begin{cases} 0 \text{ if } IQuads_j < 0.5 \\ \sin\left[\pi \cdot (IQuads_j - 0.5)\right] \text{ if } IQuads_j < 1.1 \\ 0.95 \text{ if } IQuads_j = 1.1 \\ (-1.092 \cdot IQuads_j + 2.15) \text{ if } IQuads_j > 1.1 \\ 0 \text{ if } IQuads_j > 1.97 \end{cases}$$

b) Tibialis Anterior

$$lenaugd_j := \begin{cases} 0 \text{ if } ITib_j < 0.5 \\ \sin\left[\pi \cdot (ITib_j - 0.5)\right] \text{ if } ITib_j < 1.1 \\ 0.95 \text{ if } ITib_j = 1.1 \\ (-1.092 \cdot ITib_j + 2.15) \text{ if } ITib_j > 1.1 \\ 0 \text{ if } ITib_j > 1.97 \end{cases}$$

c) Hamstrings

$$lenaugh_j := \begin{cases} 0 \text{ if } IHams_j < 0.5 \\ \sin\left[\pi \cdot (IHams_j - 0.5)\right] \text{ if } IHams_j < 1.1 \\ 0.95 \text{ if } IHams_j = 1.1 \\ (-1.092 \cdot IHams_j + 2.15) \text{ if } IHams_j > 1.1 \\ 0 \text{ if } IHams_j > 1.97 \end{cases}$$

d) Gastrocnemius

$$lenaugp_j := \begin{cases} 0 \text{ if } IGas_j < 0.5 \\ \sin\left[\pi \cdot (IGas_j - 0.5)\right] \text{ if } IGas_j < 1.1 \\ 0.95 \text{ if } IGas_j = 1.1 \\ (-1.092 \cdot IGas_j + 2.15) \text{ if } IGas_j > 1.1 \\ 0 \text{ if } IGas_j > 1.97 \end{cases}$$

4. Passive Effects (Deng and Goldsmith, 1987)

a) Quadriceps

$$pql_j := \begin{cases} 0 & \text{if } IQuads_j < 1 \\ \dfrac{qcsa1 \cdot (IQuads_j - 1) \cdot 4.28 \cdot 0.981}{\left(1 - \dfrac{IQuads_j - 1}{0.7}\right)} & \text{otherwise} \end{cases}$$

b) Tibialis Anterior

$$pdl_j := \begin{cases} 0 & \text{if } ITib_j < 1 \\ \dfrac{dfcsa1 \cdot (ITib_j - 1) \cdot 4.28 \cdot 0.981}{\left(1 - \dfrac{ITib_j - 1}{0.7}\right)} & \text{otherwise} \end{cases}$$

c) Hamstrings

$$phl_j := \begin{cases} 0 & \text{if } IHams_j < 1 \\ \dfrac{hcsa1 \cdot (IHams_j - 1) \cdot 4.28 \cdot 0.981}{\left(1 - \dfrac{IHams_j - 1}{0.7}\right)} & \text{otherwise} \end{cases}$$

d) Gastrocnemius

$$ppl_j := \begin{cases} 0 & \text{if } IGas_j < 1 \\ \dfrac{pfcsa1 \cdot (IGas_j - 1) \cdot 4.28 \cdot 0.981}{\left(1 - \dfrac{IGas_j - 1}{0.7}\right)} & \text{otherwise} \end{cases}$$

5. Force (Mullender, 1991; Cholewicki and McGill, 1995)

a) Quadriceps

$$Fq_j := qcsa \cdot \left(\frac{vastus_j}{100}\right)^{\frac{1}{nonlinear}}$$

b) Tibialis Anterior

$$Fd_j := dfcsa \cdot \left(\frac{tibant_j}{100}\right)^{\frac{1}{nonlinear}}$$

c) Hamstrings

$$Fh_j := hcsa \cdot \left(\frac{biceps_j}{100}\right)^{\frac{1}{nonlinear}}$$

d) Gastrocnemius

$$Fp_j := pfcsa \cdot \left(\frac{gastrocs_j}{100}\right)^{\frac{1}{nonlinear}}$$

6. MuscleForce!!

$$Forceq_j := Fq_j \cdot lenaugq_j \cdot velaugq_j + pql_j$$

$$Forced_j := Fd_j \cdot velaugd_j \cdot lenaugd_j + pdl_j$$

$$Forceh_j := Fh_j \cdot velaugh_j \cdot lenaugh_j + phl_j$$

$$Forcep_j := Fp_j \cdot velaugp_j \cdot lenaugp_j + ppl_j$$

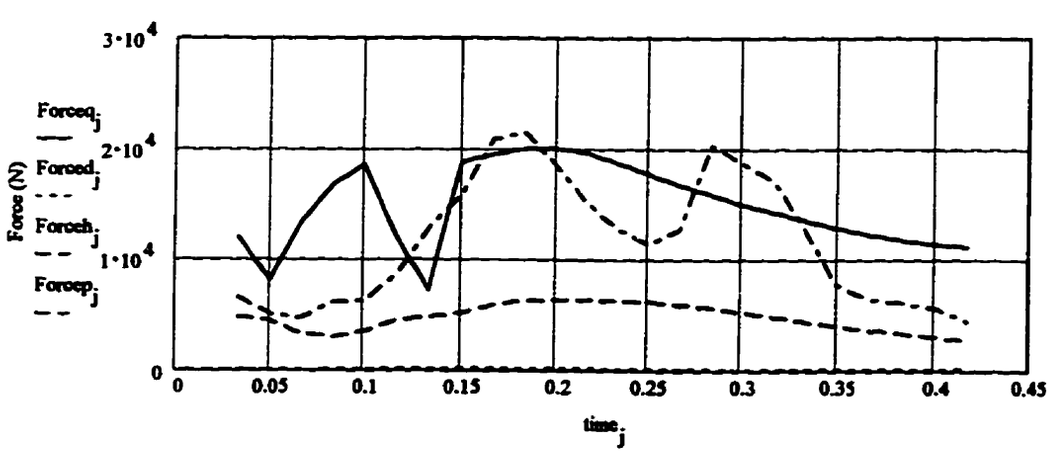

Muscle Force

Individual Parameter Contributions:

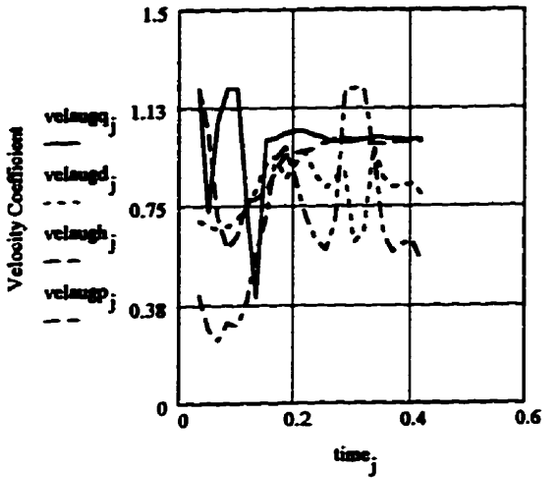

Velocity Augmentation

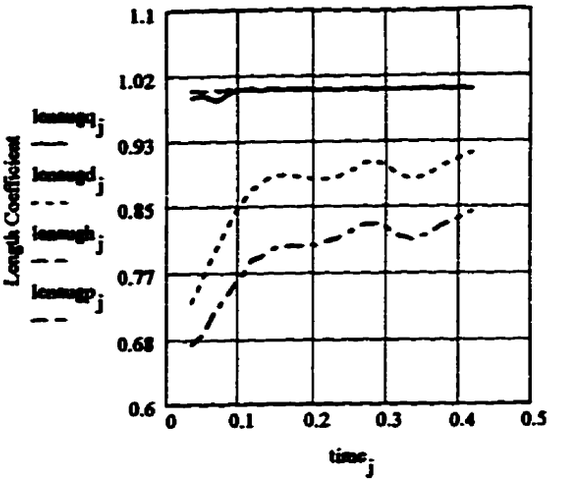

Length Augmentation

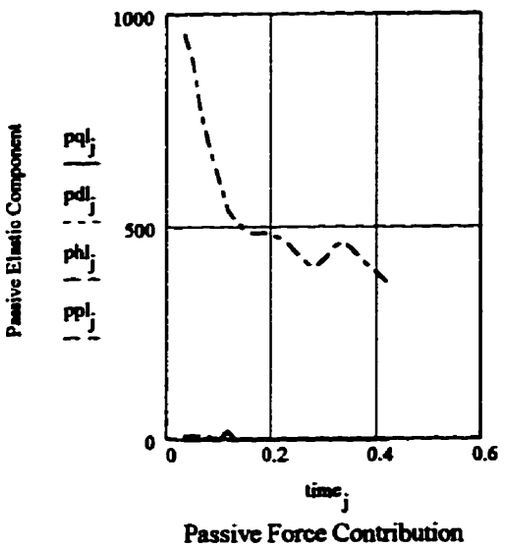

Passive Force Contribution

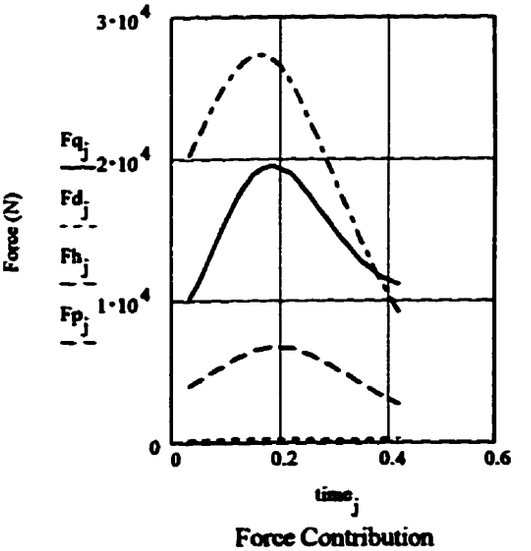

Force Contribution

Muscle Parameters:

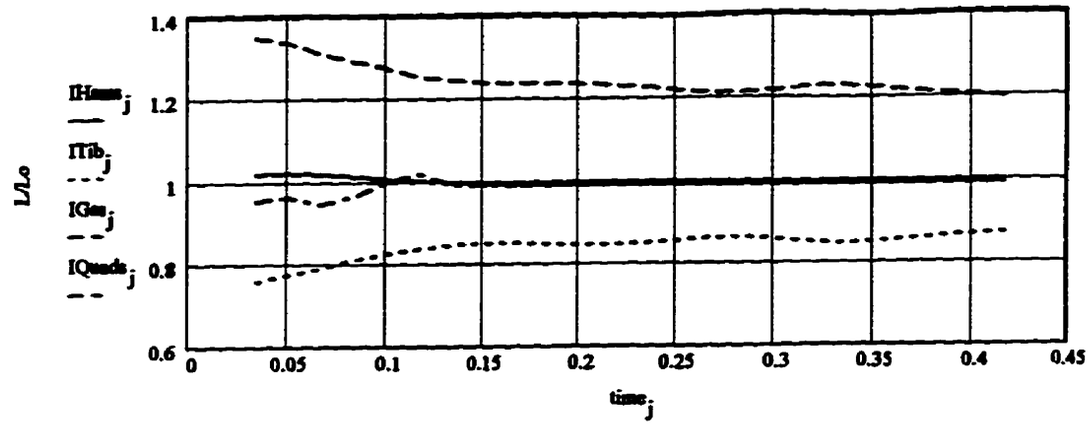

Muscle Excursion Lengths Over Time

j := 3 .. frames - 2

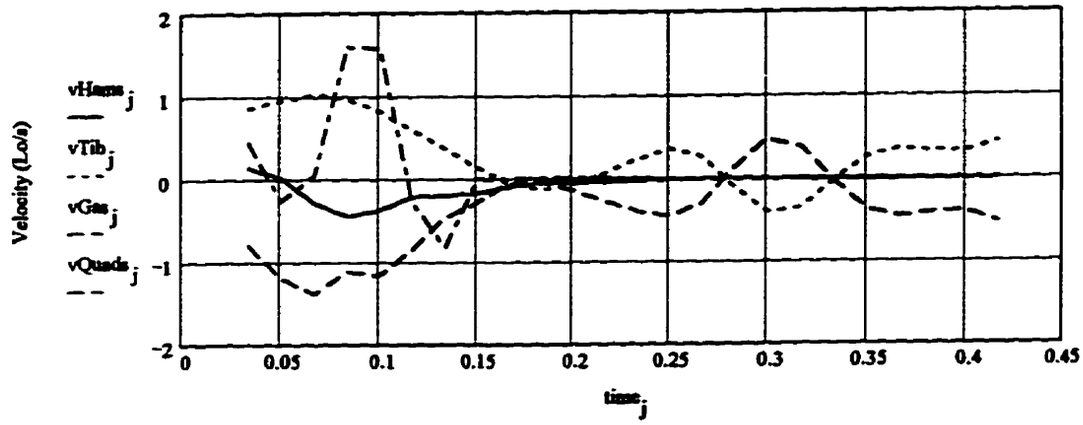

Muscle Velocities

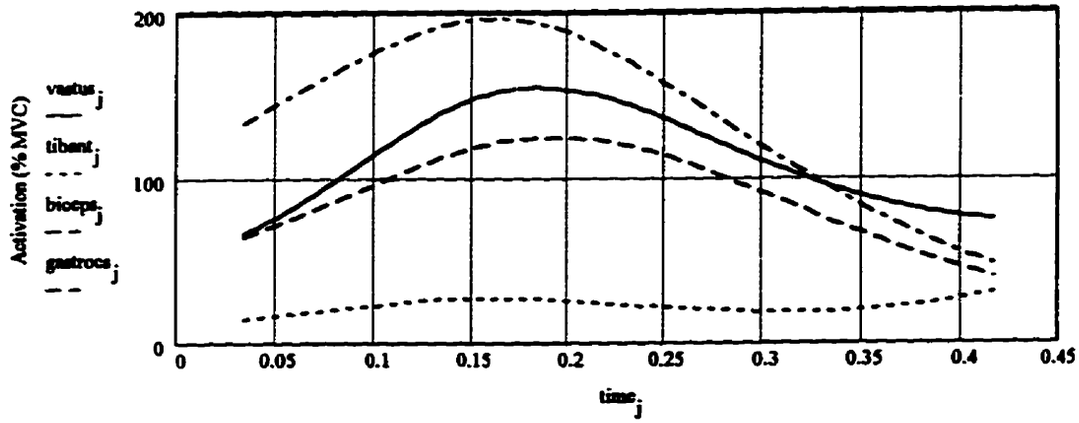

Interpolated Muscle Activation

Muscle Force Comparisons **(ie with and without Passive Stuff)**

$NForceq_j := Fq_j \cdot lenaugq_j \cdot velaugq_j$

$NForceh_j := Fh_j \cdot velaugh_j \cdot lenaugh_j$

$NForced_j := Fd_j \cdot velaugd_j \cdot lenaugd_j$

$NForcep_j := Fp_j \cdot velaugp_j \cdot lenaugp_j$

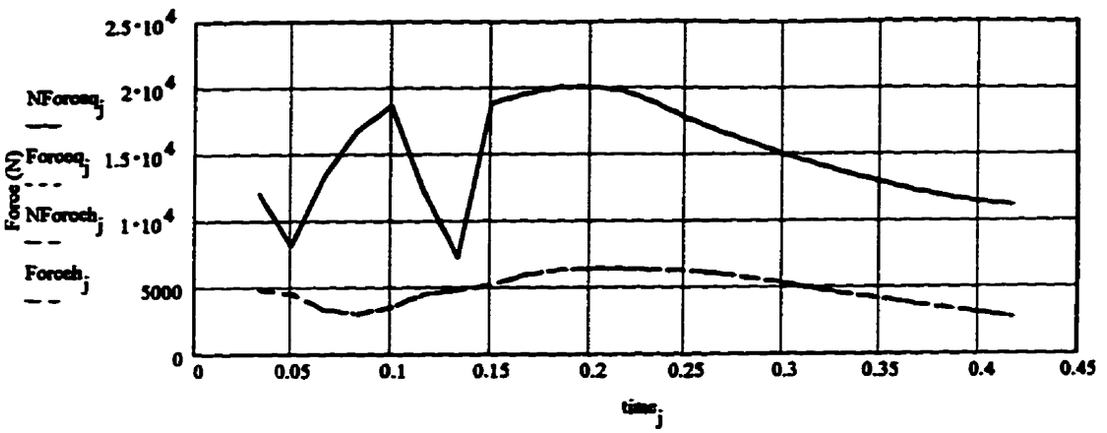

Muscle Force

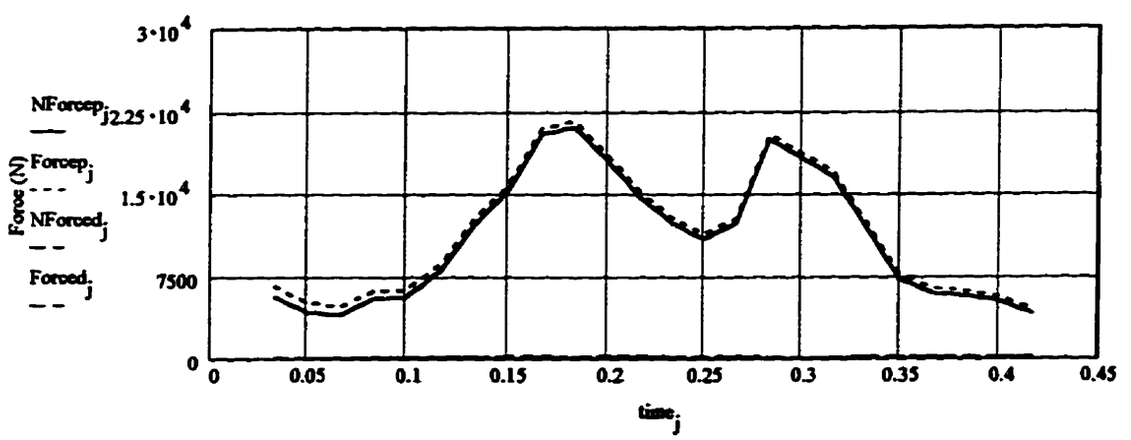

Muscle Force

THE FINAL CALCULATIONS.....

Force the muscle moments to equal the reactive moment. Apply a common gain to the dorsi/plantar flexors and a (possibly different) common gain to the knee extensors and flexors.

$$gain1_j := \frac{JM_{4,j}}{\left(Forced_j \cdot tmal_j\right) - \left(Forcep_j \cdot gmal_j\right)} \qquad gain2_j := \frac{JM_{3,j}}{\left(Forceq_j \cdot qmal_j\right) - \left(Forceh_j \cdot bmal_j\right)}$$

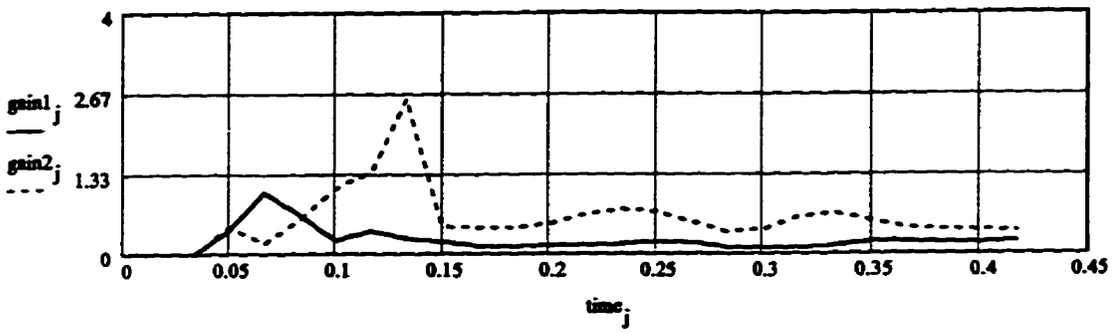

Gain Factors

Add the muscle forces to the joint reaction forces.....

Determine muscle angles of pull

$$\xi quads_j = angle\left(FQuadKx_j - FQuadIx_j, FQuadKy_j - FQuadIy_j\right)$$

$$\xi hams_j = angle\left(FHamKx_j - FHamIx_j, FHamKy_j - FHamIy_j\right)$$

$$\xi tibant_j = angle\left(FTibMx_j - FTibIx_j, FTibMy_j - FTibIy_j\right)$$

$$\xi gastrocs_j = angle\left(FGasAx_j - FGasIx_j, FGasAy_j - FGasIy_j\right)$$

The Ankle

$i := nseg$

$$BOBx_{i,j} = m_i \cdot axcm_{i,j} - Gx_j + Forced_j \cdot \cos\left(\xi tibant_j\right) \cdot gain1_j - Forcep_j \cdot \cos\left(\xi gastrocs_j\right) \cdot gain1_j$$

$$BOBy_{i,j} = m_i \cdot aycm_{i,j} + m_i \cdot g - Gy_j - Forced_j \cdot \sin\left(\xi tibant_j\right) \cdot gain1_j - Forcep_j \cdot \sin\left(\xi gastrocs_j\right) \cdot gain1_j$$

The Knee

$i := nseg - 1 .. 1$

$$BOBx_{i,j} = m_i \cdot axcm_{i,j} + Rx_{i+1,j} + Forceq_j \cdot \cos\left(\xi quads_j\right) \cdot gain2_j - Forceh_j \cdot \cos\left(\xi hams_j\right) \cdot gain2_j$$

$$BOBy_{i,j} = m_i \cdot aycm_{i,j} + Ry_{i+1,j} + m_i \cdot g - Forceq_j \cdot \sin\left(\xi quads_j\right) \cdot gain2_j - Forceh_j \cdot \sin\left(\xi hams_j\right) \cdot gain2_j$$

$$i := 1 .. nseg \qquad BOB_{i,j} = \sqrt{\left(BOBx_{i,j}\right)^2 + \left(BOBy_{i,j}\right)^2} \qquad BOBbw_{i,j} = \frac{BOB_{i,j}}{mass \cdot g}$$

Bone-on-Bone Forces at the Ankle and Knee During Jump Landings

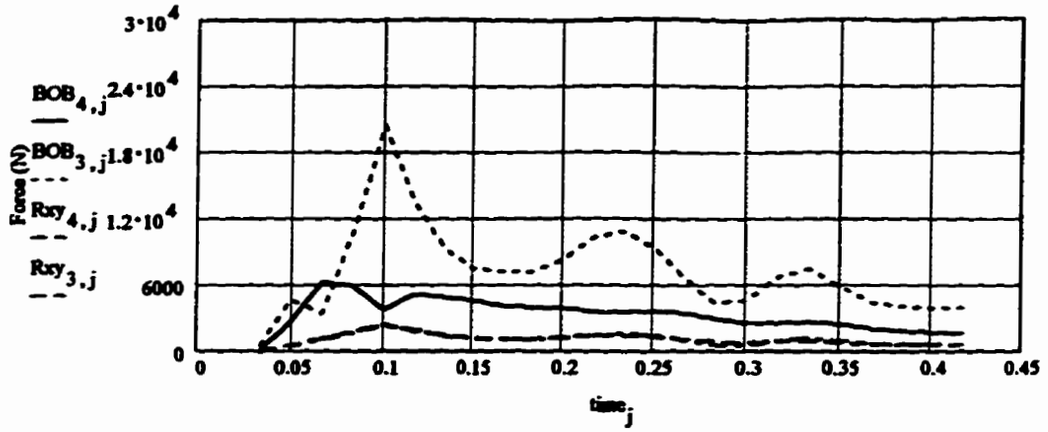

Bone-On-Bone vs Joint Reaction Forces

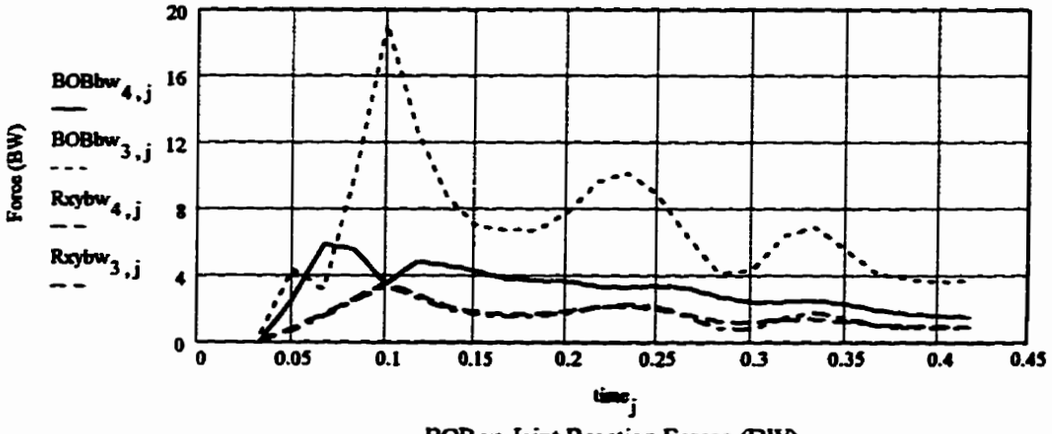

BOB vs Joint Reaction Forces (BW)

Model Outputs

$i := 1 .. npts \qquad j = jselected$

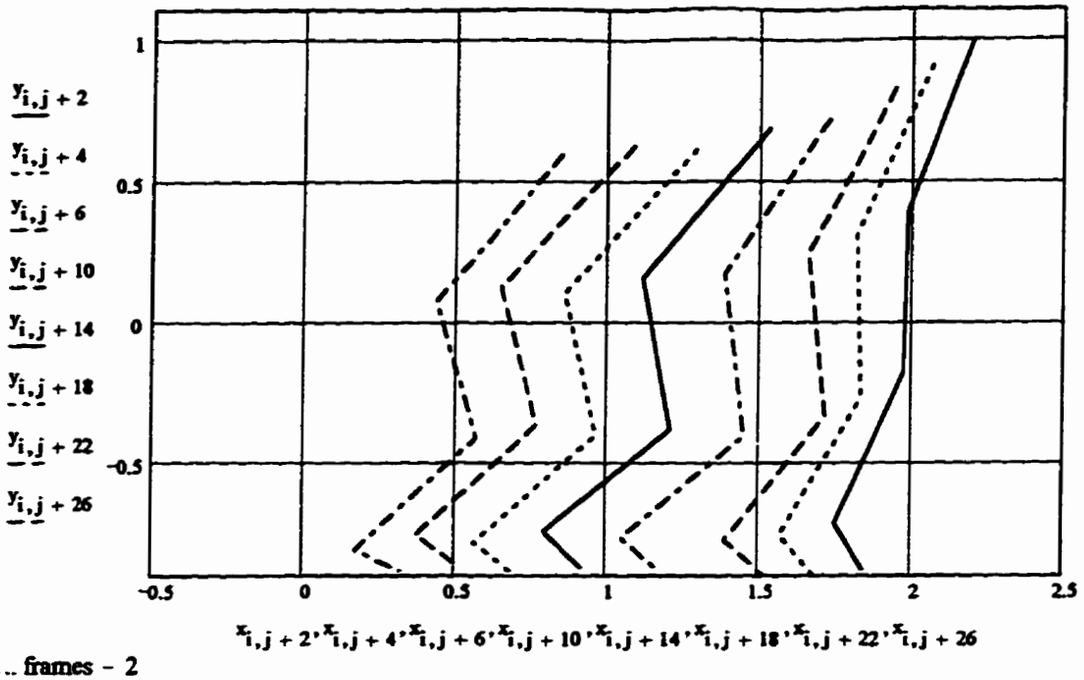

$j := 2 .. frames - 2$

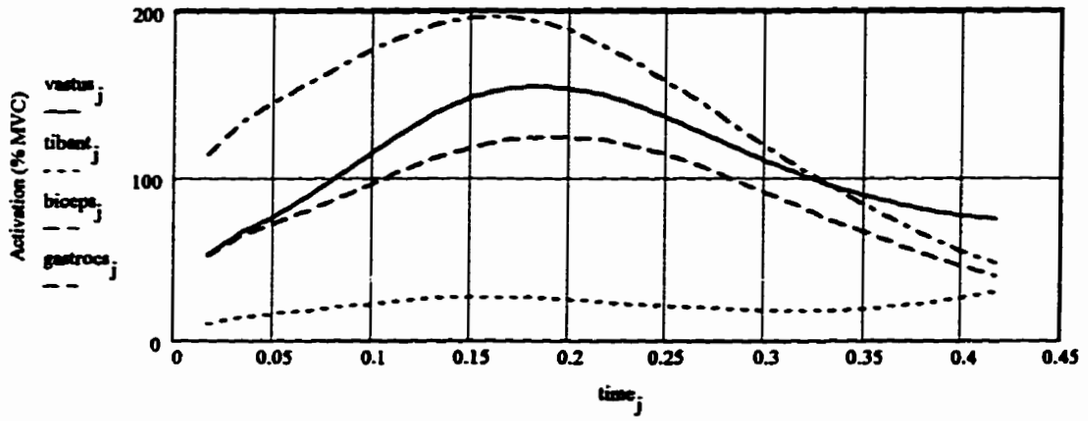

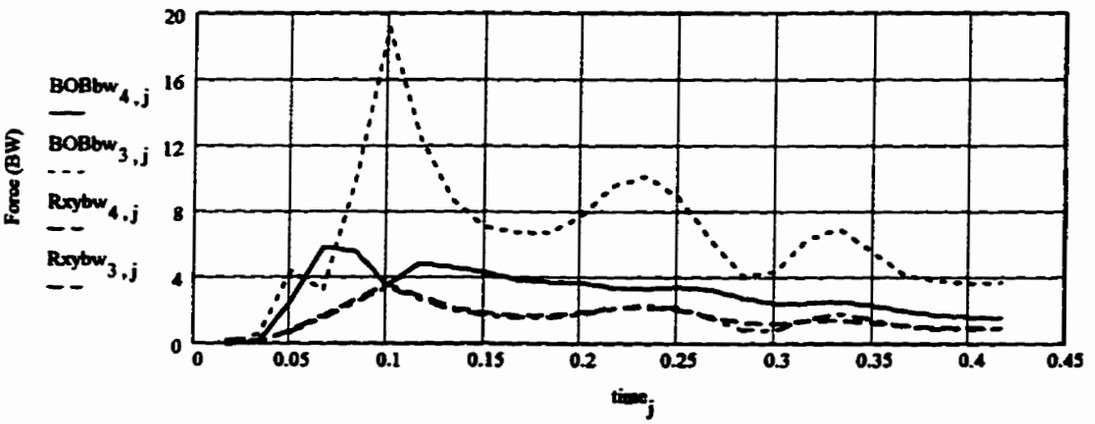

BOB vs Joint Reaction Forces (BW)

Copy Selected Results to a Single Row Output Matrix

$j := 2..frames - 2$

Time

$$Results_{1,j} := \left(\frac{j}{60} - \frac{1}{60}\right) \cdot 1000$$

$Results_{1,1} := 1$

Rx, BOB, Gain (Ankle)

$Results_{2,j} := Rxybw_{4,j}$

$Results_{3,j} := BOBbw_{4,j}$

$Results_{4,j} := gain1_j$

Rx, BOB, Gain (Knee)

$Results_{6,j} := Rxybw_{3,j}$

$Results_{7,j} := BOBbw_{3,j}$

$Results_{8,j} := gain2_j$

Ankle (4) and Knee (3) moment

$Results_{10,j} := JM_{4,j}$

$Results_{11,j} := JM_{3,j}$

Ankle (2) and Knee (1) angle

$Results_{13,j} := d\theta_{2,j}$

$Results_{14,j} := d\theta_{1,j}$

L/Lo excursions

$Results_{16,j} := lQuads_j$

$Results_{17,j} := lTib_j$

$Results_{18,j} := lHams_j$

$Results_{19,j} := lGas_j$

$Results := Results^T$

$PRNCOLWIDTH := 10$

$WRITEPRN(smsll209) := Results$

Toggle this equation to activate the saving of results from the current program settings. The Associate Filename menu item can be used to locate the output file elsewhere.

APPENDIX B

Anatomic Model Schematic

Anatomic Model
Muscle Origin-Insertion Schematic